TU Delft

Investigation on the attenuation trend of Acoustic Emission in reinforced concrete structures

Yubo Sun 4614887

Committee

Dr. ir. Y. Yang TU Delft

Dr. ir. M. A. N. Hendriks TU Delft

Abstract

Considered as an effective real-time monitoring tool, Acoustic Emission (AE) measurements is a promising technology for reinforced concrete (RC) structures. However, its application on real RC structures is still limited. Due to the lack of knowledge on the crack induced acoustic emission in large scale structures.

The aim of this study is to explore the relationship between the fracture energy and the energy of AE signals at structural level. This serves as a basis for the quantification and localization of cracking activities at structural level.

This study is based on the AE and crack propagation measurement of a series of large scale RC specimen tests. To avoid the influence of existing cracks, the first part of study focuses on the development of the first flexural crack. It was assumed that the amount of energy required for unit length of crack opening is linearly proportional to the energy of the AE signals that are generated upon the opening of this segment of the crack. These signals can only be monitored AE sensors at given locations. By then, they have travelled through the bulk concrete and possibly already existing cracks, thus their energy has attenuated due to the geometric spreading and the damping property of the material. When these effects are taken into account, the total energy of the AE signals that were obtained by the AE sensors at given location (defined as cumulative signal strength CSS) has a potential of reflecting the fracture energy of the corresponding crack. In the part of the study, this process is theoretically studied first. The theoretical result was further validated by the AE measurement obtained from experiments.

Theoretical investigation is carried out based on a simplified model considering only length of the crack and the horizontal distance between crack and AE sensor. Theoretical result shows that both crack length and horizontal distance would affect CSS. However, when the horizontal distance is big enough, crack length is no longer the dominant factor, and CSS drops significantly with the increase of horizontal distance. The CSS of different sensors in a row in the experiments are used to validate this attenuation phenomenon. Exponential curve fitting is carried out to describe the attenuation of experimental results in different tests. Finally, a comparison of attenuation in percentage terms between curve fitting results and theoretical results is carried out. In the uncracked specimens, the results fit each other well.

Furthermore, the effect of the existing cracks to the attenuation of the CSS is studied as well. In that case, a dramatic drop of CSS is observed compared to the uncracked structures.

The study shows CSS detected by AE sensors could partly indicate the cracking behavior of RC structures. The attenuation tendency gives a guidance for sensor installation in future tests.

Key words: Acoustic emission, Reinforced Concrete structures, Cumulative Signal Strength, Attenuation

Nomenclature

Abbreviations

AE	Acoustic emission
RC	Reinforced concrete
CSS	Cumulative signal strength
LVDT	Linear variable differential transformer

Greek letters

ρ_l	Reinforcement ratio
α_e	Elastic stiffness ratio between concrete and steel
Φ	Diameter of reinforcement
τ_{cm}	Bond strength between rebar and concrete
ρ_{eff}	Effective reinforcement ratio
ε_{cm}	Average strain of concrete
ε_{sm}	Average strain of steel
γ	Attenuation coefficient of wave
a	Linear relation between G_0 and G_{AE}

Roman letters

G_f	Fracture energy
W_f	Work of fracture
G_0	Total amount of energy release in a crack
s_{cr}	Estimated length of crack
l_{cr}	Spacing between cracks
l_t	Transmission length
w	Width of flexural cracks
E_0	Original energy of the propagating wave
E	Reduced energy of the propagating wave

G_{AE} Total AE energy when a crack opens

$A(x)$ Attenuation factor of AE signal

ss_0 Signal strength by unit length of crack if AE sensor is located at the crack

ss_∞ Signal strength by unit length of crack if AE sensor is located infinitely far away

g_0 Amount of energy released by unit length of crack opening

L Length of crack

b Width of specimen

dy Length of crack front

x Horizontal distance between crack and sensor

Contents

1   Introduction

The word "acoustic" is derived from the Greek word *akoustikos,* which means "hearing". For centuries, the precursor to structural collapse has been sounds that are emitted prior to the failure of a supporting member [1]. Acoustic emission testing (AET) has become a recognized nondestructive test (NDT) method commonly used to detect and locate faults in mechanically loaded structures. AE can provide comprehensive information on the origination of a crack in a stressed component and also provides information pertaining to the development of this crack as the component is subjected to continuous or repetitive stress. The application of acoustic emission to non-destructive testing of materials usually takes place between 100kHz and 1MHz. Unlike conventional ultrasonic testing, AE tools are designed for monitoring acoustic emissions produced by the material during failure or stress, and not on the material's effect on externally generated waves. Part failure can be documented during unattended monitoring [2].

Acoustic Emission (AE) has been widely used in civil structures in monitoring since the early 1980's [3]. In reinforced concrete structures, the acoustic emission is generated by several kinds of mechanisms, including cracking of the concrete, rubbing of crack surfaces during crack closure, debonding of the reinforcing steel from the surrounding concrete, etc., which could be detected by AE sensors. Thus, the AE measurements partly reflect the amount of energy release of a crack. On the other hand, no full strength would be detected by AE measurements since it's impossible to predict a completely accurate crack pattern and install the sensors just right on the crack path. CSS detected by a single AE sensor could only reflect the signal strength where the sensor is installed, and CSS of different AE sensors may vary with distance between sensor and energy source. Therefore, attenuation of AE measurement is an important factor to be investigated in this paper, and it's also possible to estimate the real fracture energy release of a certain crack. In this study CSS detected by AE sensors installed on surface of different specimens in several tests are investigated, and two important factors (attenuation and fictitious G_0) are given to show the difference of CSS detected by AE sensors in a row. With the attenuation tendency it's possible to properly indicate the cracking behavior of a RC structure with several AE sensors installed in a certain area where crack propagates.

Recently, a series of tests have been done in Delft University of Technology aiming at the evaluation on the shear capacity of reinforced members without shear reinforcement. The specimens are casted into 300, 500 and 800 mm high since the beam height would strongly affect the shear capacity of reinforced concrete structures without shear reinforcement. AE measurement is introduced in several of those tests, and the results of such tests are investigated in this study.

2   Tests configurations

A series of tests have been done in Delft University of Technology aiming at the evaluation on the shear capacity of reinforced members without shear reinforcement. The target of the tests was to investigate the transition of shear failure and bending failure, and AE signals were recorded as well during the tests. Experimental data for this study is kindly provided by *Dr. ir. Y. Yang.*

2.1   Configurations of the specimens

In general, three types of beams with different dimensions are involved in this research. In the first stage, beams of 300 mm height, 800 mm length and 300 mm width are casted and tested. AE sensors are installed on the front surface of specimens, which will be illustrated in latter chapters. Effects of concrete strength are investigated as well. In test series A, higher strength concrete (C65) are selected while test series C has lower strength concrete (C30). The numbering of the specimens in the test series is indicated in Fig. 2.1.1, where the major difference between the two series are marked by the starting letter [4].
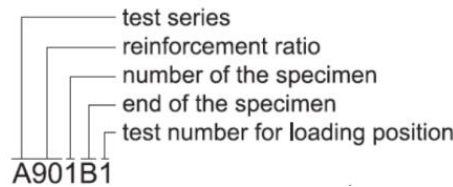

Fig. 2.1.1 Definition of test numbers in 1st stage

In the second stage, beam height increases to 500 mm while the length and width of beam remain 8000 mm and 300 mm. LVDT sensors are introduced to measure the elongation of specific part along the specimen which helps to track the initiation and propagation of cracks.

In the third stage, even larger scale beams are casted with height of 800 mm, length of 10000 mm and width of 300 mm. Both AE and LVDT sensors are installed on the surface of the specimens. Two test series can be distinguished from each other by whether beams are reinforced with plain bars or ribbed bars, namely P series and R series respectively. The test numbers in the test stage 2 and 3 are defined in Fig. 2.1.2. Details of each specimen is shown in Table. 2.2.1.1, and the difference between the several test series are summarized as well.
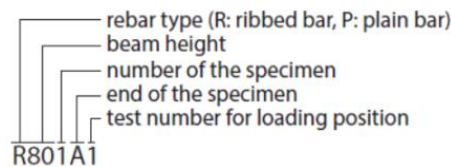

**Fig. 2.1.2 Definition of test numbers in 2nd and 3rd stage**

Table. 2.2.1.1 Summary of tested specimens

Specimen No.	Rebar config.	$f_{c,max}$ [MPa]	Height [mm]	D [mm]	ρ [%]
A602	1Ø10+2Ø16	64.36	305.5	272.5	0.59
A752	3 Ø16	64.36	306.0	273.0	0.74

| C901 | 1Ø12+2Ø20 | 19.39 | 306.5 | 271.5 | 0.91 |
R501	5Ø20(2layers)	66.04	500	455.0	1.15
R801	3 Ø25	71.47	800	762.5	0.64
P804	6Ø20(2layers)	63.51	800	755.0	0.83
R803	3 Ø25	62.07	800	762.5	0.64
R804	6Ø20(2layers)	63.51	800	755.0	0.83

2.2   Test configuration and program

In all the tests, the specimens are simply supported, and the positions of supports are shown in Fig. 2.2.1. The position of point loads varies in tests to find out the expected failure modes, which is expressed by the distance from one of the supports (distance *a*) in the figure. A long cantilever was left out of the longer end support so that the two ends of each specimen could be tested separately.
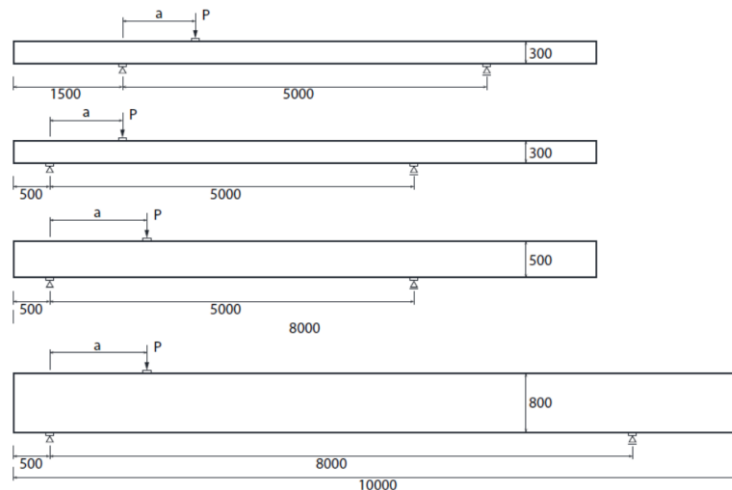

Fig. 2.2.1 Configurations of the boundary conditions of the tests

As the purpose of these tests was to find out the minimum shear force which could cause shear failure, more than one tests were conducted on the specimens with same reinforcement ratio. At the beginning of the test the point of load was placed at somewhere relatively far away from the support so that flexural failure is obtained. The second test was carried out with the point of load moved to a closer position to the support. This procedure was repeated until shear failure occurred. In order to find a critical load position, more tests were carried out by locating the load point between the first shear failure and last flexural failure. Then the failure was strengthened so that the latter tests would be less affected by cracks formed in former tests, and another series of tests were carried out on the other side on the undamaged end of the same specimen. A summary of the testing procedure is given in Fig. 2.2.2.
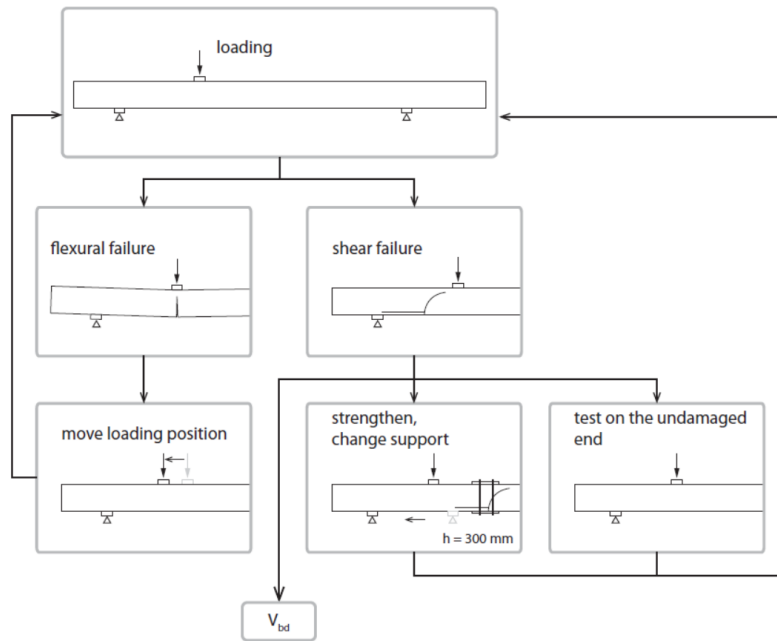
Fig. 2.2.2 Flow chat of the test program for a given beam configuration

AE and LVDT measurements are introduced in tested specimens, layouts could be found in *Appendix 1*. For this study load cycles are performed for Acoustic Emission measurements (Fig. 2.2.3).
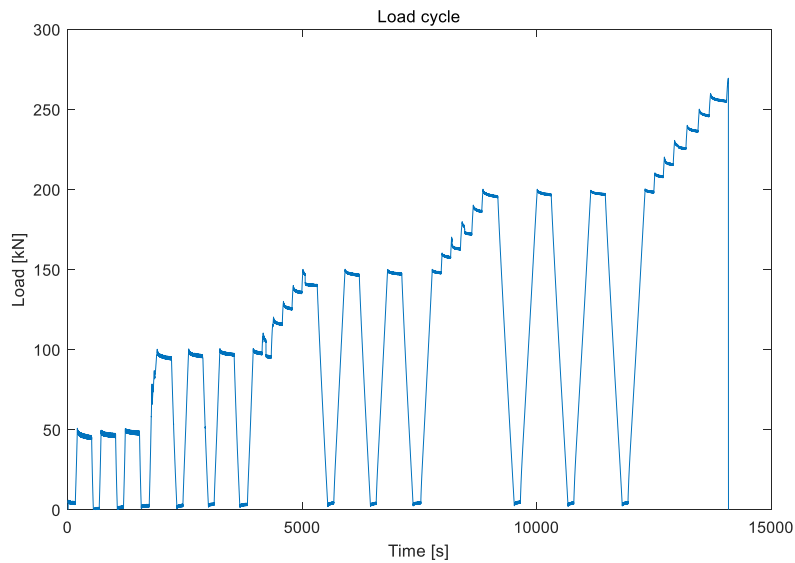
Fig. 2.2.3 Load cycles

2.2.1   AE measurement

Acoustic emission is the name given to the transient stress waves that are generated by crack growth and many other kinds of material degradation and deterioration [5]. Acoustic (elastic) waves in solids that occurs when a material undergoes irreversible changes in its internal structure, which is caused by the rapid release of localized stress energy. In particular, AE is occurring during the processes of mechanical loading of materials and structures accompanied by structural changes that generate local

sources of elastic waves. This results in small surface displacements of a material produced by elastic or stress waves generated when the accumulated elastic energy in a material or on its surface is released rapidly [6]. Acoustic emission during the test process is detected by three groups of AE sensors installed at the top, bottom and medium layer on the surface of the specimen (shown in Fig. 2.2.6).

Instrument

AE sensors transform surface motions into electric signals. Amplifiers are usually employed to magnify AE signals. Normally signals are amplified both by a pre-amplifier and by main-amplifier, and are filtered. Pre-amplifiers with sate-of-the-art transistors used to minimize the amount of electronic noise. Amplifiers with a flat response in the frequency range are best use. The gain of the amplifier is given in dB(decibels). A filter of variable band-width between 1kHz and 2MHz is generally employed. The choice of the frequency range depends on noise level and attenuation property of concrete.

Data acquisition

Main concern for data acquisition results from the A/D (analog to digital) conversion and the triggering. Fast A/D units gave to be used to ensure that a large number of events are recorded. Usually, the A/D converter is equipped for each channel of recording unit. Anti-aliasing filters are required so that signals can be properly transformed to frequency domain. A monitoring system could analyze such parameters as count, hit, event, rise time, duration, peak amplitude, energy, RMS (root mean square) voltage, frequency spectrum, and arrival-time difference.

Identification of AE Signal

AE signals emerge rapidly and randomly in a test. Therefore, the discrimination of AE signals from running waves is the first step of analyzing AE activity. Since the increase of the cumulative signal strength is strongly correlated to the opening of a crack locally [7]. Normally, to get rid of other energy sources other than crack opening, a voltage threshold level is set and AE signals are processed after amplitude exceeds threshold level.

Parameters

Elastic waves generated by fracture phenomena is detected by AE sensors as electrical signals (AE signals). Therefore, characteristics of AE parameters are studied to reveal the physical phenomena of cracking. In what follows, signal parameters (shown in Fig. 2.2.4) most widely used are explained from definitions (ISO 12716 2001) [3].
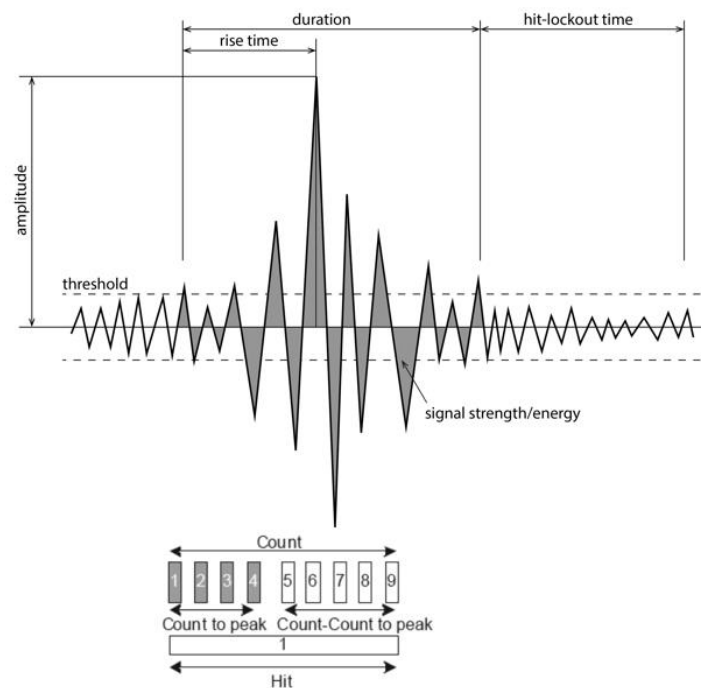
Fig. 2.2.4 Conventional AE signal features

- Hit: a signal that exceed the threshold and causes a system channel to accumulate data. It is frequently used to show the AE activity with counted number for a period or accumulated numbers.

- Count: the number of times within the duration, where one signal strength exceeds a present threshold.

- Amplitude: a peak voltage of the signal waveform is usually assigned, which is closely related to the magnitude of source event.

- Duration: a time interval between the triggered time of one AE signal and the time of disappearance is assigned.

- Rise time: a time interval between the triggering time of AE signal and the time of the peak amplitude is assigned.

- Signal strength: a measured area under the rectified signal envelope.

- Average frequency: a calculated feature obtained from *Count* divided by *Duration*, which determines an average frequency over one AE hit.

Previous study [8] showed that the signal strength of AE hits received by the sensors has strong relationship to the cracking activities. In this study, *Signal strength* of a rectified signal detected by AE sensors is selected to investigate the fracture behavior of RC specimens, which represent the total energy of an AE hit.

2.2.2   LVDT measurement

A linear variable differential transformer (LVDT) is a sensor used for measuring linear displacement [9]. The operation is based on that of a transformer with three coils that are placed around a tube in succession. The middle coil is the primary, the two outer coils are secondary, both secondary coils must have the same number of turns. A rod-shaped ferromagnetic core, which is attached to the object whose position is to be measured, slides along the axis of the tube (Fig. 2.2.5).
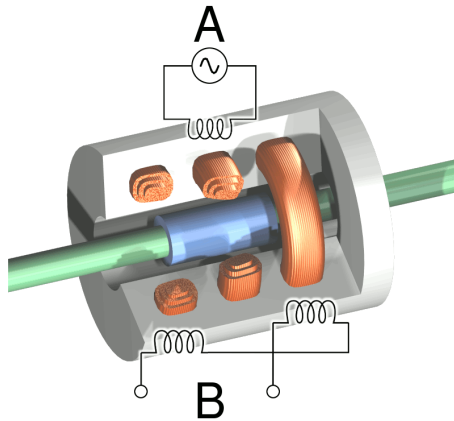
Fig. 2.2.5 Cross-section of LVDT

An alternating current through the primary coil causes an electric voltage in each of the secondary coils, this voltage is proportional to the mutual coil ratio with the primary coil. The frequency of the alternating current is usually between 1 and 10 kHz.

Crack openings are measured by LVDT grid shown in Fig. 2.2.6. Elongation of specific part of concrete specimen could be measured so that the crack openings could be tracked.

Fig. 2.2.6 AE and LVDT grid

3 Related parameters

3.1 Fracture energy

As defined as the energy required to open unit area of crack surface, the *fracture energy* is considered as a material property which is independent of the size of structure. Fracture energy could be obtained either by a three-point bending test [10] or a wedge-splitting test [11]. From any of those tests, the load-displacement or load-COD (crack open displacement) curve is obtained.
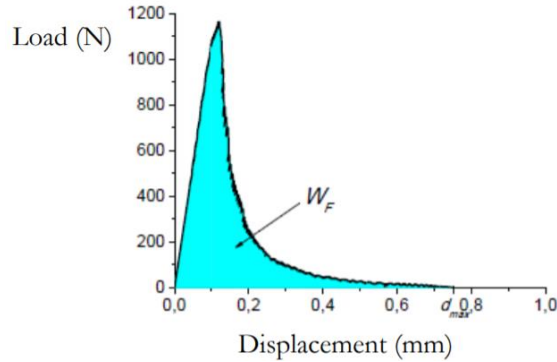
Fig. 3.1.1 Load-displacement curve of concrete specimens

The area under the envelop represents the work of fracture (W_f), and the fracture energy (G_f) is defined as $G_f = \frac{W_f}{A}$, where A is a ligament area, determined by the geometry of fracture surface [12]. Therefore, it is possible to roughly estimate the amount of energy release of a certain crack by doing integration along the crack path. Then a relation could be found between the energy release of a crack and signal strength detected by sensor. Furthermore, the fracture of a structure could be assessed as well by AE measurements.

3.2 G_0

G_0 is defined as the total amount of energy release in a crack, which is related to fracture energy of a concrete structure. It is for sure that the generation and propagation of cracks in reinforced concrete beams will be accompanied with some energy release during loading progress, and thus the amount of energy release is expected to have some certain relationship with the fracture energy.

Because of the loading condition and boundary conditions given in previous chapter, location of the first main flexural crack is expected to be under the loading point. Assuming a linear stress distribution in compression zone, the height of crack s_{cr} is given by

$$s_{cr} = (1 + \rho_l \alpha_e - \sqrt{2\rho_l \alpha_e + (\rho_l \alpha_e)^2})d \tag{1}$$

Here, ρ_l is the reinforcement ratio, α_e is the ratio of elastic stiffness between concrete and steel. A rough estimation of spacing between cracks is given by $l_{cr} = 1.5 l_t$, where l_t is the transmission length given by

$$l_t = \frac{f_{ctm}\Phi}{4\tau_{cm}\rho_{eff}} \tag{2}$$

With f_{ctm} is the mean tensile strength of concrete, Φ is diameter of reinforcement, τ_{cm} is the bond strength between rebar and concrete, and ρ_{eff} is the effective reinforcement ratio. The width of the flexural cracks could also be given by the difference between average strain of steel and concrete along two cracks

$$w = (\varepsilon_{cm} - \varepsilon_{sm})l_{cr} \tag{3}$$

Discussion above shows that the height and width of a certain flexural crack in formation stage is determined by configuration of beam. Therefore, with the definition of fracture energy, the amount of energy release could be considered as a constant once the configuration of beam is given, or in other words, G_0 is constant.

3.3   Fictitious G_0

No full strength would be detected by AE measurements since it's impossible to predict a completely accurate crack pattern and install the sensors just right on the crack path. CSS detected by a single AE sensor could only reflect the signal strength where the sensor is installed. However, it's always fascinating to know what is real G_0, and how much energy is released while crack opening. Furthermore, attenuation could be investigated only if the initial value is known.

The AE signal detected by sensors will attenuate since the energy wave are reflected and dissipated while travelling in concrete structures due to the existing pores and cracks in concrete matrix. Therefore, the signal detected by the sensor closest to the crack is selected as a fictitious source of crack to account for AE measurements.

On the other hand, in a three-point bending test, at the very beginning, the first main flexural crack will occur at the bottom of the specimen under load point and propagate upward in vertical direction. Then more flexure cracks and shear cracks occur with the increase of load. In this research, to avoid the energy released by different cracks during propagation affecting each other, only the first critical crack is considered to investigate the fracture energy.

Therefore, in this study, the CSS detected by AE sensor located at the bottom surface of specimen closest to loading point is regarded as Fictitious Source. For instance, AE layout of specimen R804A1 is given in Fig. 3.3.1. The AE sensors (No.1 – No.14) are divided into three rows and installed on the surface of concrete beam, and AE signals of 14 channels are recorded in computer memories. In this test, the first flexural crack is expected to occur at the position where external load is applied at the bottom of the beam and propagate upward due to the longest lever arm according to the support position. It is obvious that AE sensor No.14 is the closest one to the first crack and the attenuation is smallest, and therefore, AE signal recorded in channel 14 is selected as the Fictitious G_0.
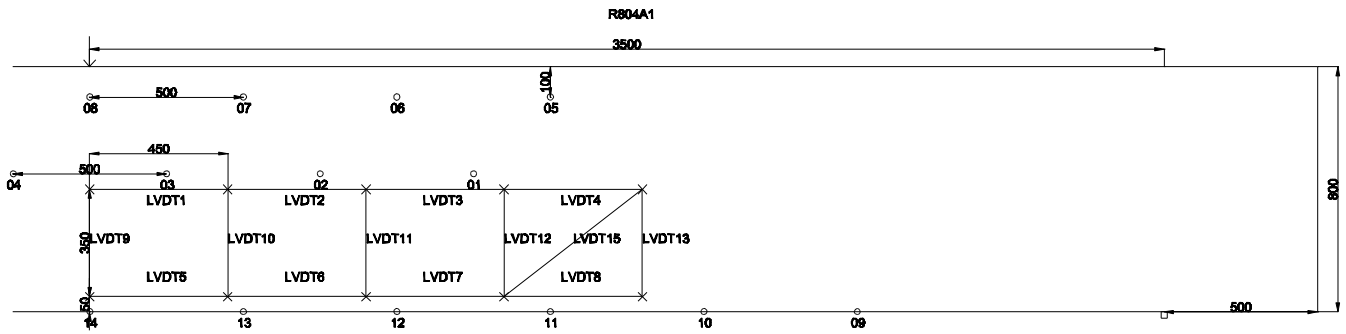
Fig. 3.3.1 AE layout of R804A1

3.4 CSS

Cumulative signal strength (CSS) is defined as the summation of impulse strength detected by AE sensor in a certain time period. Theoretical results show that CSS detected by a single AE sensor tends to be a constant value as crack length grows. However, the selection of the period is rather strict to get rid of other noises except energy released by crack opening.

3.5 Linear hypothesis

In this study, structural behavior is monitored with the help of AE sensor, which contains a transducing element that turns AE waves motion into an electrical voltage. An acoustic signal (G_0 expressed in [J]) is transferred into electrical signal (G_{AE} expressed in [mVs]) in this process. G_{AE} is defined as the total AE energy when a crack opens here.

A linear hypothesis is put forward between the amount of energy of energy required for unit length of crack opening and energy of AE signals generated by unit length of crack opening to represent the amount of energy release by electrical signal detected by AE sensors. The linear relationship could be expressed by $G_{AE} = \alpha G_0$, where α is the linear coefficient.

Then attenuation effect is considered as well to determine the CSS (can be directly measured) since it's not always possible to measure AE signal strength right on the crack path. It is assumed that $CSS = A(x)G_{AE}$, and A(x) is the attenuation factor. Therefore, $CSS = \alpha A(x)G_0$.
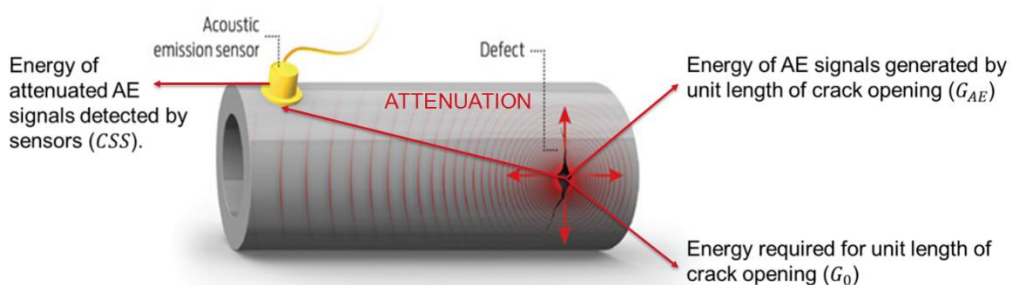
Fig. 3.5.1 Linear hypothesis

4   Signal detected by a single AE sensor

In this chapter signal detected by a single AE sensor is investigated. The definition of G_0 is given firstly, theoretical derivation shows that G_0 is determined by configuration of beam. Then CSS is defined to show which part of the discrete signal is selected to investigate along loading history. Finally, fictitious G_0 is given to approximately represent the total amount of energy release of a crack. Result of test R804A1 is selected as an example.

4.1   Attenuation of acoustic waves

The intensity of acoustic wave diminishes with distance when it travels in a medium. In idealized materials, sound pressure (signal amplitude) is only reduced by the spreading of wave. Natural materials, however, all produce an effect which further weakens the wave, which results from scattering and absorption. Absorption is the conversion of the sound energy to other forms of energy. The combined effect of scattering and absorption is called attenuation [13].

The energy change of a decaying plane wave can be expressed as $E = E_0 e^{-\gamma x}$.

In this expression E_0 is the original energy of the propagating wave at some location. E is the reduced amount of energy after the wave has traveled a distance x from the initial location. The quantity γ is the attenuation coefficient of the wave travelling, in neper per meter or simply reciprocal of meter (m^{-1}). That is, if $\gamma = 1 m^{-1}$, the wave's amplitude decreases by a factor of 1/e for each meter traveled [14].

In this study, an exponential attenuation model is applied to investigate the attenuation of AE signals.

4.2   Theoretical results

The signal strength will decrease before being detected by sensors, part of the energy is dissipated while propagating in a medium. It is for sure that full strength will be detected by a sensor if the sensor located right at the signal source, however, no signal will be detected if the sensor is infinitely far away from the source. Theoretical analysis is conducted to find out factors which may affect CSS detected by AE sensors.

First of all, the factor "length of crack" is investigated by a simplified model shown in Fig. 4.2.1. It is assumed that a straight crack is propagating upward just through the AE sensor, and only half of the crack is modelled due to symmetricity. For unit area of differential crack front, full signal strength will be detected if energy is released at the coordinate origin where AE sensor is installed ($ss_0 = \alpha g_0 A(x), A(x) = 1$), and for sure signal strength per unit crack will attenuates to zero at somewhere infinitely far away from the sensor ($ss_\infty = 0$). Therefore, the attenuation could be represented by

$$ss_x = \alpha g_x A(y), \ A(y) = e^{-y}. \tag{4}$$
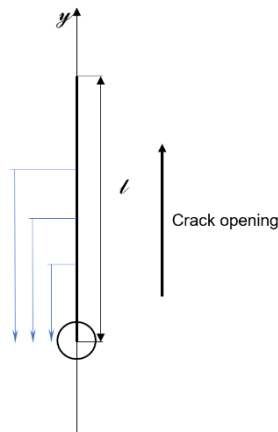
**Fig. 4.2.1 Simplified model of crack length factor**

CSS (cumulative signal strength) could be derived by integration of each unit area of crack

$$\text{CSS} = \alpha \int_0^L A(y) g_f b dy \qquad (5)$$

where L is the length of crack, $A(y)$ is the attenuation factor, g_f is the energy released by cracking of unit area, b is the width of concrete specimen, and dy is the length of crack front. On the other hand, the total energy released by crack propagation is

$$G_0 = \int_0^L g_f b dy. \qquad (6)$$

Result is plotted in Fig. 4.2.2 (unknown constants are assumed to be 1), and it is obvious that after crack has grown to a certain length the CSS detected by a single AE sensor nearly approaches a constant while the total amount of energy release of a crack increases linearly as crack propagates.
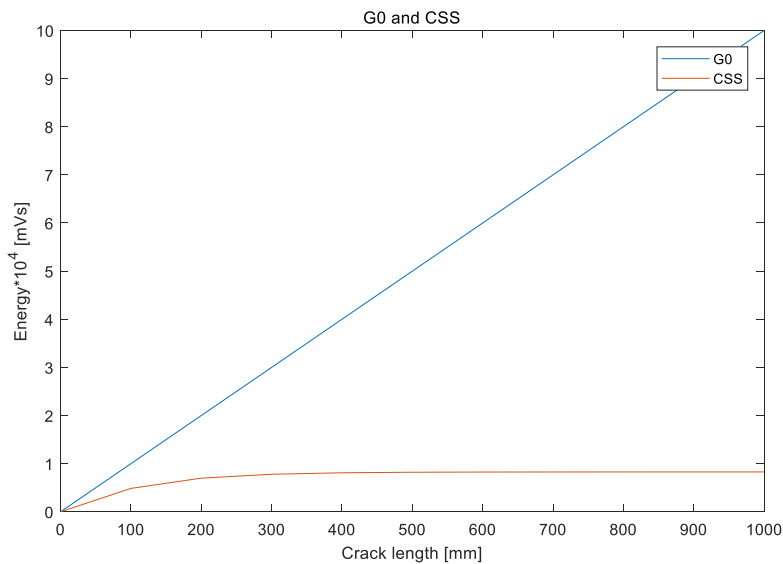
Fig. 4.2.2 Comparison between CSS and G_0

Besides, the horizontal distance between crack and AE sensor could also affect CSS. The model is given in Fig. 4.2.3, x represents the horizontal distance between crack and sensor, and length of crack is considered as a constant L. Then CSS of the sensor at x could be represented by

$$CSS = \alpha \int_0^L e^{-\sqrt{x^2+y^2}} g_f \, b \, dy \qquad (7)$$

Here, the attenuation factor of signal strength is given as a function of distance $A(x) = A_0 e^{-\sqrt{x^2+y^2}}$, and $\sqrt{x^2+y^2}$ is the distance between AE sensor and crack front.
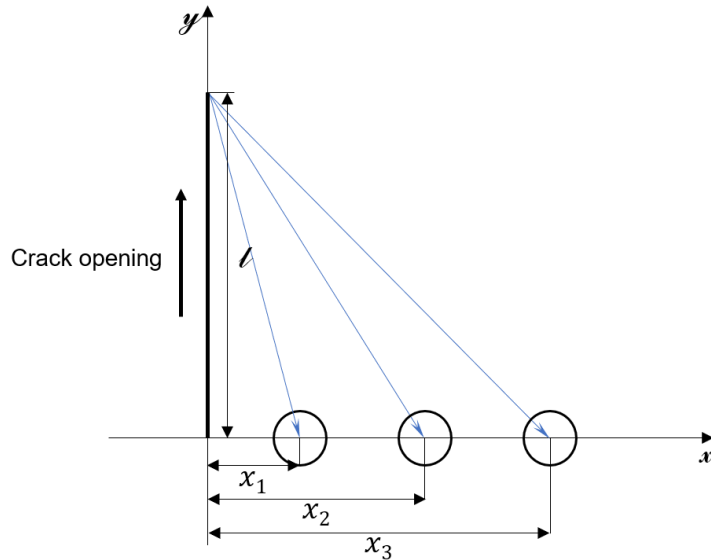
Fig. 4.2.3 Simplified model of horizontal distance model

Setting the horizontal distance $x = 0.5, 1.0, 1.5$ and 2.0 m respectively, CSS of each sensor against crack length is plotted in Fig. 4.2.4. An obvious decrease in CSS is observed with the increase of horizontal distance. The result shows that as the horizontal distance between sensor and crack increases, CSS detected by a single AE sensor would decrease since the propagating distance is longer and more energy is dissipated.
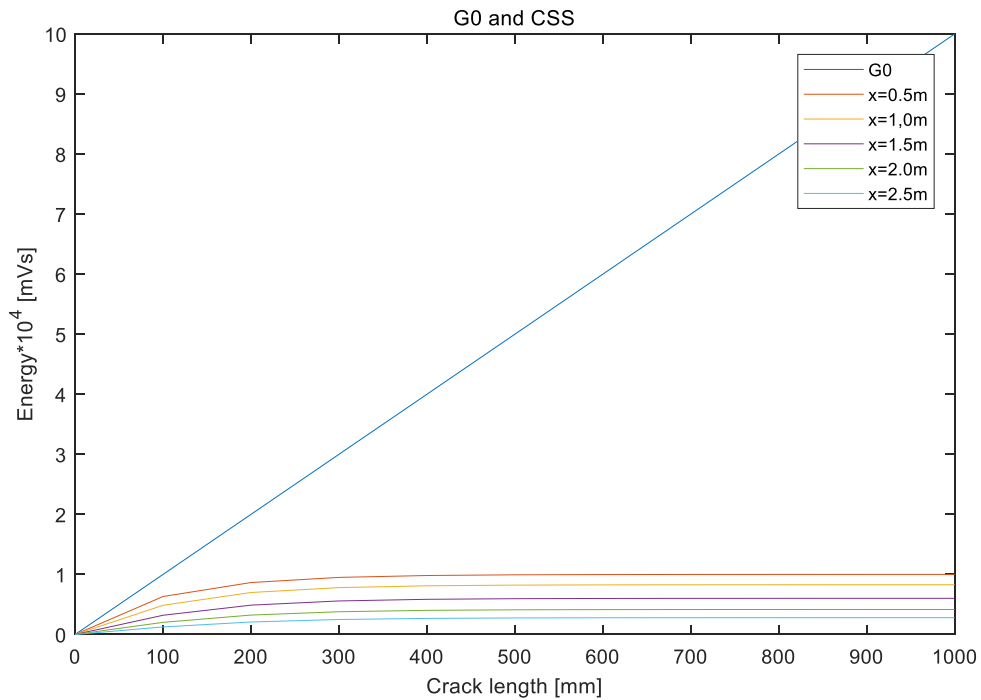
Fig. 4.2.4 CSS of a single sensor versus Horizontal distance

4.3   Experimental results

The energy release of cracking in reinforced concrete specimens are detected by AE sensors, the total amount of energy release during crack initiation and propagation is represented by cumulative signal strength (CSS) in loading history.

As mentioned above, AE signals are detected at discrete points in time, the cumulative signal strength is defined as the summation of AE signal strength within a certain time period. On the other hand, in RC structures, acoustic emission is generated by several kinds of mechanisms, including cracking of the concrete, rubbing of crack surfaces during crack closure, debonding of the reinforcing steel from the surrounding concrete, etc., which could be detected by AE sensors. Therefore, the selection of time period is very strict to get rid of any other noises other than energy release while crack opening. Load-time curve together with instant signal strength-time curve are plotted in the same figure Fig. 4.3.1 to show the relation between loading history and amount of energy release.
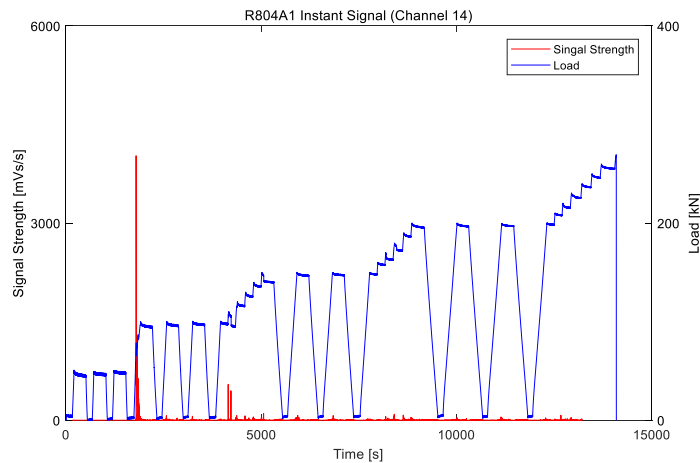
Fig. 4.3.1 Load-time and SS-time curve of R804A1 (Channel 14 instant signal)

It is obvious that there is a high concentration of AE impulse within loading phase. Since AE signals are detected at discrete points in time, this graph could not show the amount of energy release accurately. To solve this problem, a modified graph is shown in Fig. 4.3.2 by summing up and plotting the AE signal strength in every three seconds (dt=3s). An obvious energy release phenomenon is observed in loading phase. The occurrence of peak values of signal strength are always accompanied with a significant drop of slope in loading curve, which represents the generation of a crack. On the other hand, however, energy release phenomenon is also observed at the end of unloading phase, which is suspected to be induced by crack closing or friction. Energy induced by these kinds of mechanisms should not be accounted into the amount of energy release in crack opening. Therefore, the time period of CSS is strictly limited within the loading phase where the first crack occurs and grow to full length. In addition, noises introduced by other mechanisms such as rubbing of crack surfaces during crack closure, debonding of the reinforcing steel from the surrounding concrete, and environmental noises should always be avoided. Unloading where other mechanisms would be dominant are excluded.

.
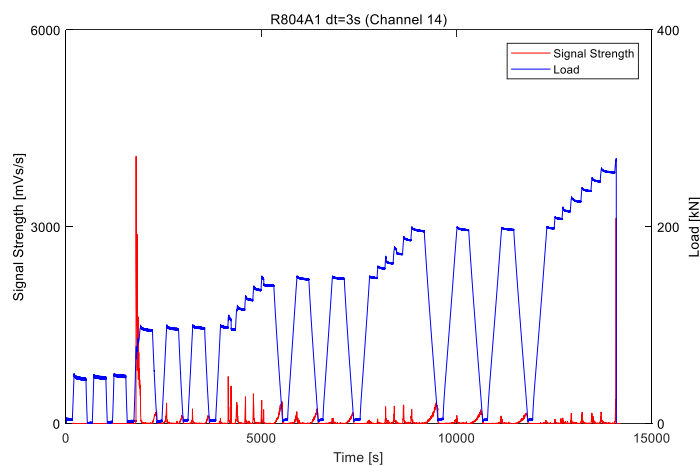
Fig. 4.3.2 Load-time and SS-time curve of R804A1 (Channel 14 dt=3s)

Zooming in to examine loading phase, shown in Fig. 4.3.3, the time period where the first SS peak occurs is taking out individually to account for the amount of energy release in the first main flexural crack. However, an obvious overlap of SS peaks is observed, which means several cracks are growing together and affecting each other in AE signals. This kind of phenomena occurs in several tests because the crack pattern is hard to predict. The solution is to separate each peak in loading history and only the first peak is selected to account for the 1st main flexural crack. By summing up all signal strength in channel 14 from 1773s to 1812s (Fig. 4.3.3), the CSS is 14239 mVs. As a matter of fact, G_0 should be little bit greater than CCS of AE14 since there is an attenuation while the signal wave travels from crack front to the position of AE sensor.
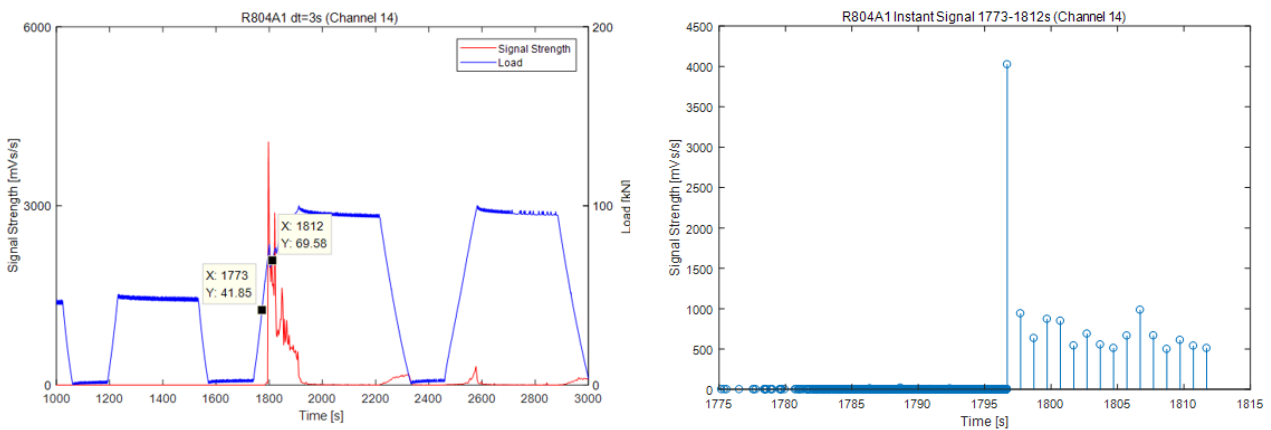
Fig. 4.3.3 1773-1812s R804A1 (Channel14 dt=3s)

CCS of the rest specimens are derived in the same way, results are shown in Table. 2.2.2.1, and dimension and AE sensors layout of each specimen could be found in *Appendix 1*.

Table. 2.2.2.1 CSS of each specimen

Specimen No.	dt=3s plot	Instant signal plot	CSS [mVs]
A602B1			7.3070e+03

A752B1		1.0825e+04
C901A1		361.2496
C901B1		129.5784
R501B1		1.2728e+04

R801B1		2.8377e+04
P804A1		2.2468e+03
P804B1		4.0888e+03
R803A1		8.8936e+03

R803B1			4.4859e+03
R804A1			1.4239e+04
R804B1			5.4286e+03
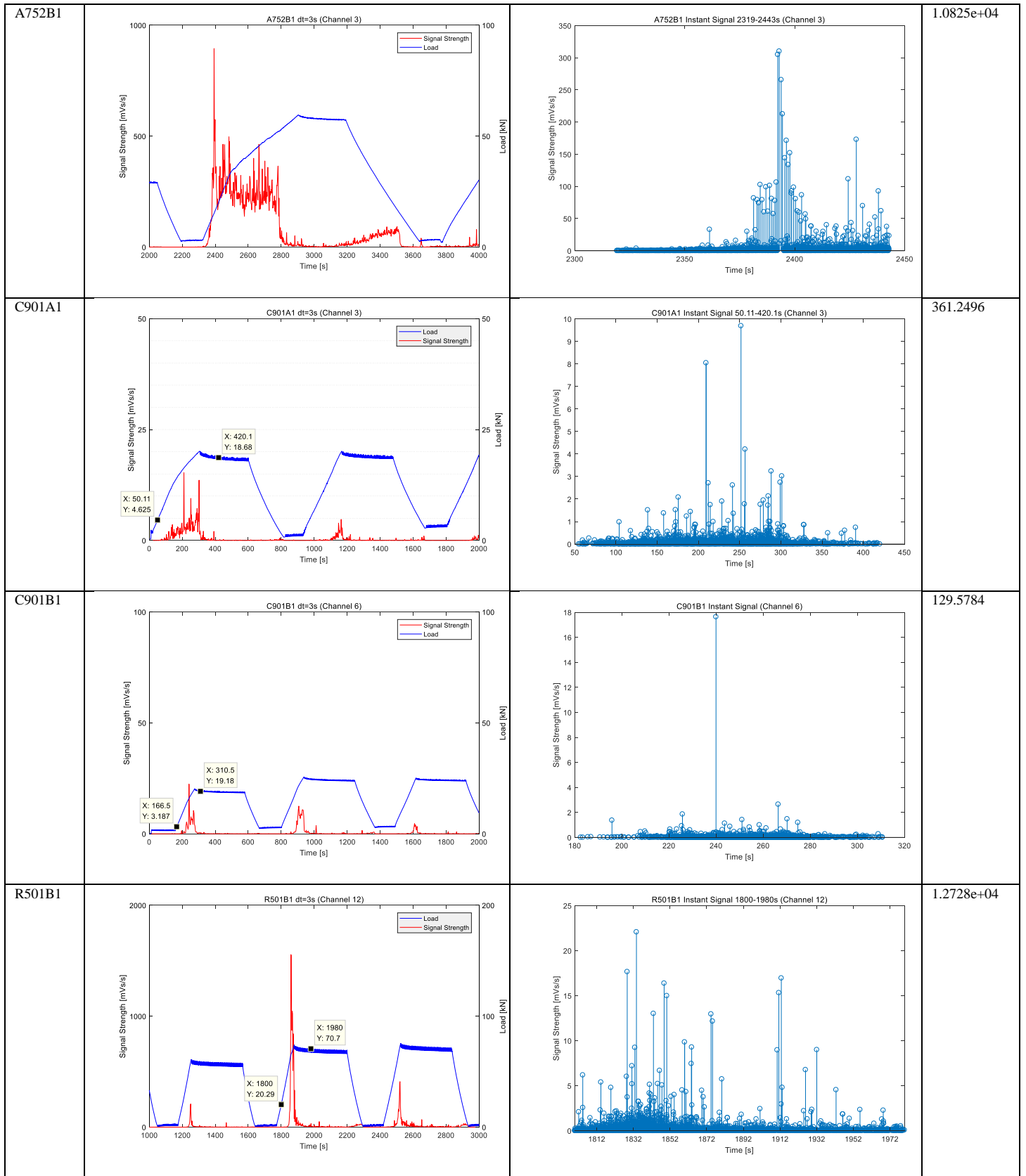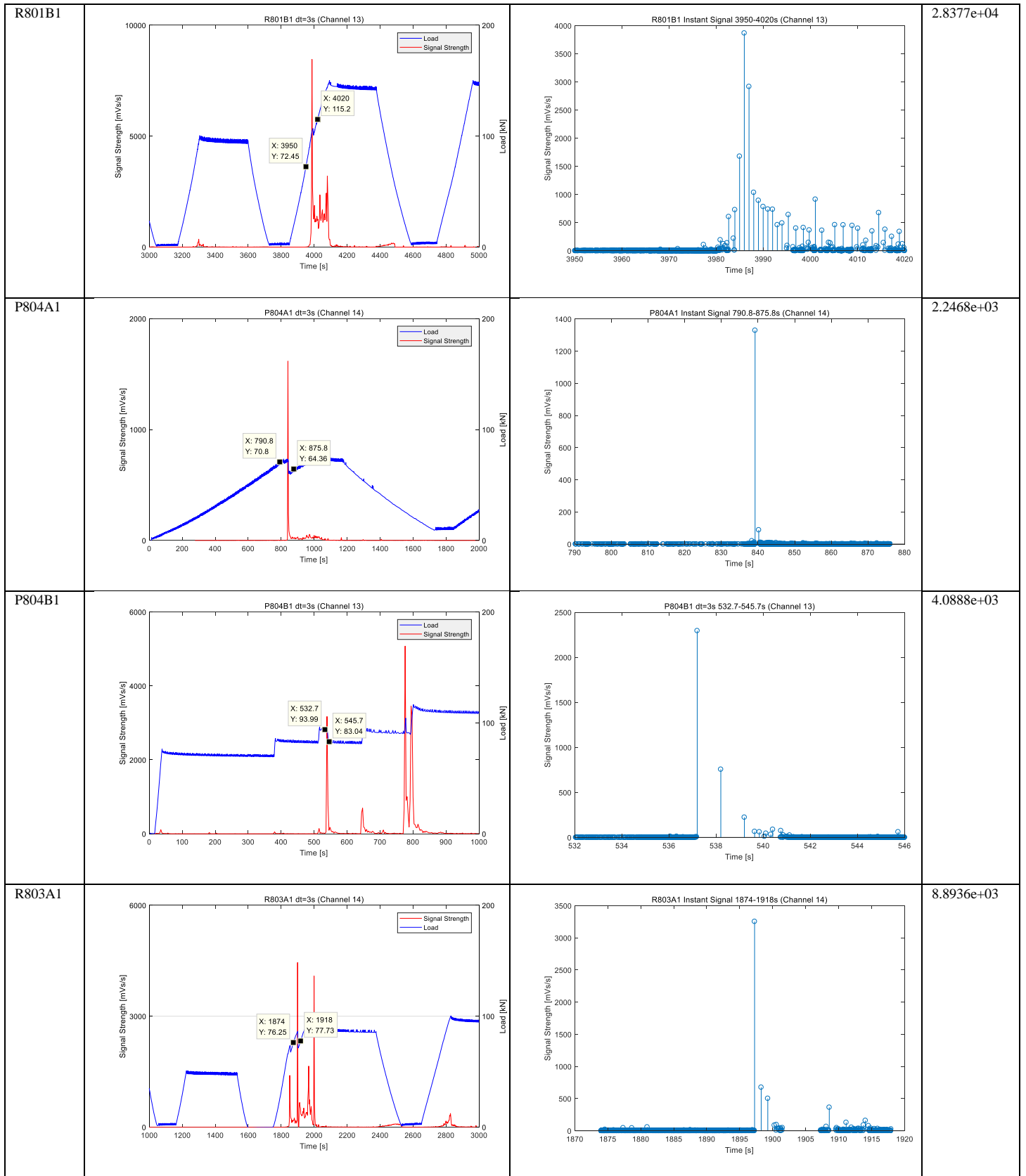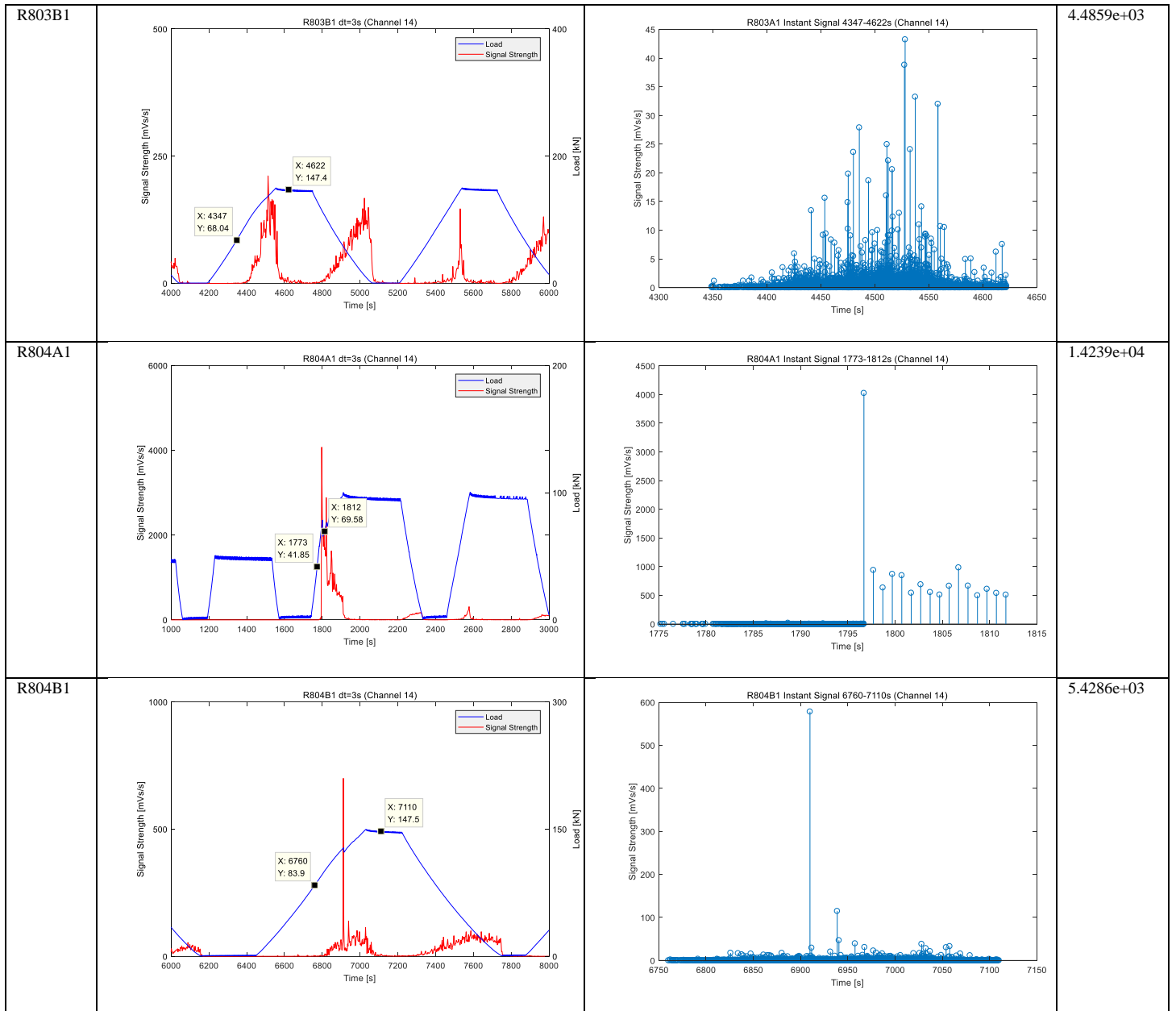
5   CSS in a row of AE sensors

Due to the porosity of the concrete matrix, strength of signal waves will attenuate while travelling in concrete matrix. The phenomena of attenuation is concluded in this chapter by comparing cumulative signal strength (CSS) of different AE sensors in a row as a function of distance from AE source. Longitudinal LVDT sensors are installed in 500 mm and 800 mm beams as well to monitor the crack opening. A-series of tests are primarily investigated due to the integrity of specimens that there are no cracks in the concrete beam before load is applied. However, in B-series the attenuation could be affected by the existing cracks due to previous tests, the signals detected by sensors to the right of the newly generated cracks are selected. Result of test R804A1 is selected as an example.

5.1   Theoretical results

As mentioned before, horizontal distance between AE sensor and crack is an important factor affecting CSS detected by a single sensor. In this chapter, CSS of several sensors installed in the same row with different horizontal distance are compared to each other to find attenuation (Fig. 5.1.1).
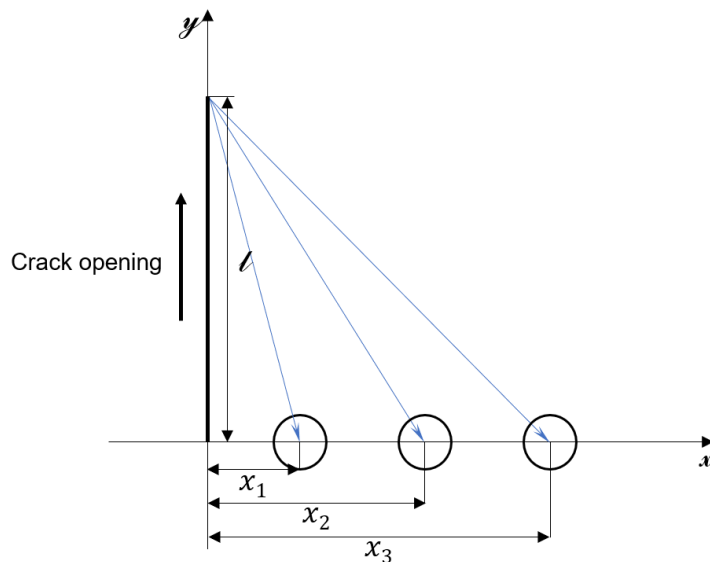
Fig. 5.1.1 Simplified model of horizontal distance model

CSS of different sensors in a row are plotted against distance in Fig. 5.1.2. A significant attenuation of CSS is observed as horizontal distance between AE sensors and crack increases. CSS drops rapidly at the beginning, and while the horizontal distance is big enough, almost no signal would be detected by AE sensor. The phenomena unambiguously illustrate that as the horizontal distance increases, crack length is no longer the dominant factor affecting CSS, since the vertical length of crack is negligible comparing with horizontal distance.
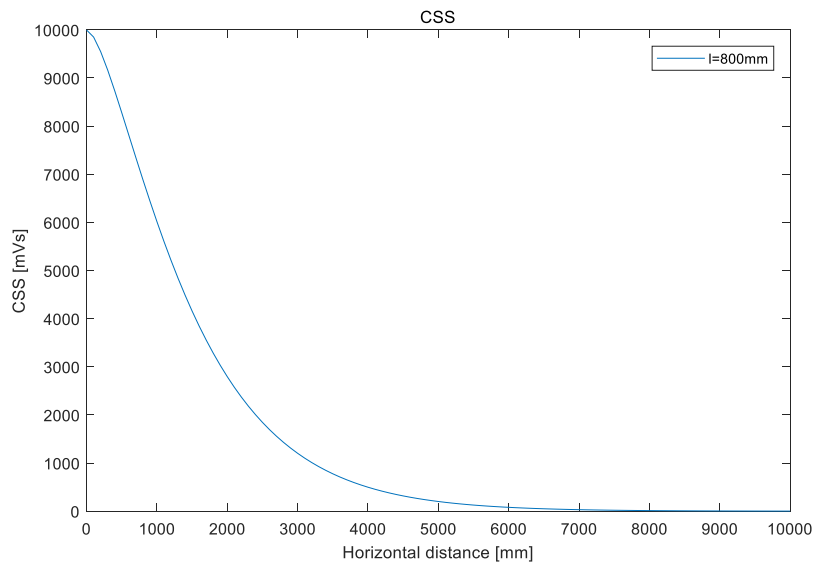
Fig. 5.1.2 CSS of different sensors versus Horizontal distance

The results of A-series tests are expected to be more accurate science the effect of existing cracks could be avoided. Energy released by the first main flexural crack in A-series are investigated here to find the attenuation.

Crack length may also affect the attenuation. Setting crack length l=800, 500, 300, 200 and 100mm respectively (Fig. 5.1.3). While the crack length decreases to 1/8 of initial length, approximately only 40% percent energy is detected. In horizontal direction, a quite clear attenuation is observed in each crack length. After the horizontal distance increasing to approximately 6000mm, CSS of each case almost decrease to zero.
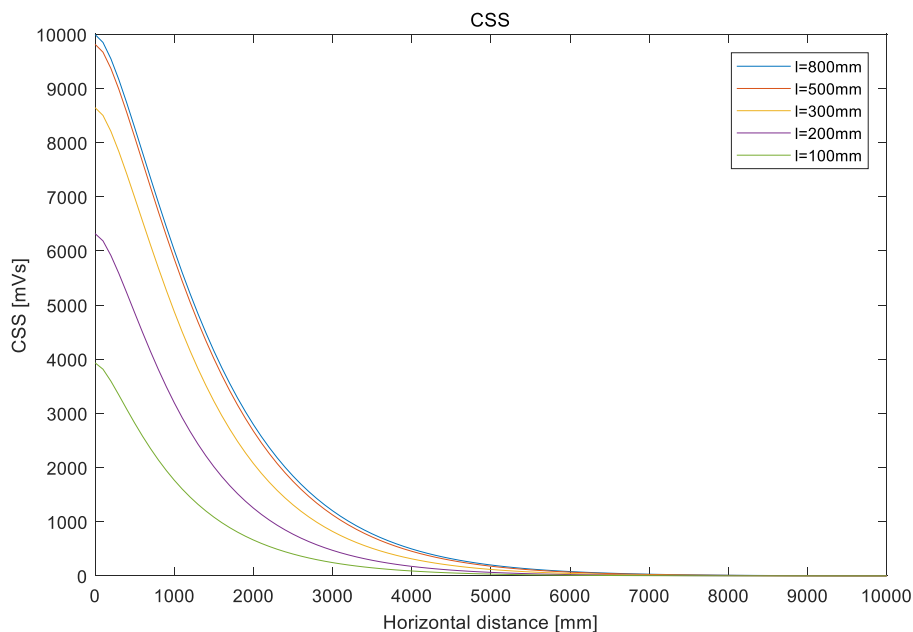
Fig. 5.1.3 CSS versus Horizontal distance (different crack length)

Based on theoretical analysis, both crack length and horizontal may affect the CSS. While the horizontal distance is big enough, crack length is no longer the dominant factor affecting CSS, since the vertical length of crack is negligible comparing with horizontal distance. In reality, attenuation could be affected by multiple mechanisms.

5.2 Experimental results

Experimental results are divided into two parts, according to whether there are any existing cracks in the specimen. Attenuation without cracks and attenuation with cracks are investigated separately in this chapter.

5.2.1 Attenuation without cracks

Attenuation without cracks is investigated mainly in A-series of tests due to there's no existing cracks in specimens. The first main flexural crack is selected as source of energy release. However, in B-series tests, existing cracks caused by previous tests may affect signals detected by sensors. Therefore, the first crack to the right of loading point is selected as energy source to get rid of those effects.

In test R804A1, for instance, AE signals detected by sensors 14, 13, 12 and 11 are plotted against time in the same graph as shown in Fig. 5.2.1(time period 1600-250s). It is quite clear that there is no distinct time delay of peak values in different channels, only the peak signal strength of each channel varies. Several cracks propagate almost together according to this graph, which is quite hard to distinguish.
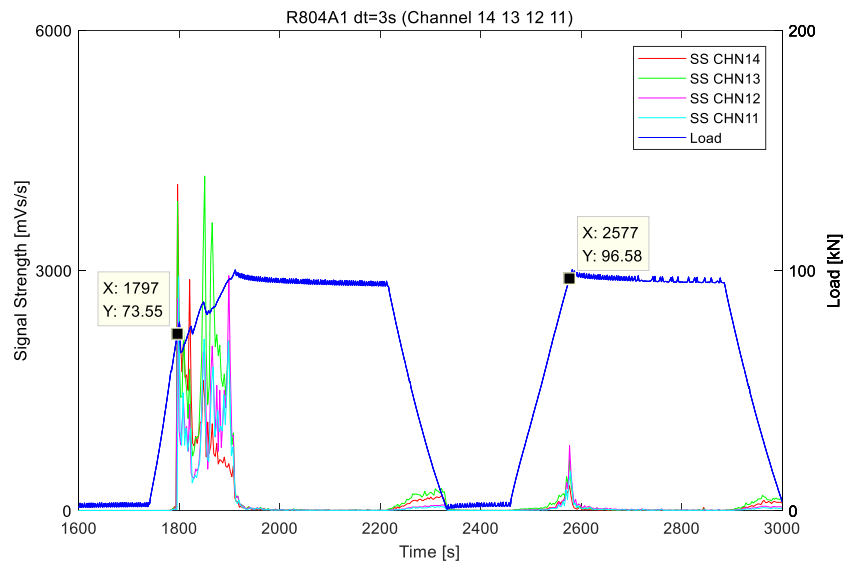
Fig. 5.2.1 Load and Signal strength against Time (R804A1)
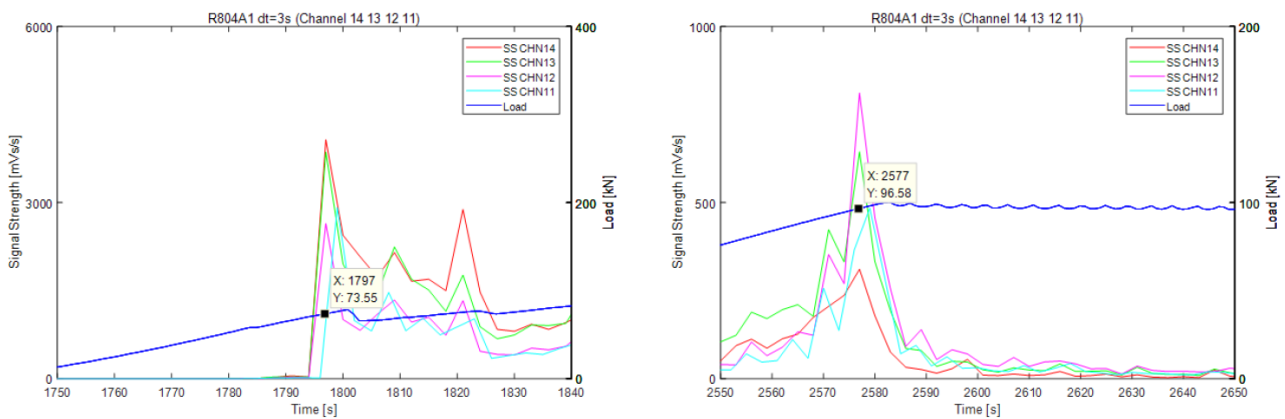
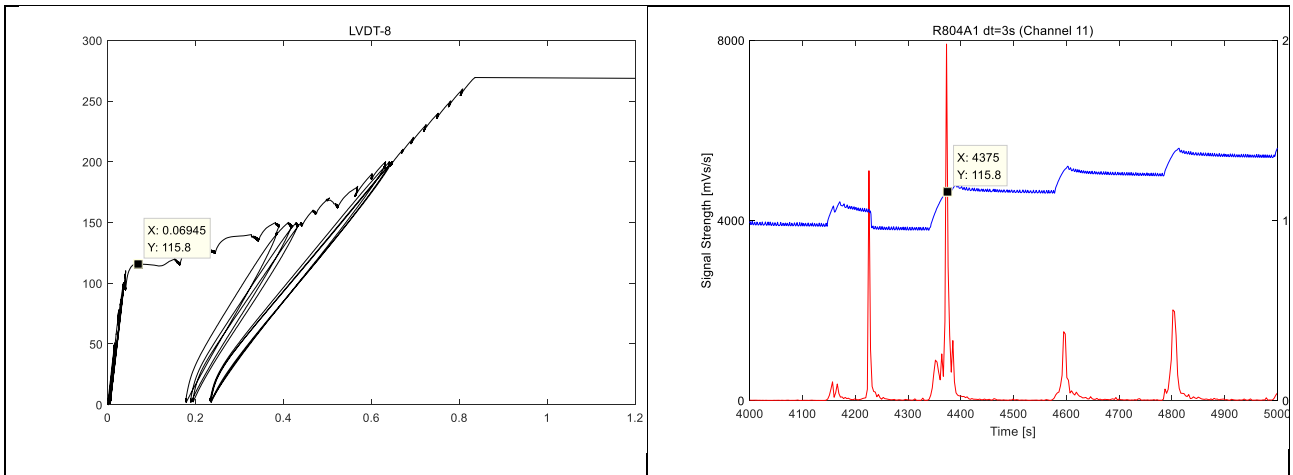**Fig. 5.2.2 Load and signal strength against time (R804A1)**

Zooming in the first peak at 73.55kN load level (signal strength at period 1750-1840s), Signal strength detected by AE14 is the highest, and the attenuation is quite clear. According to LVDT measurements, the highest signal strength at 73.55kN load level is due to energy release of the crack within the area where LVDT5 is measuring, or where AE14 is the closest to the crack (the first main flexural crack). Signal strength of AE13, 12 attenuates as the horizontal distance increases. A little delay is observed in channel 11, since the horizontal distance is much greater comparing to other sensors. However, signal strength of AE11 is little bit higher than that in AE12, which may be affected by other cracks on the bottom surface. Zooming in the second peak at 96.58kN level (Fig. 5.2.2), the highest signal strength is corresponding to the crack measured by LVDT7, where AE12 is governing. Therefore, signal strength of channel 12 is the highest.

With respect to AE grid of specimen, the closer the distance between sensor and crack, the higher the energy detected by sensor. Therefore, the AE signal strength detected by different sensors varies with the location of sensors, and attenuation of CSS in different AE sensors could be expressed as a function of distance between crack and sensor.

LVDT measurements are introduced as well to locate the cracks, and load-crack width figures of each LVDT shown in Table. 4.2.1.1. The first crack opening is represented by an obvious drop in slope, which means a sudden growth in crack width while the load remains same level. According to Table. 4.2.1.1, the first crack occurs at 66.66kN load level and is and is detected by LVDT5, where AE13 is governing. Then with respect to load-time curve (Fig. 5.2.3), the first flexural crack occurs at load step 2.

Table. 5.2.1.1 LVDT plot and corresponding AE plot (R804A1 uncracked)

LVDT-5	AE-14
LVDT-6	AE-13
LVDT-7	AE-12
LVDT-8	AE-11
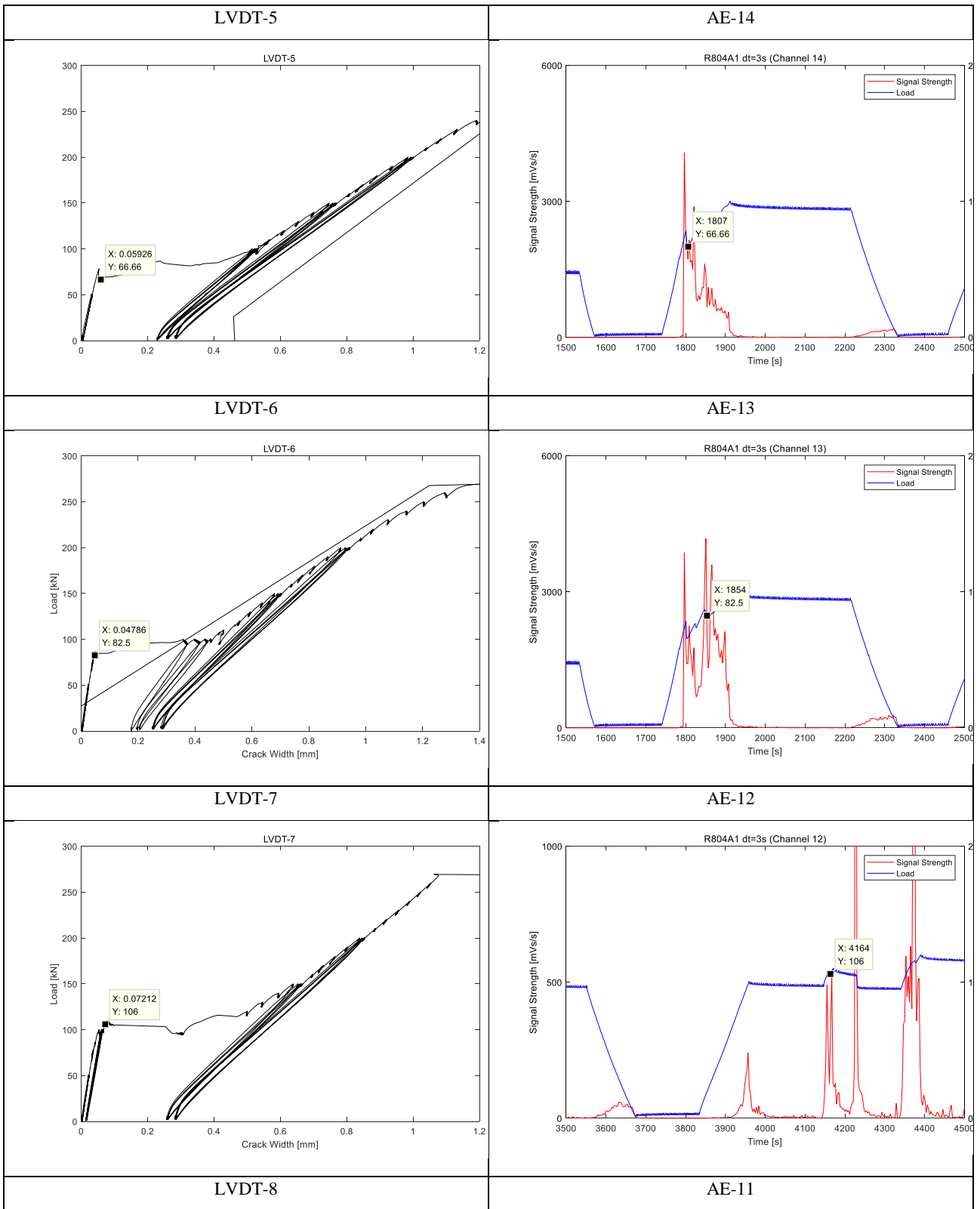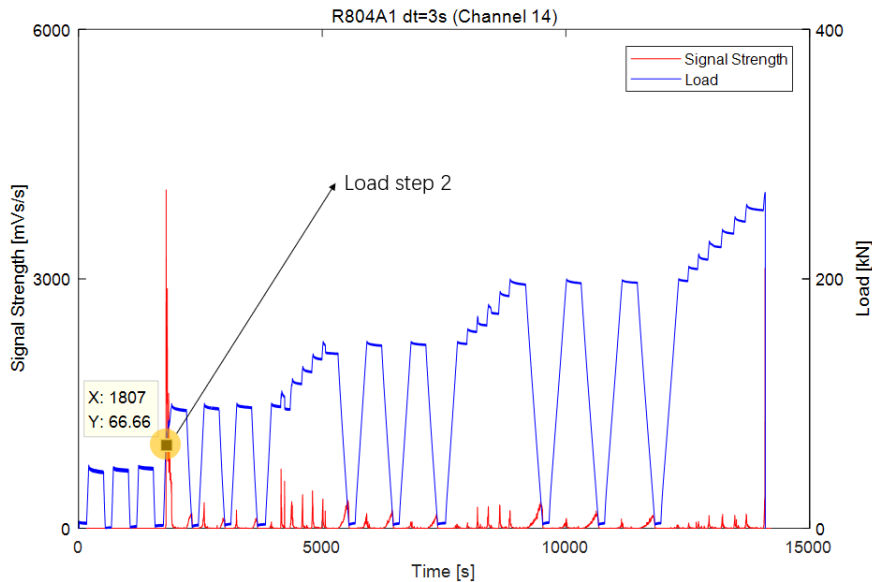
Fig. 5.2.3 Load and Signal strength against Time (R804A1 CHN14)

The crack pattern at the end of each load step is recorded by camera, and crack path generated specifically within the load step 2 is sketched as shown in Fig. 5.2.4. The distance between crack and load position could be derived according to ratio between beam height measured in sketch and that in reality. Here the horizontal distance between crack and loading point is $\frac{291.99*800}{1448.62} =$ 161.25mm. Then horizontal distances between crack and each sensor could be derived as well. Finally, attenuation of CCS which are divided into three layers could be given as a function of distance between crack and AE sensor.

Crack pattern of load step 2 of R804A1 is given in Fig. 5.2.4, the 1st main flexural crack is located to the left of loading point, which it is not detected by LVDT6. According to Fig. 5.2.5, energy release of the first crack is in the time-period 1773-1812s, and CCS within this period detected by each sensor is given in Table. 5.2.1.2.
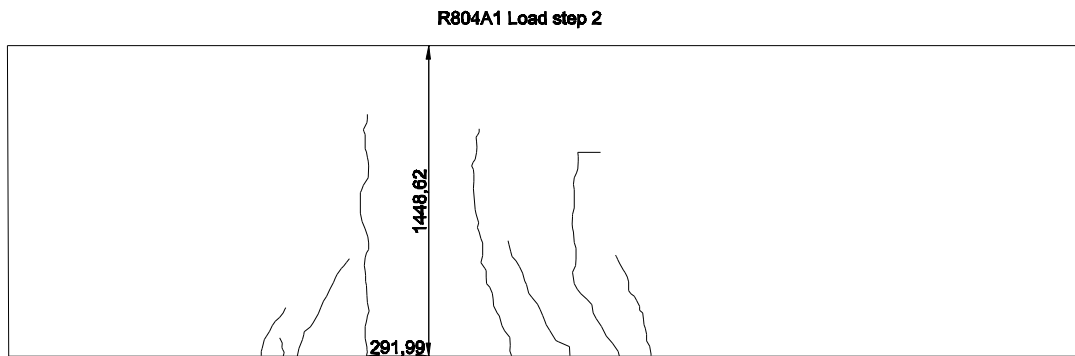
Fig. 5.2.4 Crack pattern of R804A1 load step 2
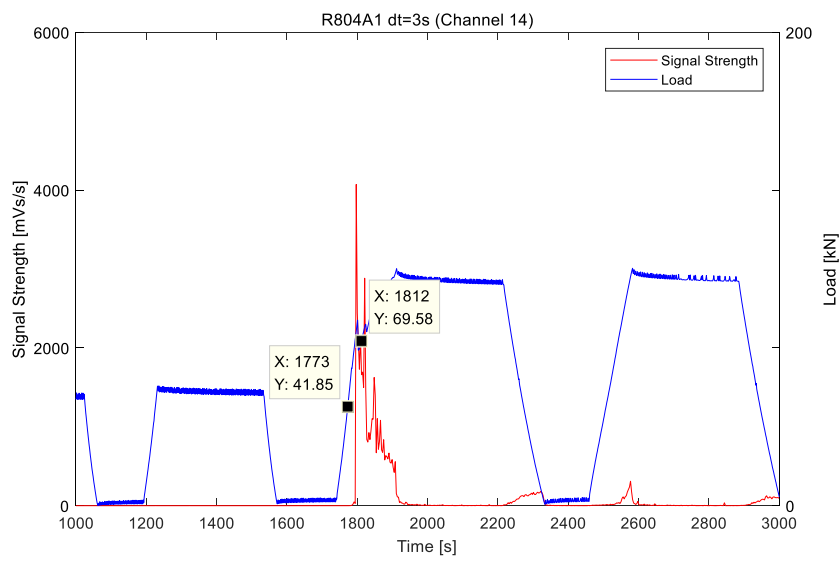
Fig. 5.2.5 SS-time curve of R804A1

Table. 5.2.1.2 CCS of each sensor (R804A1 1773-1812s)

	1773-1812s	Distance [mm]
Channel 1	5.0044e+03	1803.88
Channel 2	6.2128e+03	1303.88
Channel 3	5.9188e+03	803.88
Channel 4	6.7311e+03	303.88
Channel 5	1.2017e+04	-196.12
Channel 6	4.1987e+03	1553.88
Channel 7	4.3900e+03	1053.88
Channel 8	8.1120e+03	553.88
Channel 9	9.4139e+03	53.88
Channel 10	1.0073e+04	-446.12

Channel 11	3.6700e+03	1803.88
Channel 12	4.9490e+03	1303.88
Channel 13	7.4231e+03	803.88
Channel 14	8.8936e+03	303.88

According to AE grid, sensors are divided into three layers, and attenuation of each AE row could be investigated. CCS against time is plotted in Fig. 5.2.6 in three groups. An obvious attenuation is observed in each layer as horizontal distance increases.
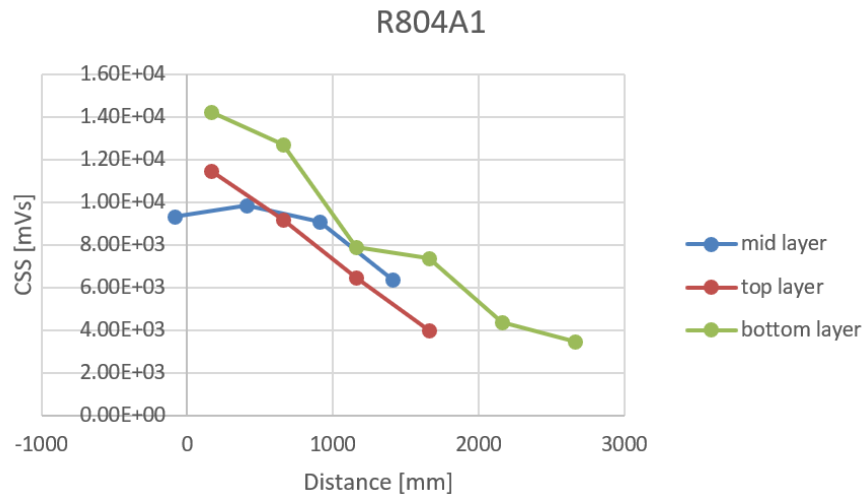
Fig. 5.2.6 CCS-Distance R804A1 (uncracked)

Results of other tests could be found in *Appendix 2*.

The feature of CSS curve could be expressed by two important indicators, namely G_0 and attenuation. G_0 reflects the total amount of energy release in a specific crack, and attenuation shows the amount of energy dissipated before being detected by a sensor. The CSS detected by AE sensors could be affected by several kinds of factors, such as existing cracks, newly generated cracks, propagating distance and top surface reflection etc.

CSS are plotted in three layers against distance since different factors would be dominant, as shown in Fig. 5.2.7. The factor G_0 could be estimated by reading the signal strength of AE sensor closest to the crack. According to figures above, G_0 of bottom layer is always higher than mid layer and top layer. The bottom layer AE sensors would be more affected by those newly generated cracks on bottom surface of specimen, which would increase the total amount of energy release, and therefore the CCS of bottom layers are higher. Besides, CSS of top layer is expected to be the lowest since the propagating distance is the longest, however, it's also interesting to find that there is no apparent difference between CSS of mid layer and top layer. It is suspected that the reflection of AE signals from top surface of specimen may affect the signal strength of top layer.
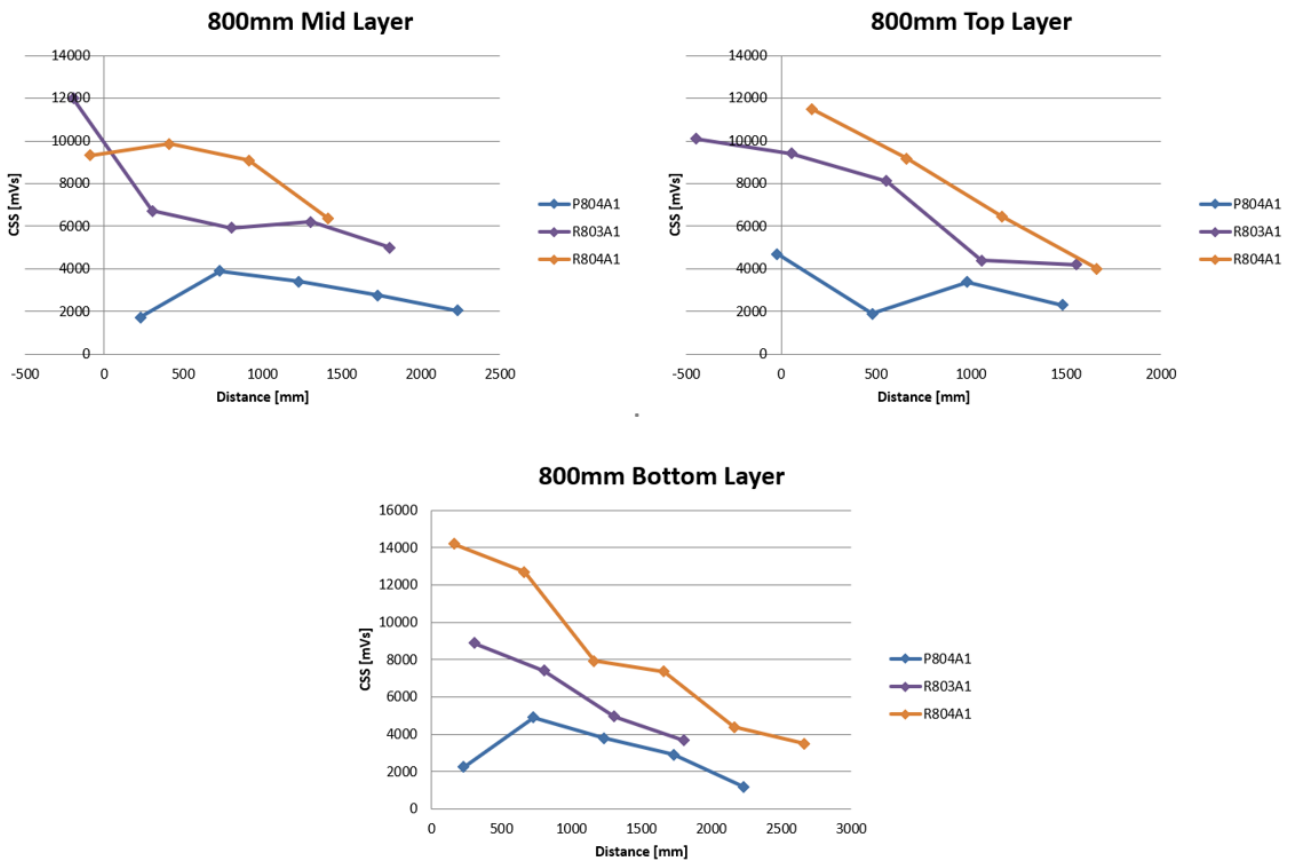
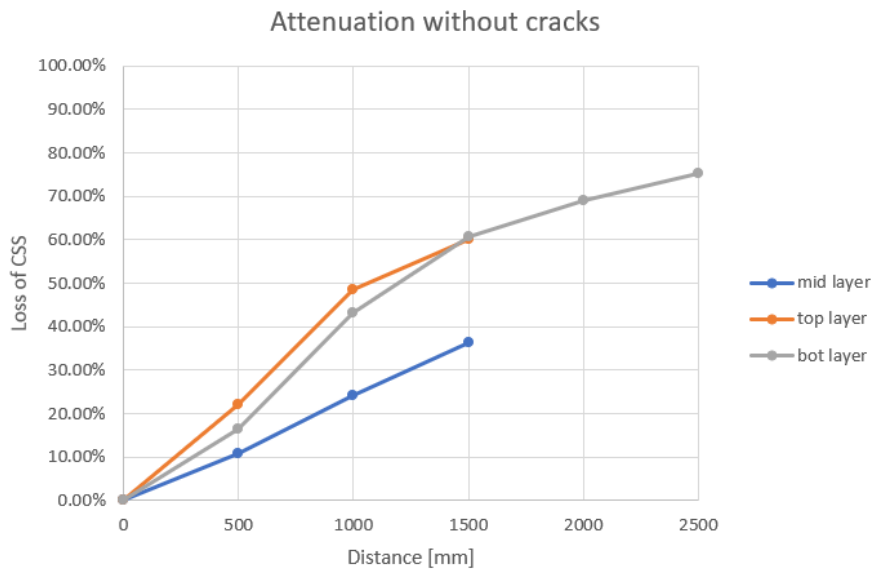**Fig. 5.2.7 CSS of 800 mm beam in different layers (uncracked)**

Averaged attenuation of 800mm beams of different layers are plotted in Fig. 5.2.8.
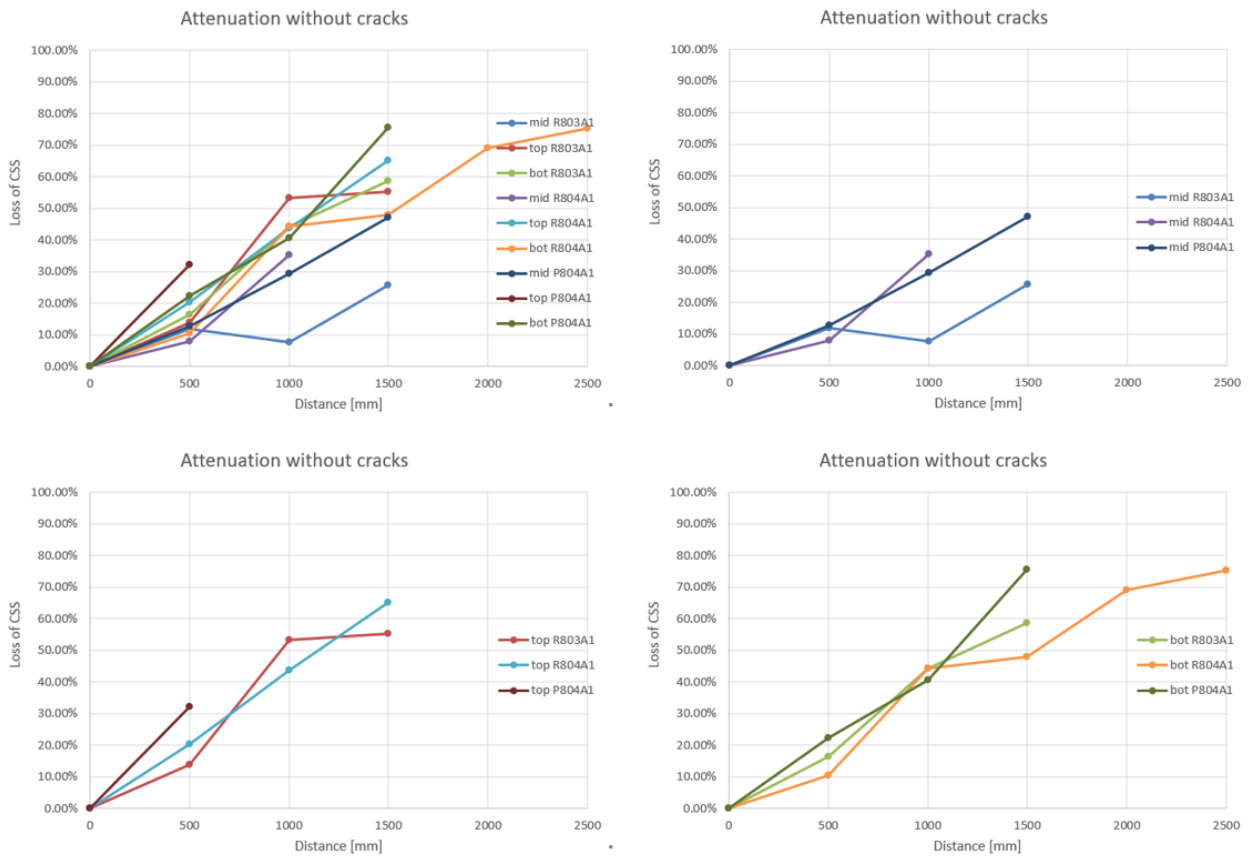
Fig. 5.2.8 Attenuation of 800 mm beam in different layers (uncracked)

An averaged attenuation curve of three layers is derived in Fig. 5.2.9. Standard deviation and coefficient of variation are given in Fig. 5.2.10 to quantify the amount of variation or dispersion.

It's obvious in the figure that attenuation of top layer and bottom layer are higher than mid layer. However, this might be caused by different mechanisms. In bottom surface of specimen, there are many existing and newly generated cracks which would increase energy dissipation, and therefore the attenuation in bottom layer would be higher. As for top layer, the propagating distance would be dominating since bottom-initiated cracks have to travel farther to be detected by a top layer sensor than a mid-layer sensor. Finally, it is hard to tell whether the attenuation of top layer or bottom layer is higher since CSS would be affected by many factors and data derived from tests is limited.

Fig. 5.2.9 Averaged attenuation of 800 mm beam in different layers (uncracked)
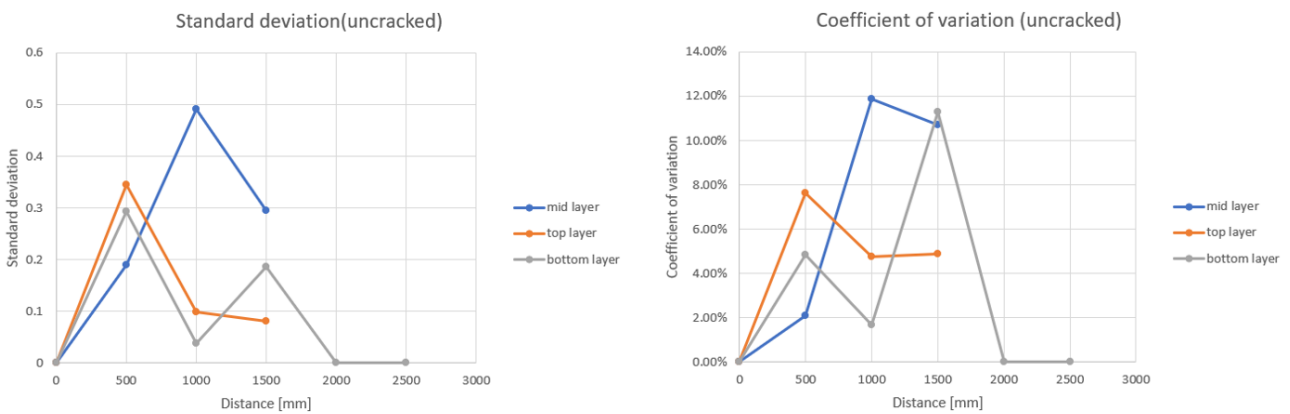
Fig. 5.2.10 Standard deviation and Coefficient of variation (uncracked)

An exponential curve fitting is carried out here to determine the attenuation curve and try to look for real G_0. The AE sensor closest to the crack in horizontal direction is selected as the fictitious source, then by checking the CSS of other sensors in the same layer a formula of attenuation could be derived through exponential curve fitting. Real G_0 could be derived as well by substituting distance between real source and fictitious source into the formula. For instance, test R804A1, attenuation from fictitious source and real source are given in Table. 5.2.1.3 and Table. 5.2.1.4 respectively.

Table. 5.2.1.3 Attenuation from fictitious source

Horizontal distance x [mm]	0	500	1000	1500
Loss of CSS	100%	89.08%	75.88%	63.58%

Table. 5.2.1.4 Attenuation from real source

Horizontal distance x [mm]	0	411.25	911.25	1411.25
Loss of CSS	100%	88.53%	76.34%	65.83%
CSS [mVs]		9870	9080	6380
Curve fitting results [mVs]	11149	9870	8511	7339

CSS of each layer could be expressed as a function of distance given in Table. 5.2.1.5. (uncracked structures). Fitting results are shown in

Table. **5.2.1.6** comparing with real results detected by AE sensors.

Table. 5.2.1.5 Formulas derived from curve fitting (uncracked)

Mid layer	$CSS = \exp(-0.0002963x)$
Top layer	$CSS = \exp(-0.0006266x)$
Bottom layer	$CSS = \exp(-0.0005883x)$

Table. 5.2.1.6 Curve fitting vs. CSS(uncracked)

Top layer	R803A1 top layer cracked / R804A1 top layer uncracked / R803A1 top layer uncracked
Bottom layer	R803A1 bottom layer crackerd / R804A1 bottom layer uncracked / R803A1 bot layer uncracked
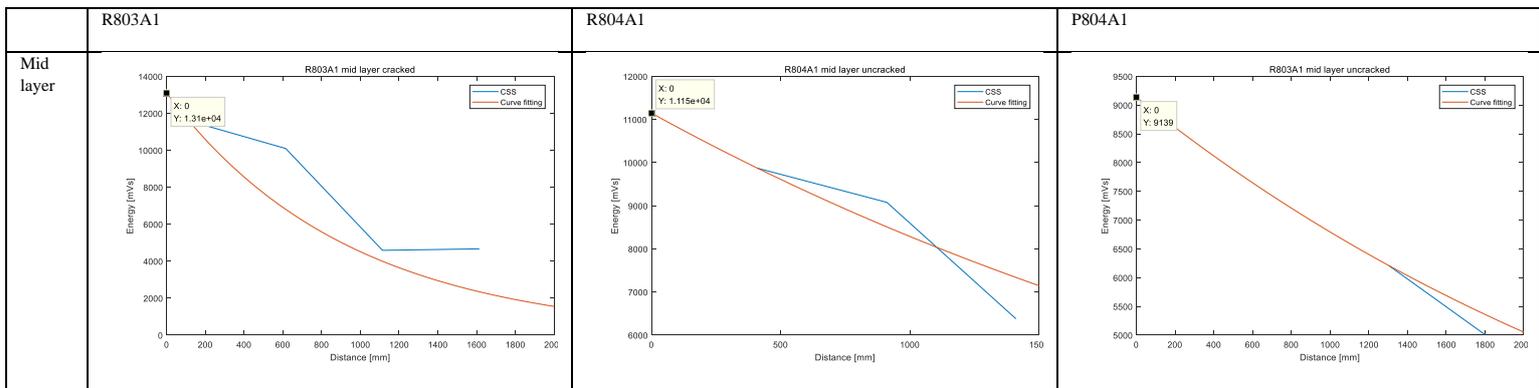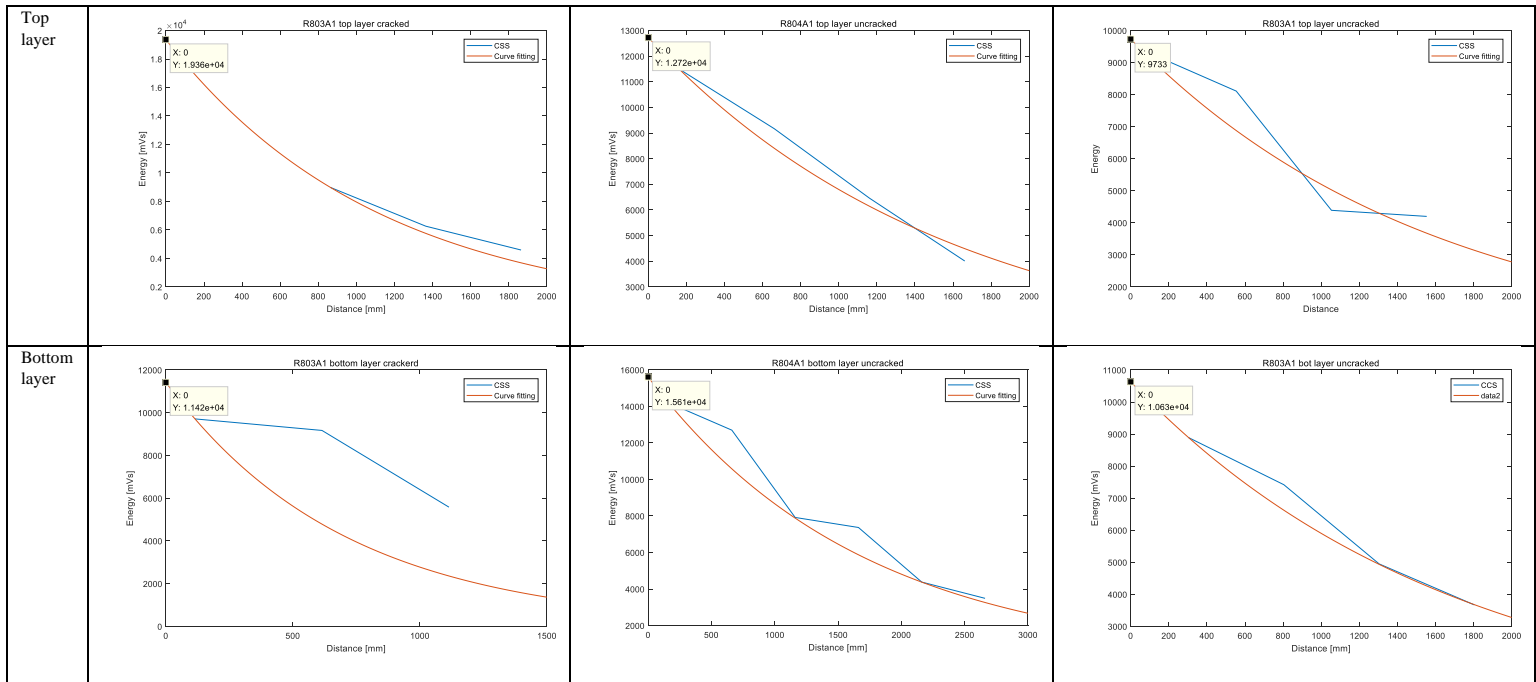
In B-series, to get rid of existing cracks due to previous tests, only cracks to the right of loading point which are newly created are considered. CSS results are shown in Table. 5.2.1.7. Several vertical or diagonal cracks may occur within the selected time period since main flexural cracks are already formed in previous A series tests, which may affect the CSS detected by sensors on the right side. On the other hand, B series are more suitable for the investigation of attenuation with cracks by checking CSS in the cracked zone. The number of longitudinal sensors is limited, and the sensors installed in the uncracked part are not sufficient to find attenuation, as shown in R803B1 and R804B1.

Table. 5.2.1.7 CSS results of B series (uncracked)
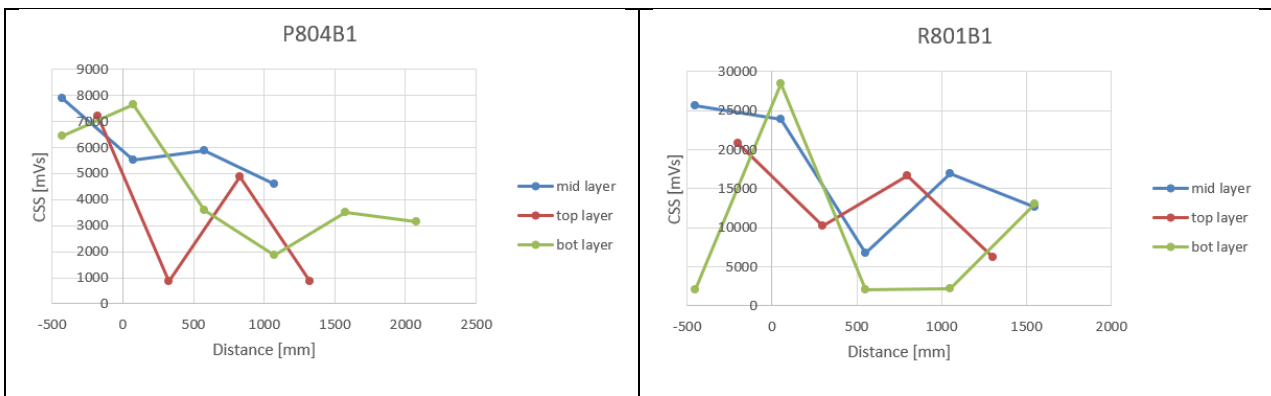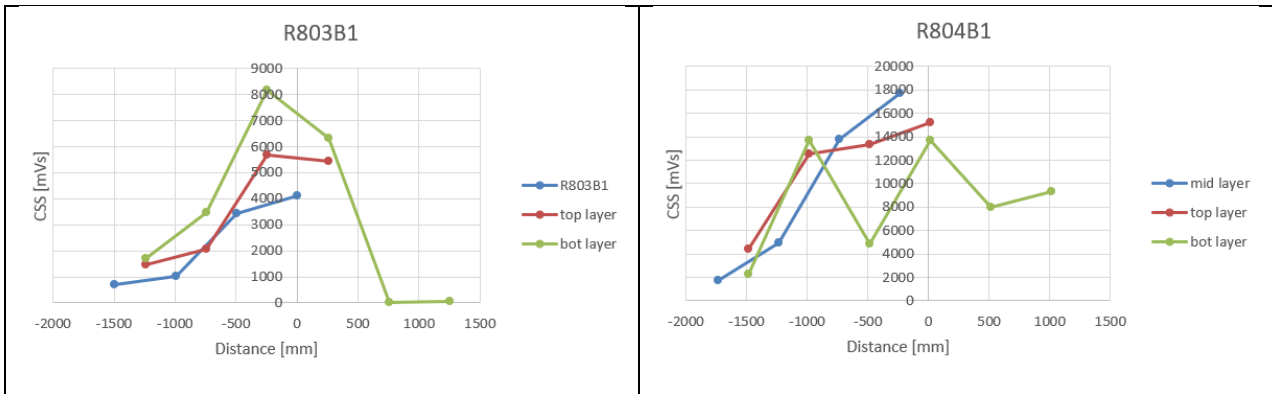
5.2.2   Attenuation with cracks

It is suspected that cracks in concrete structures may result in further decrease of CSS since signals would reflect and dissipate while travelling through crack surface in concrete matrix. Attenuation of CCS in cracked concrete structures is investigated in this chapter.

A crack detected by the LVDT farthest from loading point is selected to make sure that there are sufficient sensors working in the cracked zone. For instance, according to LVDT layout of R804A1 (shown in Fig. 5.2.11), the crack detected by LVDT8 is selected to be investigated. Cracks occurred prior to this one which were detected by LVDTs on left side are regarded as target cracks affecting attenuation of CSS.
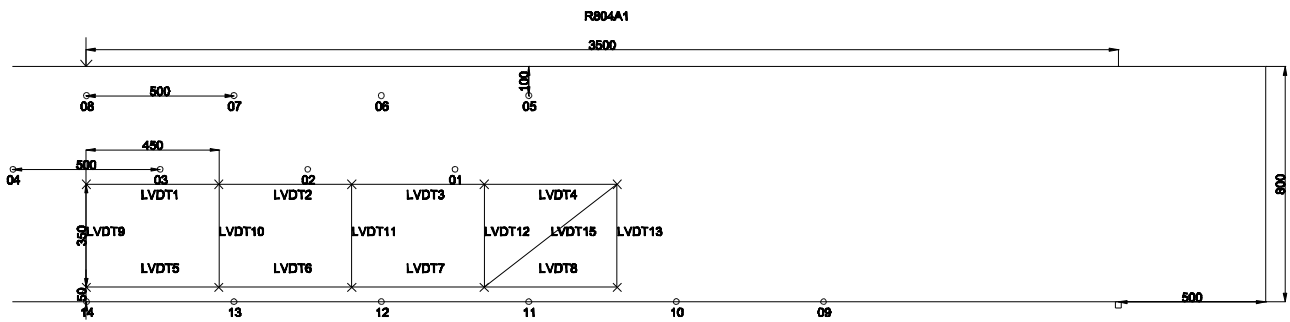
Fig. 5.2.11 LVDT layout of R804A1

Load-displacement curve of LVDT8 and signal strength of AE11 are given in Table. 5.2.2.1. It's obvious that crack detected by LVDT8 occurs at load step 3. Pattern of newly generated cracks within load step 3 is given in Fig. 5.2.12. The distance between crack and load position could be derived according to ratio between beam height measured in sketch and that in reality. Then horizontal distances between crack and each sensor could be derived as well. Here the horizontal distance between crack and loading point is $\frac{2936*800}{1461.38} = 1607.25$mm.

Table. 5.2.2.1 LVDT plot and corresponding AE plot (R804A1 cracked)
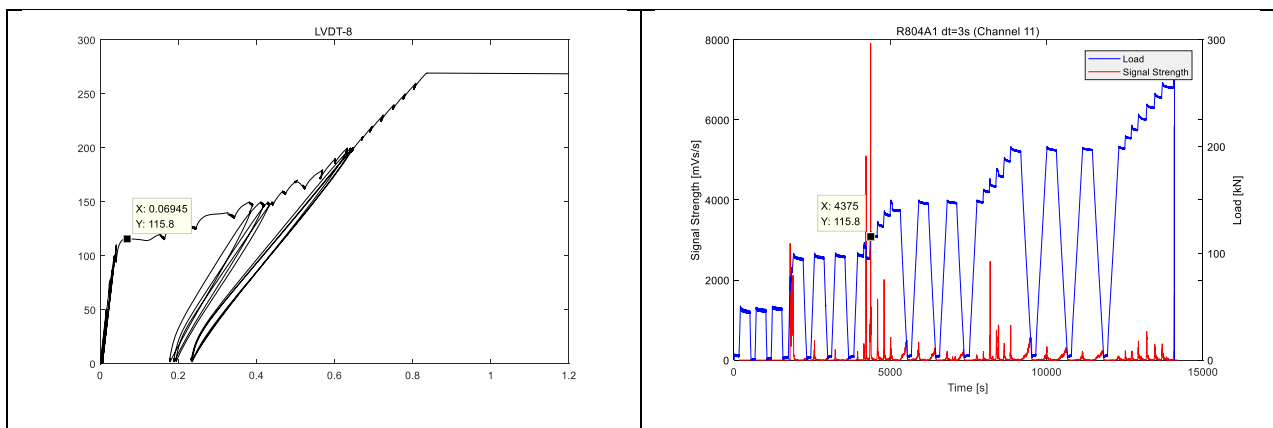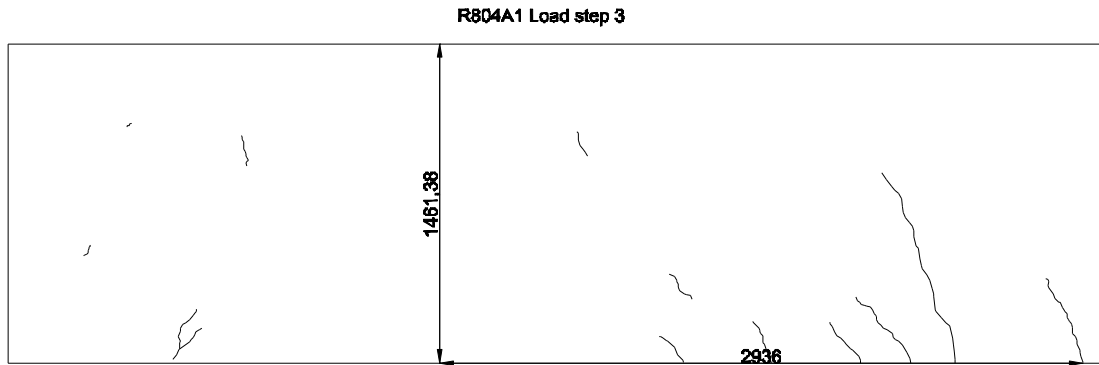
Fig. 5.2.12 Crack pattern of R804A1 load step 3

Zooming in signal strength plot of AE11 (Fig. 5.2.13), peak value of signal strength at load level 115.8kN is in time period 4335-4380s. CSS of other AE sensors within this period is given in Table. 5.2.2.2.
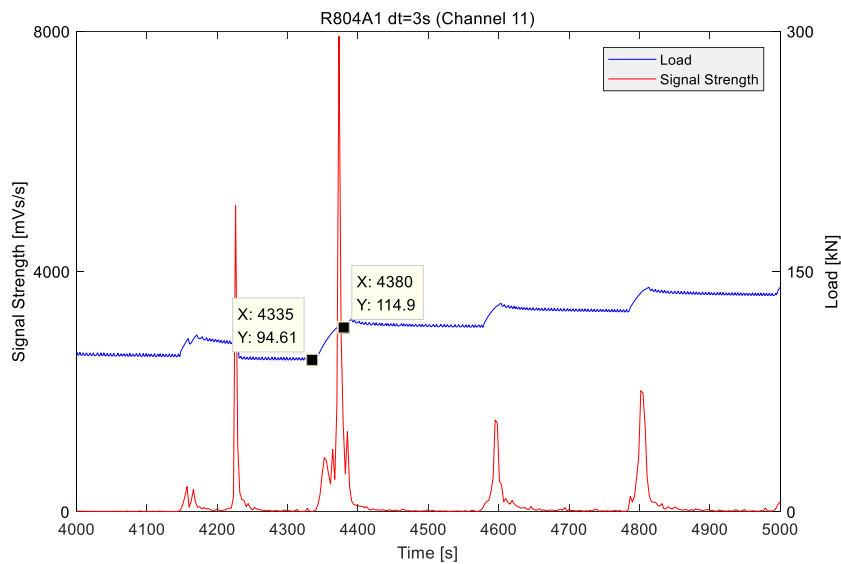

Fig. 5.2.13 Load and Signal strength against Time (R804A1 CHN11)

Table. 5.2.2.2 CCS of each sensor (R804A1 4335-4380s)

	4335-4380s	Distance
Channel 1	1.44E+04	-357.25
Channel 2	1.15E+04	-857.25
Channel 3	5.54E+03	-1357.25
Channel 4	2.43E+03	-1857.25
Channel 5	8.26E+03	-107.25
Channel 6	1.17E+04	-607.25

Channel 7	8.34E+03	-1107.25
Channel 8	5.43E+03	-1607.25
Channel 9	7.41E+03	892.75
Channel 10	9.85E+03	392.75
Channel 11	1.98E+04	-107.25
Channel 12	8.31E+03	-607.25
Channel 13	4.88E+03	-1107.25
Channel 14	1.85E+03	-1607.25

According to AE grid, sensors are divided into three layers, and attenuation of each AE row with cracks could be investigated. CCS against time is plotted in Fig. 5.2.14 in three groups. Attenuation in both cracked and uncracked part are observed in bottom layer as horizontal distance increases. In top and mid layer all AE sensors are installed in cracked part, obvious attenuation is observed as well.

Comparation between attenuation with and without cracks will be discussed in latter chapters. Results of other tests could be found in *Appendix 3*.
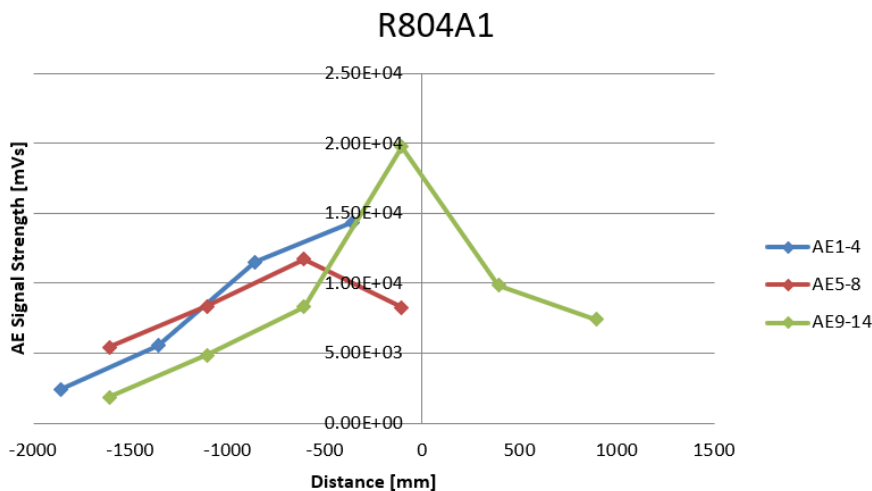
Fig. 5.2.14 CCS-Distance R804A1 (cracked)

CSS are plotted in three layers against distance as shown in Fig. 5.2.15. The factor G_0 could be estimated by reading the signal strength of AE sensor closest to the crack. According to figures, G_0 of bottom layer is higher than mid layer and top layer since bottom layer AE sensors would be more affected by newly generated cracks on bottom surface of specimen. In general, however, the attenuation in cracked concrete structure is not that characteristic since several cracks may propagate simultaneously, as shown in figures that sub-peaks occur at somewhere far away from main crack.
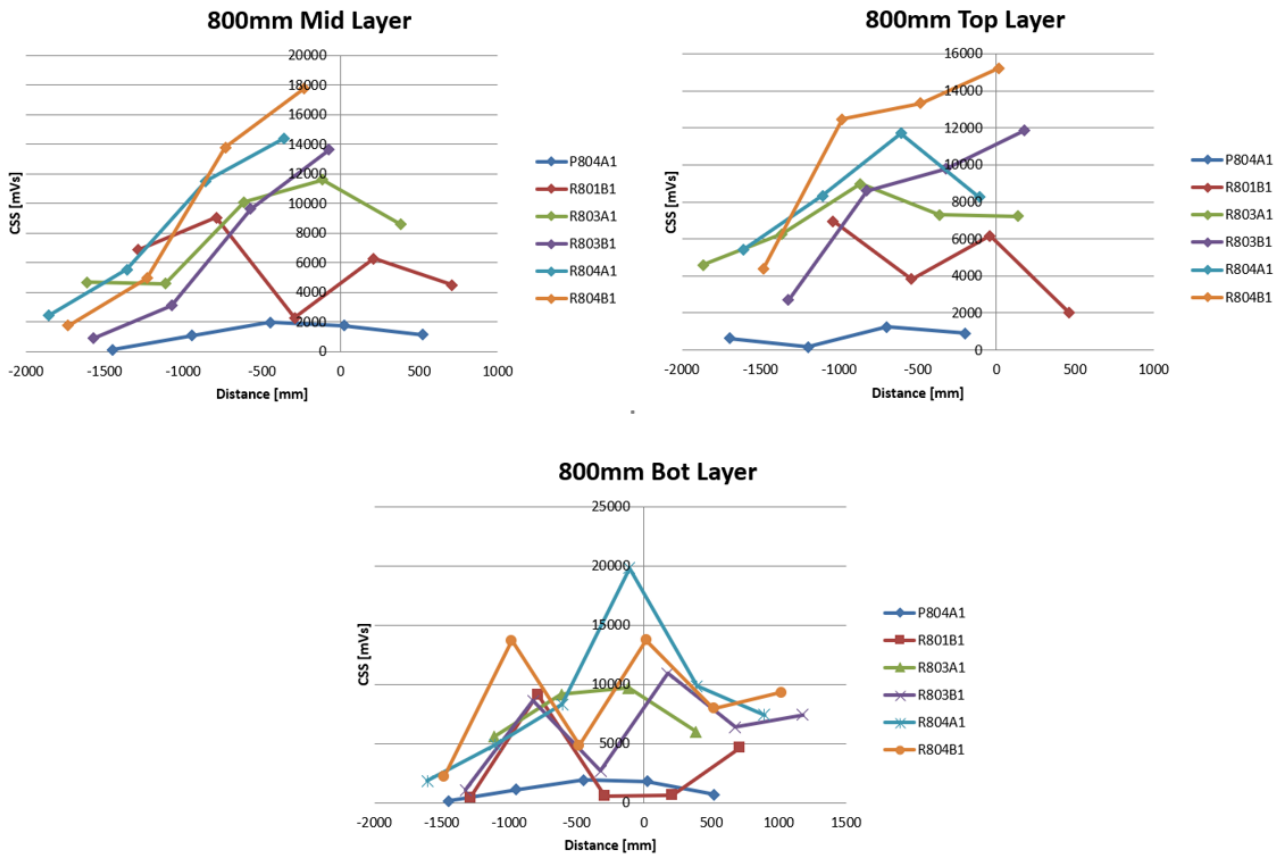
Fig. 5.2.15 CSS of 800 mm beam in different layers (cracked)

The CSS attenuation of cracked structure are divided into three layers, plotted in Fig. 5.2.16. The first sensor to the right of the crack is regarded as fictitious source as mentioned in previous chapter. By doing so, attenuation could be expressed as percentage of loss CSS with respect to the fictitious G_0. Then attenuations of different layers are plotted in Fig. 5.2.16.

The averaged attenuation curve of three layers is given in Fig. 5.2.17. Standard deviation and coefficient of variation are given in Fig. 5.2.18 to quantify the amount of variation or dispersion.

At a horizontal distance from 0 to 500 mm the attenuation trend is the same as that observed in uncracked structures. However, the attenuation in greater distance would be hard to predict since the existing crack would significantly affect CSS detected by sensors, and crack pattern varies with each beam.
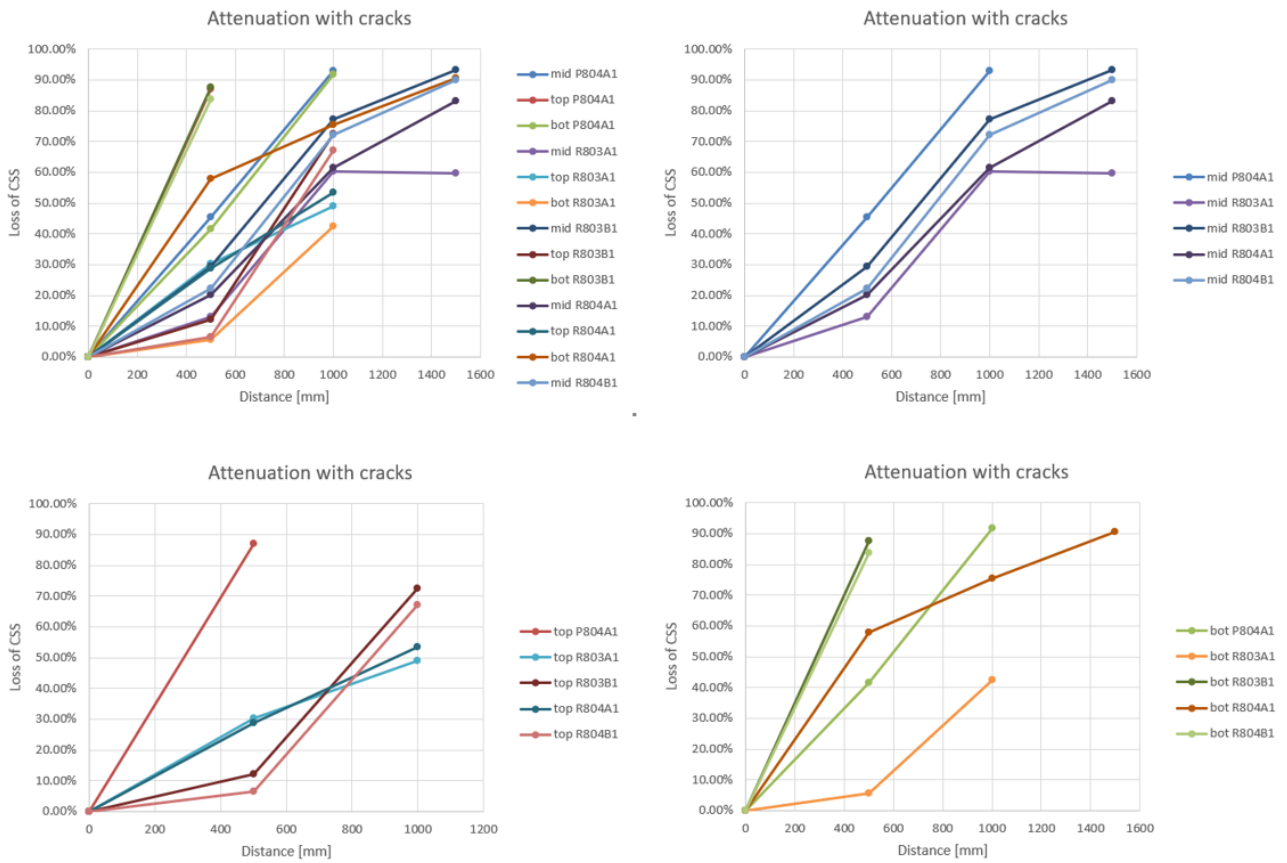
Fig. 5.2.16 Attenuation of 800 mm beam in different layers (cracked)
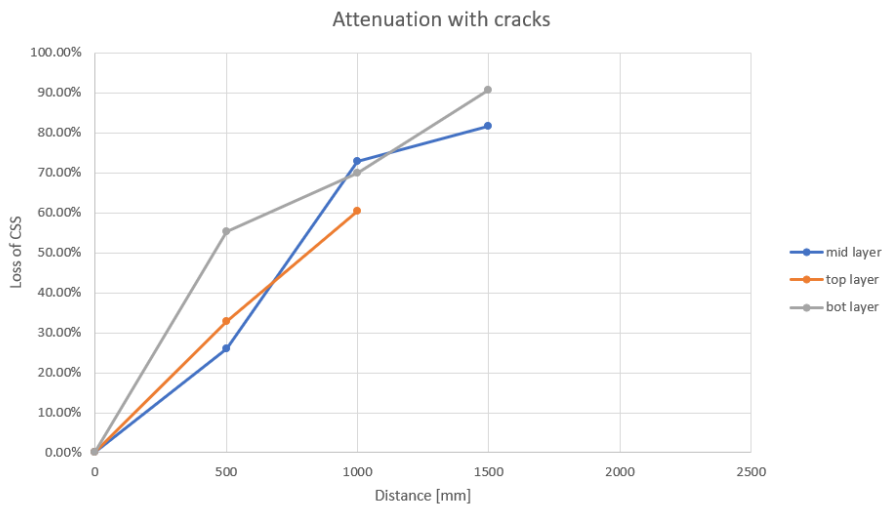
Fig. 5.2.17 Averaged attenuation of 800 mm beam in different layers (cracked)
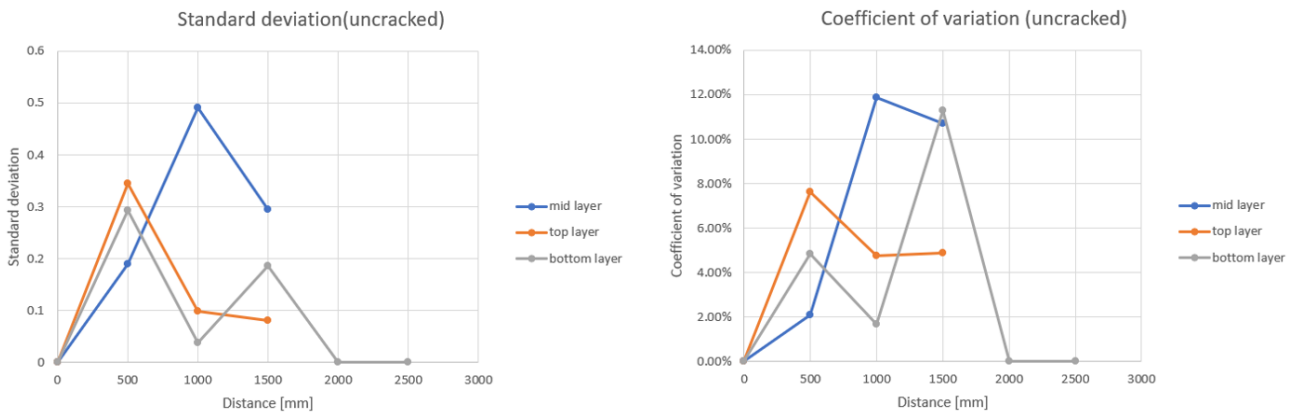
Fig. 5.2.18 Standard deviation and Coefficient of variation (cracked)

Exponential curve fitting is conducted again to determine the attenuation curve and try to look for real G0. CSS of each layer could be expressed as a function of distance given in Table. 5.2.2.3. (cracked structures). Fitting results are shown in
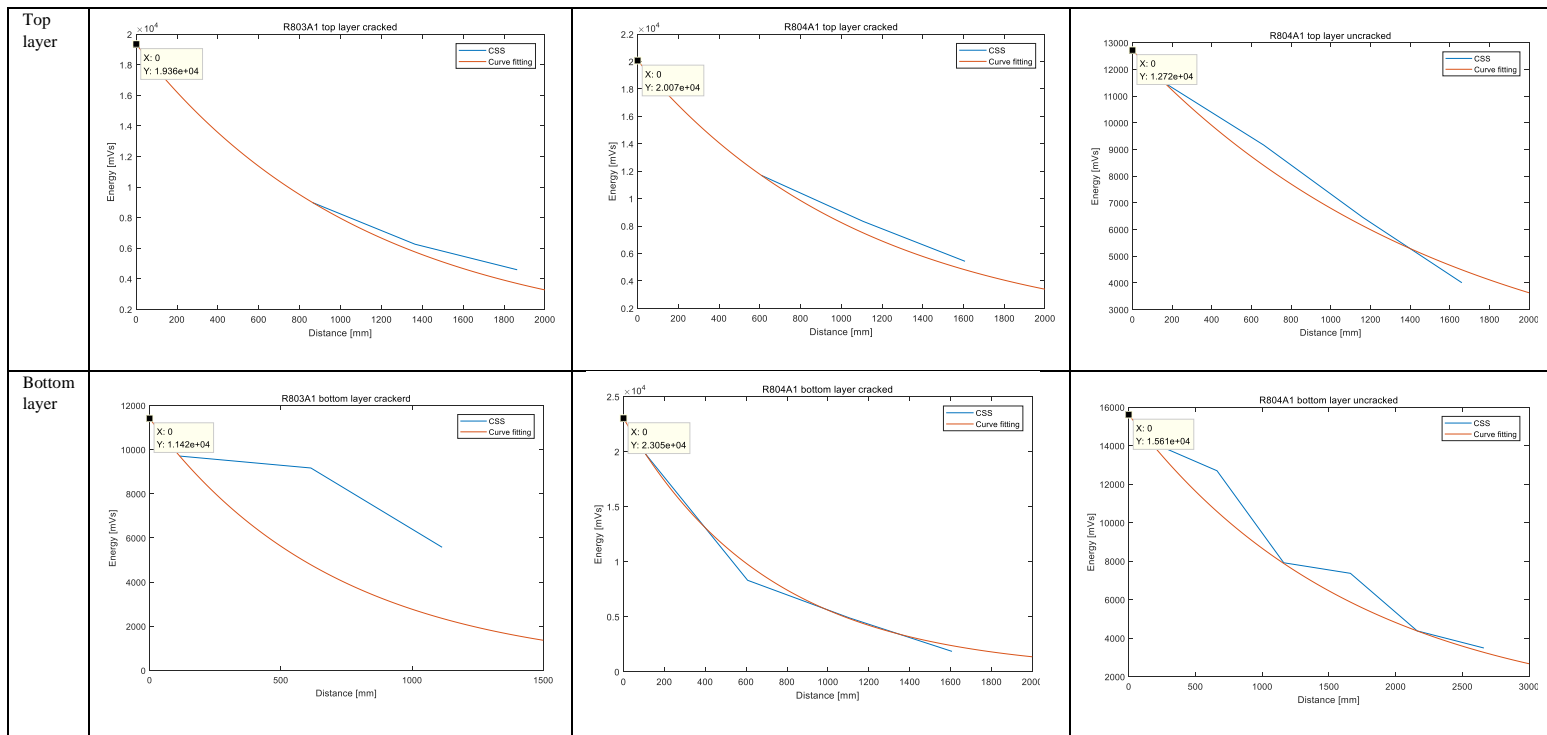
Table. **5.2.2.4** comparing with real results detected by AE sensors.

Table. 5.2.2.3 Formulas derived from curve fitting (cracked)

Mid layer	$CSS = \exp(-0.001065x)$
Top layer	$CSS = \exp(-0.0008888x)$
Bottom layer	$CSS = \exp(-0.001415x)$

Table. 5.2.2.4 Curve fitting VS CSS (cracked)

	R803A1	R804A1	P804A1
Mid layer			

Top layer			

Bottom layer			
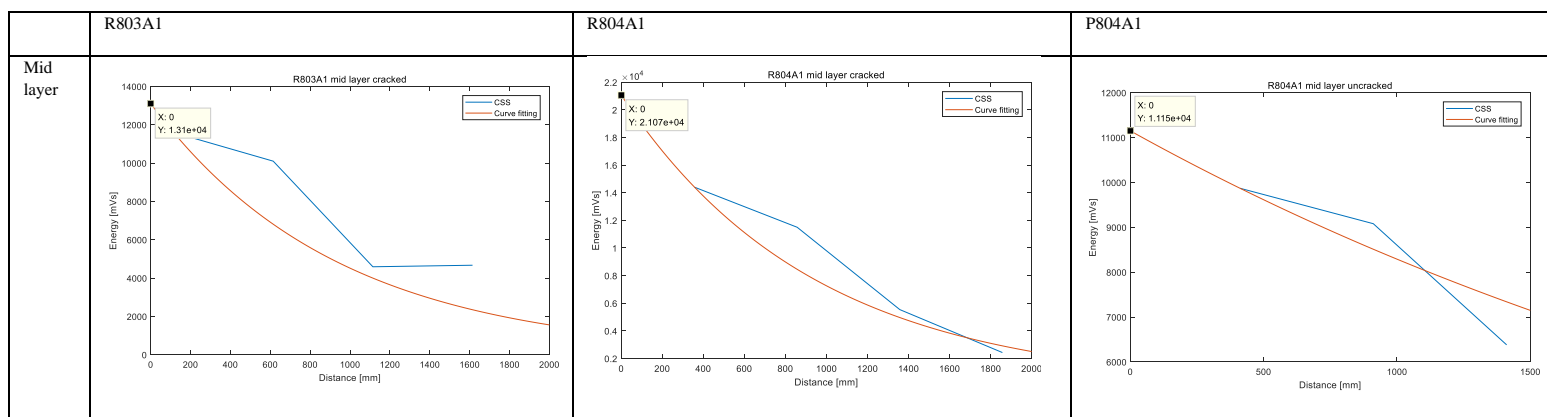
5.3 Cracked versus uncracked structures

The difference of attenuation between cracked and uncracked structures are given in Fig. 5.3.1, it is quite obvious that the attenuation of cracked structures is much higher than uncracked structures in all three layers. On the other hand, the difference in top layer is not that great since the propagating distance plays an important role in attenuation as well. In general, the existing cracks would result in significant energy dissipation and decrease in CSS.
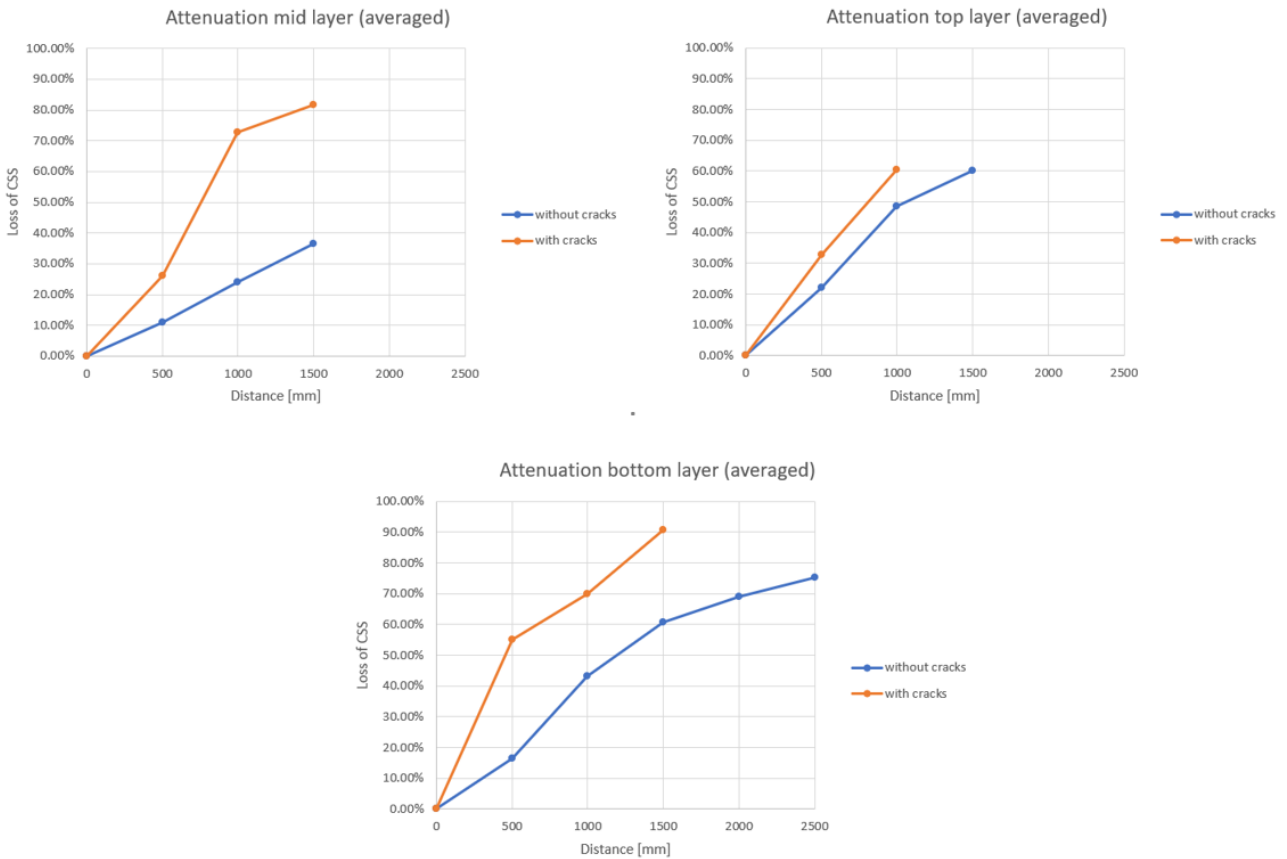
Fig. 5.3.1 Attenuation in cracked and uncracked structures

5.4 Theoretical results versus experimental results

A comparison between theoretical results and experimental results (curve fitting results) is carried out in percentage to check the accuracy.

According to the crack pattern of R804A1 in load step 2 and 3 (shown in Fig. 5.4.1 and Fig. 5.4.2 respectively), the length of crack path in uncracked specimen is $\frac{1127.72 * 800}{1448.62} = 622.78$ mm (approximately 600mm level), and the length of crack path in cracked specimen is $\frac{419.55 * 800}{1461.38} = 229.67$ mm (approximately 200mm level). Comparison between theoretical results and curve fitting results is given in Fig. 5.4.3 and Fig. 5.4.4.
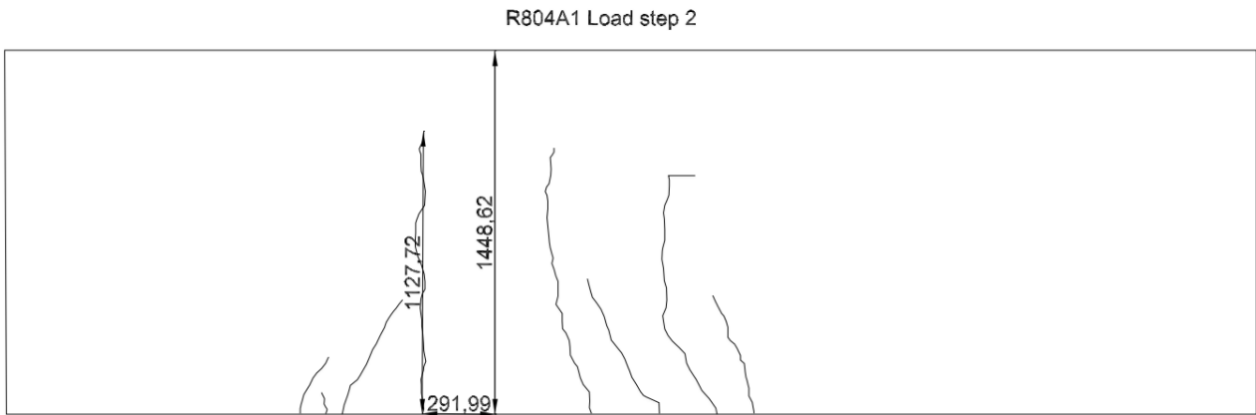
Fig. 5.4.1 rack pattern of R804A1 load step 2
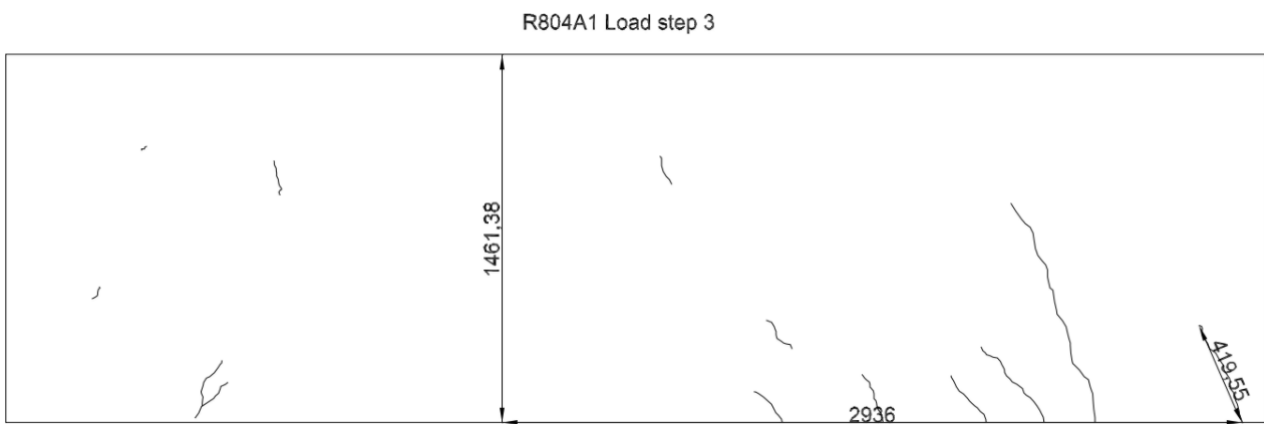
Fig. 5.4.2 Crack pattern of R804A1 load step 3
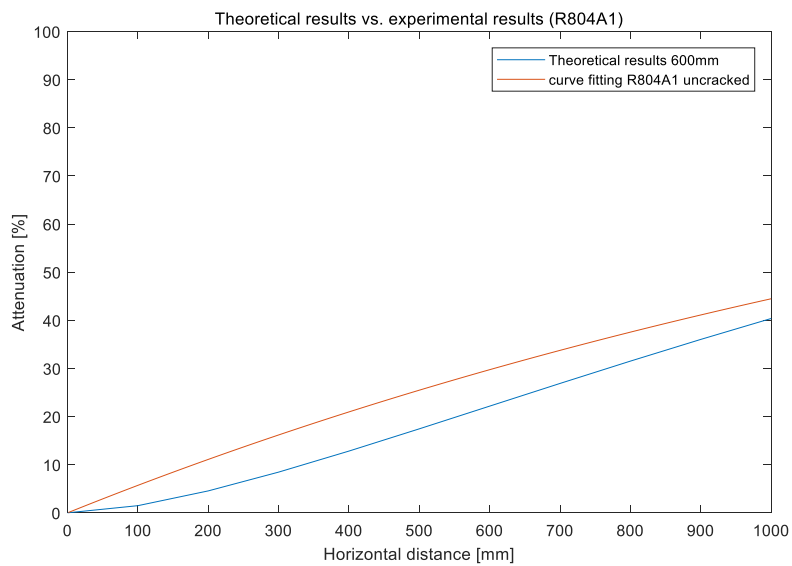
Fig. 5.4.3 Theoretical results vs. experimental results (R804A1 uncracked)
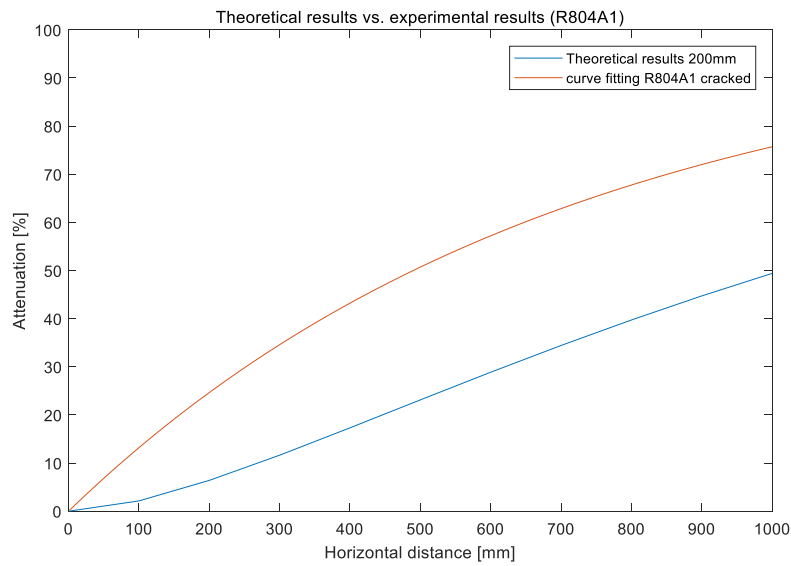
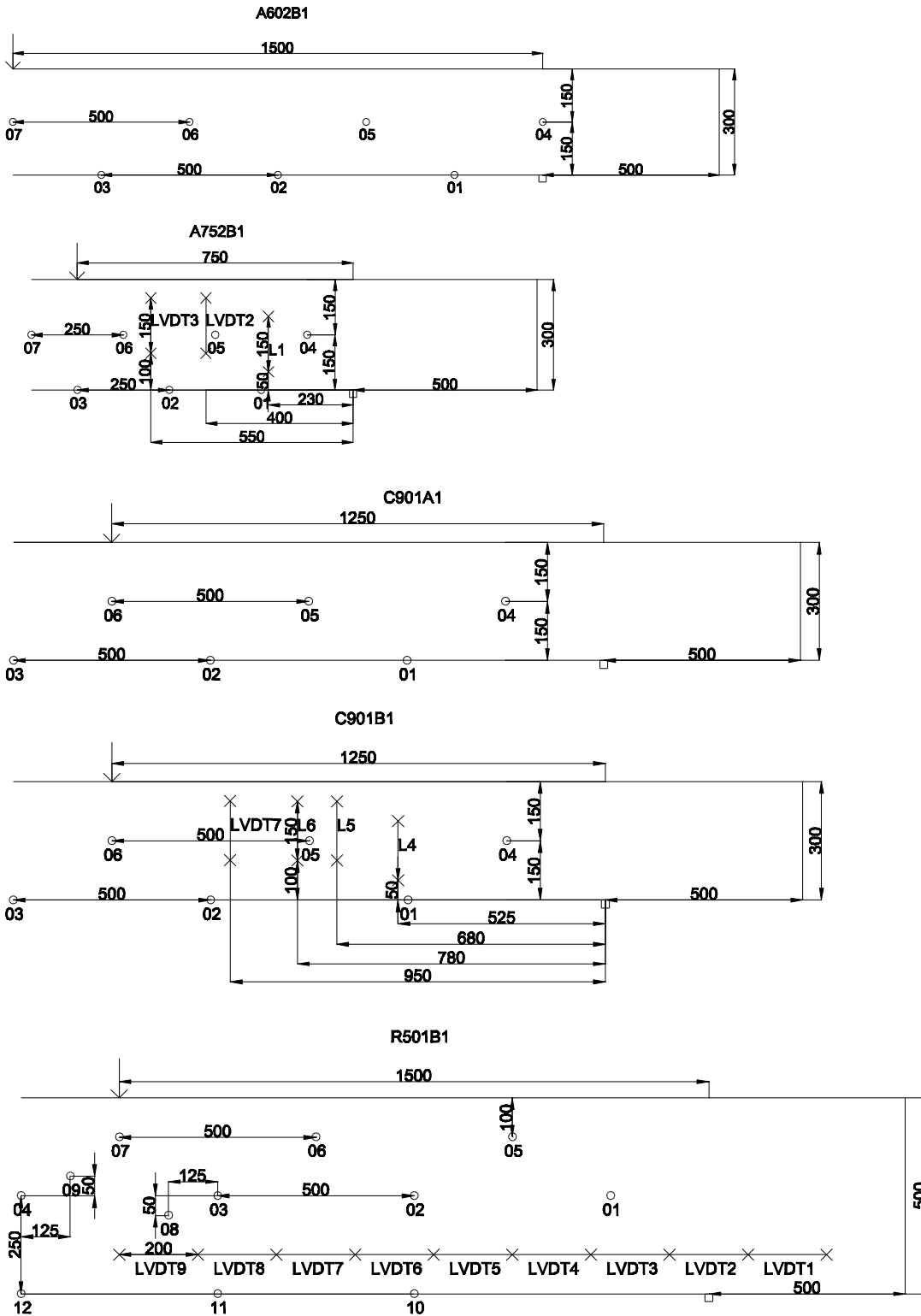**Fig. 5.4.4 Theoretical results vs. experimental results (R804A1 cracked)**

The experimental and theoretical results fit good in uncracked structures, and the attenuation curve almost parallel to each other (Fig. 5.4.3). CSS of experimental result is always higher than that of curve fitting result, which may be affected by other cracks occurred in the same time period within load step 2. In addition, it is also interesting to notice that at the very beginning the exponential model could not simulate the sharp drop of CSS. Modifications are required for the exponential curve fitting. However, things are different in cracked structures. A dramatic drop of CSS is observed in experimental curve, and it is no longer parallel to theoretical curve or the uncracked curves, which serves well to illustrate that the effect of existing cracks in specimens have not been taken into account in exponential model. Furthermore, the slope of CSS of cracked specimen at the very beginning is much higher than that in uncracked specimen. This is because that the flexural crack has been transited into shear cracks, where many cracks occur at the same period (as shown in Fig. 5.4.4) and are recorded by sensors.
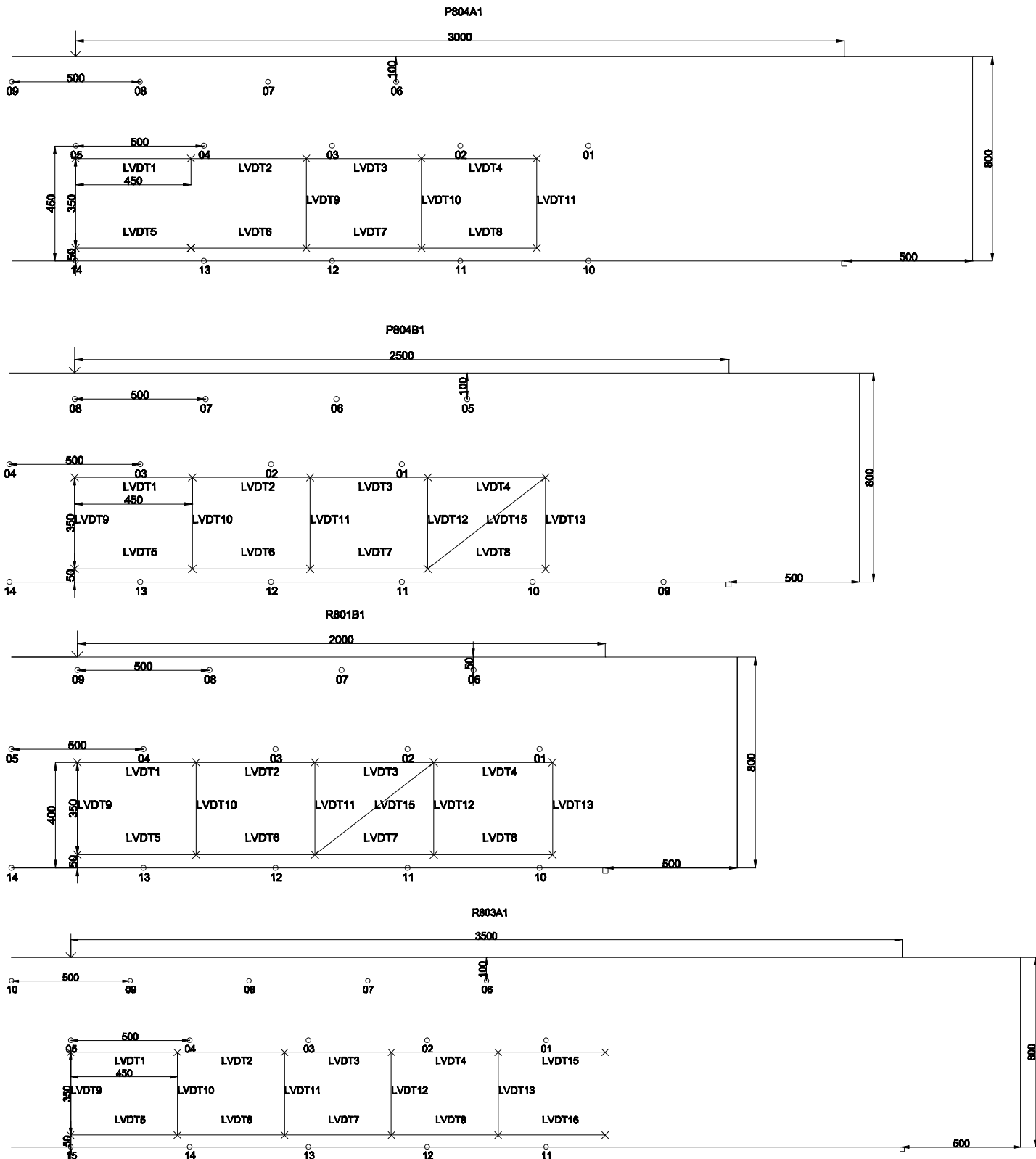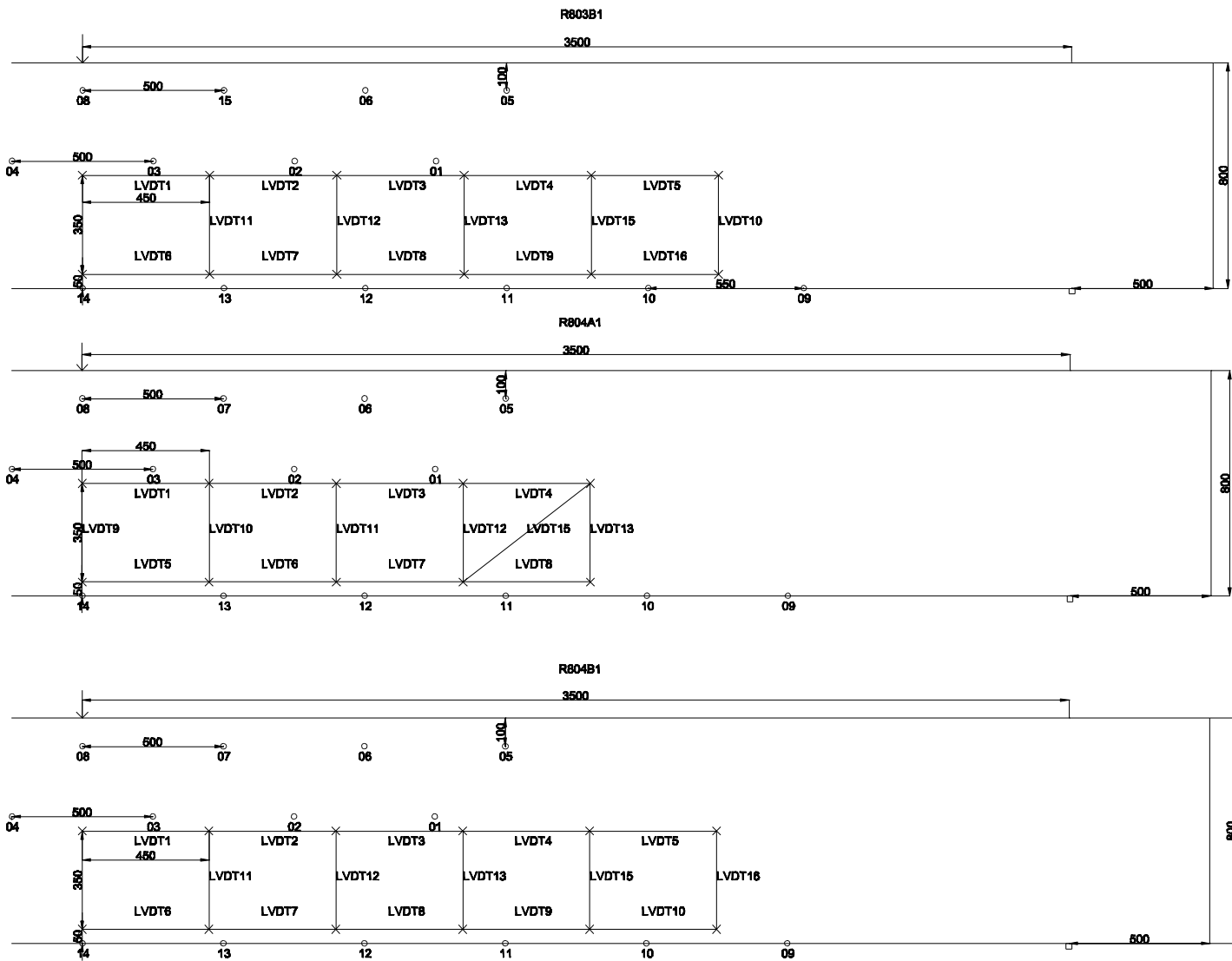
6 Conclusions

A-series of tests on reinforced concrete beams are carried out to investigate the relationship between AE measurement results and fracture energy. AE measurements could only partly represent the amount of energy release in crack propagation due to attenuation. Then G_0 and attenuation, which are two important factors to describe the CSS curve, are investigated in each beam. However, here the G_0 is a "fictitious G_0" by assuming AE sensor closest to crack as the "fictitious source". Real G_0 could be determined by curve fitting and taking into account the distance between crack and AE sensor. Attenuation is represented as a function of distance between crack and AE sensor. The following conclusions may be derived, and they are listed in the sequel.

- CSS detected by a single AE sensor nearly approaches a constant while the total amount of energy release(G_0) of a crack increases linearly as crack propagates.

- Crack length and horizontal distance between crack and sensor are two main factors affecting CSS. A dramatic drop in CSS is observed with the increase of horizontal distance, and crack length is no longer the dominant factor, since the vertical length of crack is negligible comparing with horizontal distance.

- G_0 reflects the total amount of energy release in a crack. G_0 of bottom layer is always higher than mid layer and top layer since bottom layer AE sensors are the closest to energy source and would be more affected by those newly generated cracks on bottom surface of specimen.

- Attenuation of CSS could be affected by several kinds of mechanisms, such as existing cracks, newly generated cracks, propagating distance and top surface reflection. Attenuation in bottom layer is always the highest since there are many sub cracks which are not fully developed initiating on bottom surface.

- CSS detected by AE sensors in a cracked structure drops faster than that in uncracked structures. Existing cracks would result in more energy dissipation while signal travels in concrete matrix.

Appendix 1

R603B1

3500

08   500   15   06   05

100

04   500   03   02   01

LVDT1   LVDT2   LVDT3   LVDT4   LVDT5

450

350

LVDT11   LVDT12   LVDT13   LVDT15   LVDT10

LVDT6   LVDT7   LVDT8   LVDT9   LVDT16

50   550

14   13   12   11   10   09

800

500

R804A1

3500

08   500   07   06   05

100

04   500   03   02   01

450

LVDT1   LVDT2   LVDT3   LVDT4

500

350   LVDT9   LVDT10   LVDT11   LVDT12   LVDT15   LVDT13

LVDT5   LVDT6   LVDT7   LVDT8

50

14   13   12   11   10   09

800

500

R804B1

3500

08   500   07   06   05

100

04   500   03   02   01

LVDT1   LVDT2   LVDT3   LVDT4   LVDT5

450

350

LVDT11   LVDT12   LVDT13   LVDT15   LVDT16

LVDT6   LVDT7   LVDT8   LVDT9   LVDT10

50

14   13   12   11   10   09

800

500

Appendix 2

Attenuation without cracks

R501B1

Only one test of 500mm beam is conducted named R501B1, however, it's very interesting to focus on this specific test result since a dense array of AE sensors are installed at the bottom of the specimen (as shown in Fig.A2. 1). Therefore, cracks could be located accurately, and it's easier to tell energy detected by different sensors are released by which crack as well. Top layer sensors are AE sensors 05-07 installed at 50 mm from the top surface of specimen, while the bottom layer sensors are AE sensors 10-12, arranged at the bottom surface of specimen. Mid layer sensors are AE sensors AE 01-04 and 08, 09, they are installed in the central axis of the beam. AE08 and AE09 are slightly adjusted 50 mm upward and downward in vertical direction respectively as shown in Fig.A2. 1.
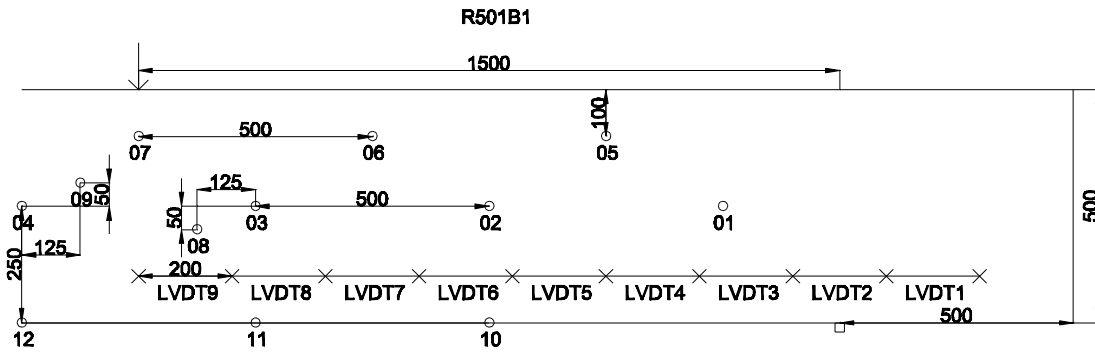
Fig.A2. 1 LVDT and AE grid (R501B1)

According to load-crack width figures shown in Table.A2. 1, the first crack opening is represented by an obvious drop in slope, which means a sudden growth in crack width while the load remains same level. Then with respect to load-time curve (Fig.A2. 2), the load step where the first crack occurs could be decided. The crack pattern at the end of each load step is recorded by camera, and crack path generated within the specific load step is sketched as shown in Fig.A2. 3, the distance between crack and load position could be derived according to ratio between beam height measured in sketch and in reality. Finally, attenuation of CCS which are divided into three layers could be given as a function of distance between crack and AE sensor.

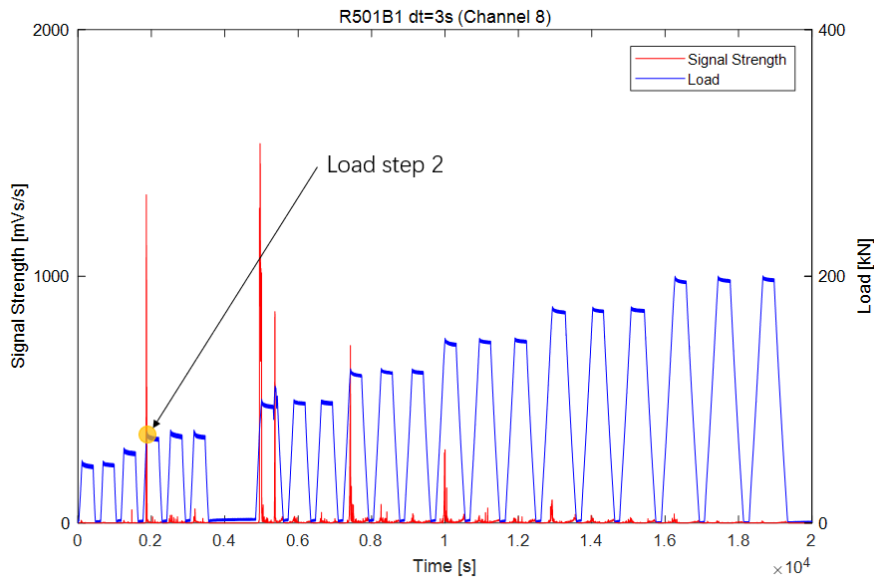**Table.A2. 1 LVDT plot and corresponding AE plot (R501B1)**
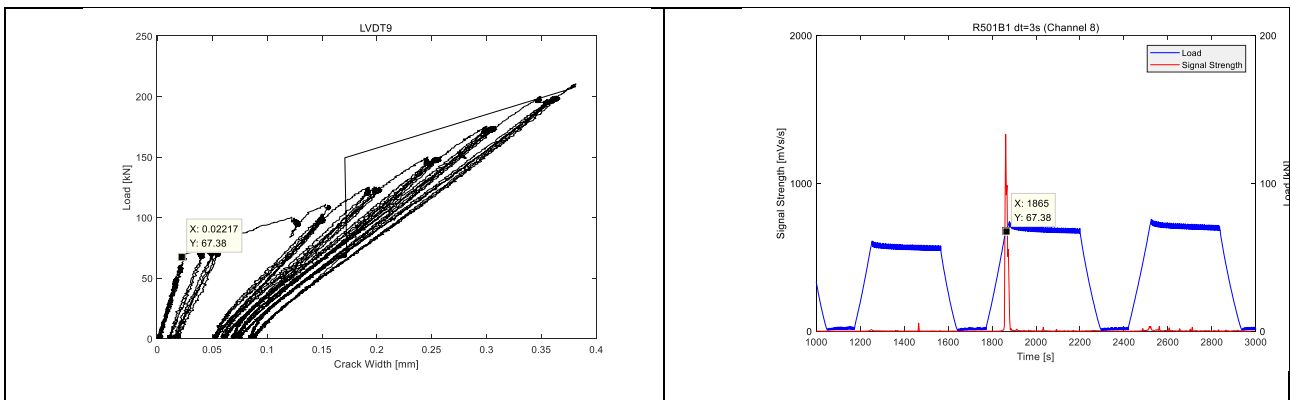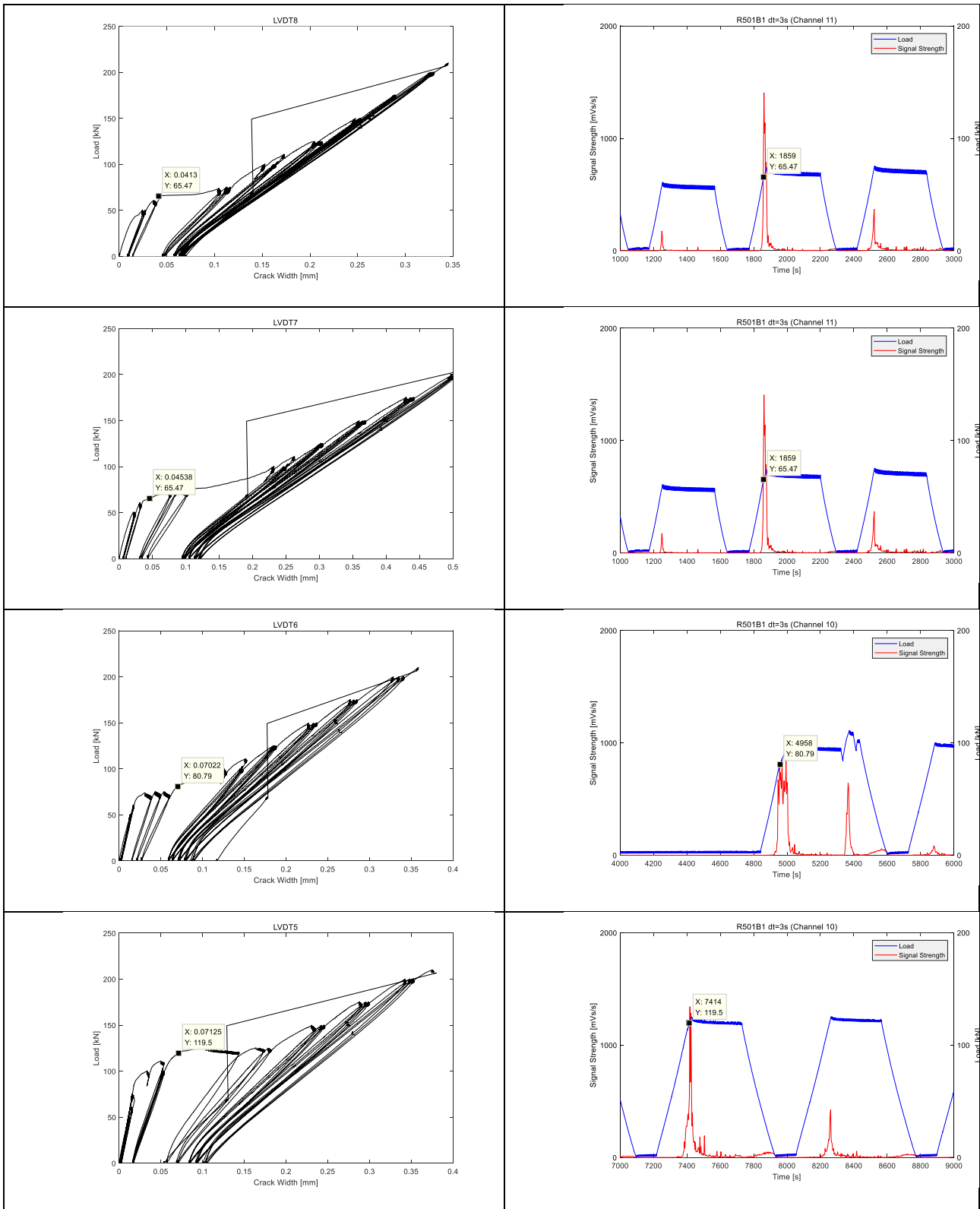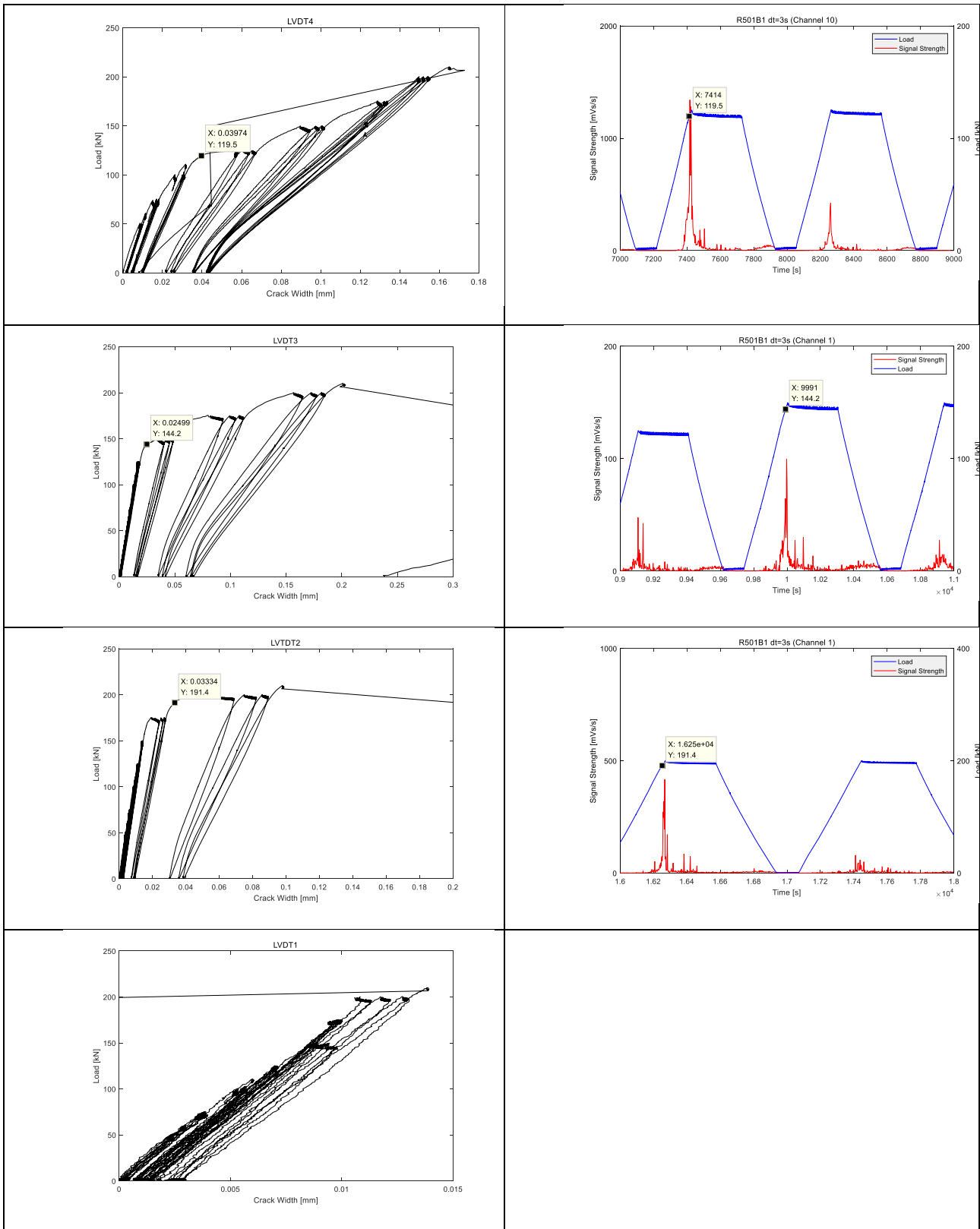
In Table.A2. 1, by comparing Load-crack width plot and corresponding AE plot, it is obvious that at the same load level, each crack opening detected by LVDT is accompanied with a peak value of

signal strength detected by AE sensor, which proves again that the crack propagation could be monitored by AE sensors.


**Fig.A2. 2 Load and Signal strength against Time (R501B1)**

The crack pattern of R501B1 is given in Fig.A2. 3 and Fig.A2. 4, the 1st major flexural crack is located approximately 179.11 mm to the left of loading point, which it is not detected by LVDT9. According to Fig.A2. 5, energy release of the first crack is in the time-period 1800-1980s, and CCS within this period detected by each sensor is given in Table.A2. 2.
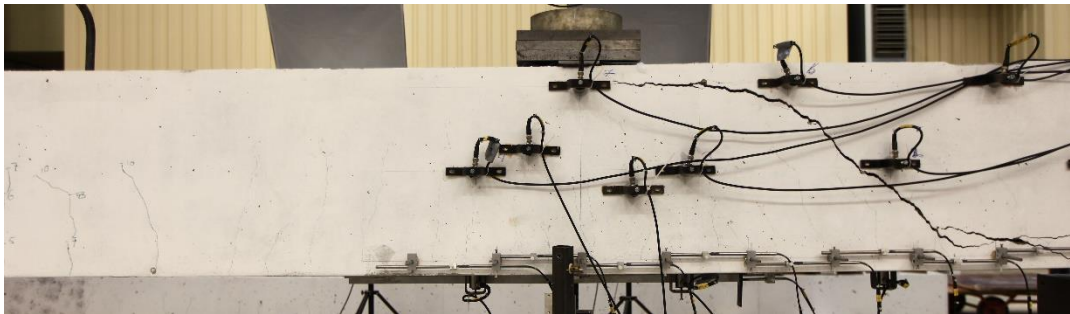
Fig.A2. 3 Crack pattern of R501B1
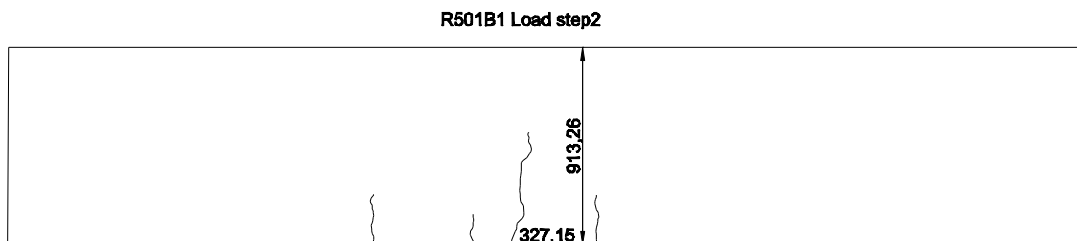
Fig.A2. 4 Crack pattern sketch of R501B1 load step 2
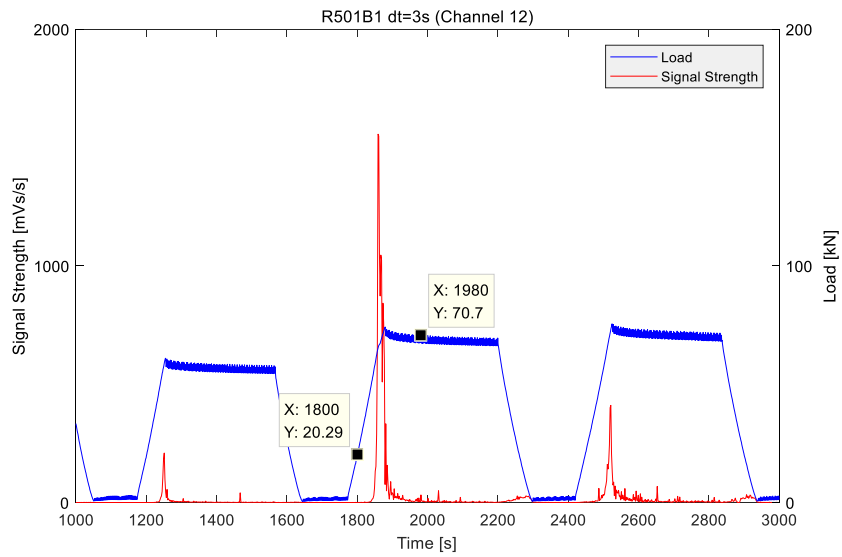
Fig.A2. 5 SS-time curve of R501B1

Table.A2. 2 CCS of each sensor (R501B1 1800-1980s)

	CSS [mVs]	Distance [mm]
Channel 1	1150.00	2228.55
Channel 2	2260.00	1728.55
Channel 3	3870.00	1228.55
Channel 4	8770.00	728.55
Channel 5	1460.00	228.55
Channel 6	3480.00	1478.55
Channel 7	6760.00	978.55
Channel 8	5720.00	478.55
Channel 9	7300.00	-21.45
Channel 10	5120.00	2228.55
Channel 11	8460.00	1728.55
Channel 12	12700.00	1228.55
Channel 13	1150.00	728.55
Channel 14	2260.00	228.55

By dividing the AE sensors into three groups, CCS against time is plotted in Fig.A2. 6, and the trends of attenuation is quite clear as the distance between AE sensors and crack increases.
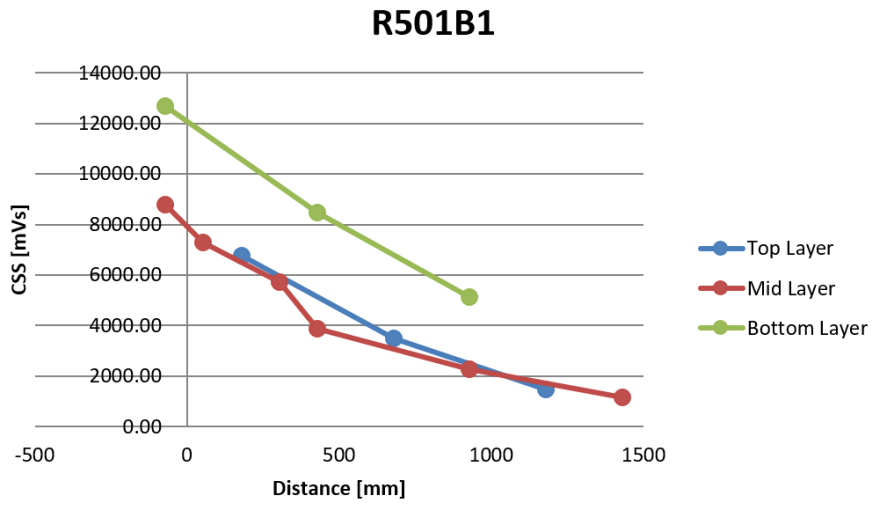
Fig.A2. 6 CCS-Distance R501B1

R803A1

Crack pattern of R803A1 is given in Fig.A2. 7, the 1st main flexural crack is located to the right of loading point. Due to installation failure, no signal is detected by AE15 in this test, and AE14 is selected as the one closest to 1st crack. According to result of LVDT measurement, the crack occurs at the second load step, and the corresponding energy release is in the time period 1874-1918s (Fig.A2. 8).
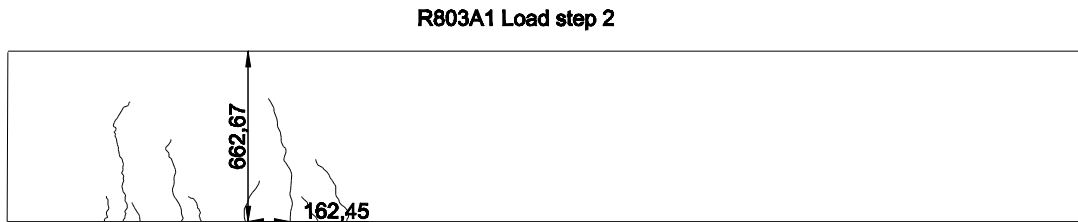

Fig.A2. 7 Crack pattern of R803A1 load step 2
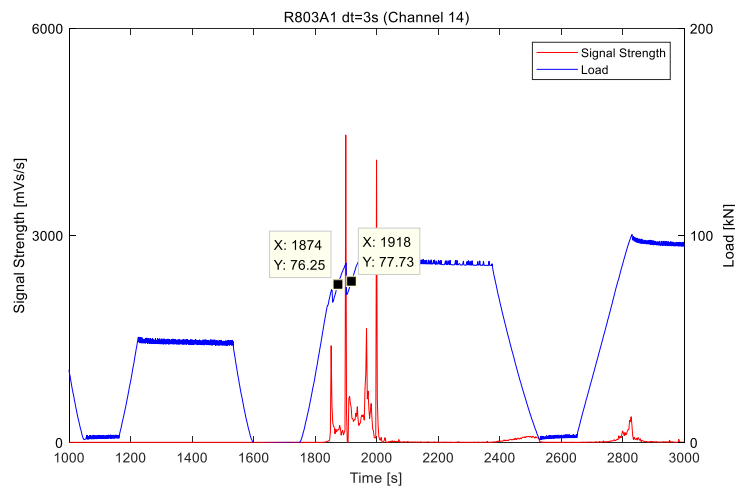
Fig.A2. 8 SS-time curve of R803A1

Table.A2. 3 CCS of each sensor (R803A1 1874-1918s)

	1874-1918s	Distance [mm]
Channel 1	5.0044e+03	1803.88
Channel 2	6.2128e+03	1303.88
Channel 3	5.9188e+03	803.88
Channel 4	6.7311e+03	303.88
Channel 5	1.2017e+04	-196.12
Channel 6	4.1987e+03	1553.88
Channel 7	4.3900e+03	1053.88
Channel 8	8.1120e+03	553.88
Channel 9	9.4139e+03	53.88

Channel 10	1.0073e+04	-446.12
Channel 11	3.6700e+03	1803.88
Channel 12	4.9490e+03	1303.88
Channel 13	7.4231e+03	803.88
Channel 14	8.8936e+03	303.88

CCS within this period detected by each sensor is given in Table.A2. 3. By dividing the AE sensors into three groups, CCS against time is plotted in Fig.A2. 9.
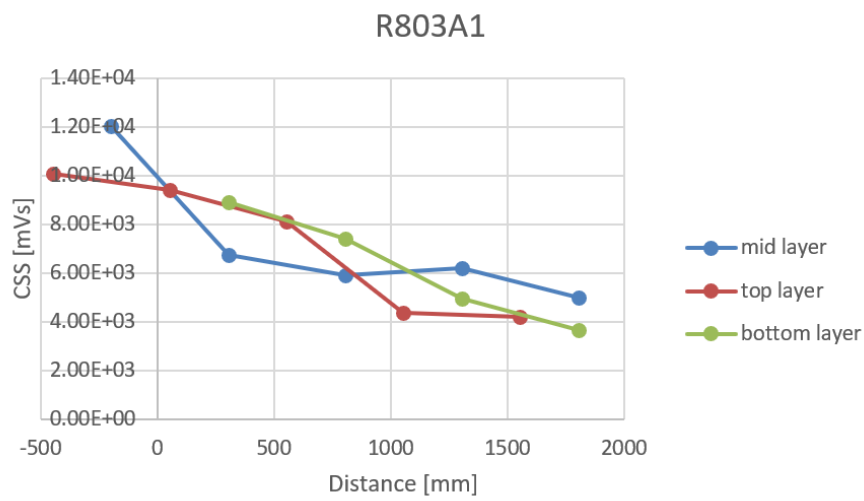
Fig.A2. 9 CCS-Distance R803A1

P804A1

The crack pattern of P804A1 is given in Fig.A2. 10, the 1st main flexural crack is located to the left of loading point, which it is not detected by LVDT14. According to Fig.A2. 11, energy release of the first crack is in the time period 790.8-875.8s, and CCS within this period detected by each sensor is given in Table.A2. 4.
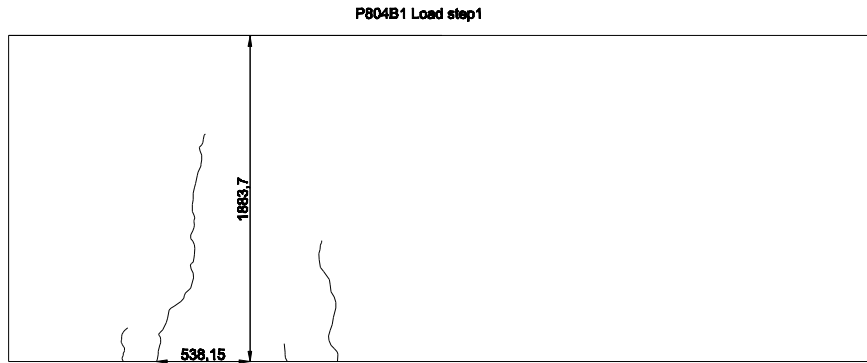
Fig.A2. 10 Crack pattern of P804A1 load step 1
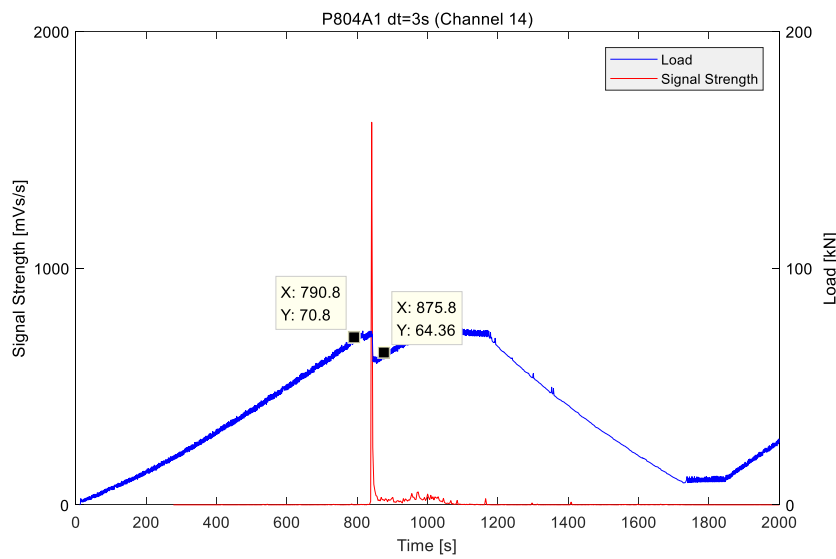
Fig.A2. 11 SS-time curve of P804A1

Table.A2. 4 CCS of each sensor (P804A1 790.8-875.8s)

	CSS [mVs]	Distance [mm]
Channel 1	2.0594e+03	2228.55
Channel 2	2.7555e+03	1728.55
Channel 3	3.4000e+03	1228.55
Channel 4	3.8952e+03	728.55
Channel 5	1.7195e+03	228.55
Channel 6	2.2987e+03	1478.55

Channel 7	3.3926e+03	978.55
Channel 8	1.8900e+03	478.55
Channel 9	4.7070e+03	-21.45
Channel 10	1.1977e+03	2228.55
Channel 11	2.9036e+03	1728.55
Channel 12	3.8015e+03	1228.55
Channel 13	4.8979e+03	728.55
Channel 14	2.2468e+03	228.55

By dividing the AE sensors into three groups, CCS against time is plotted in Fig.A2. 1.
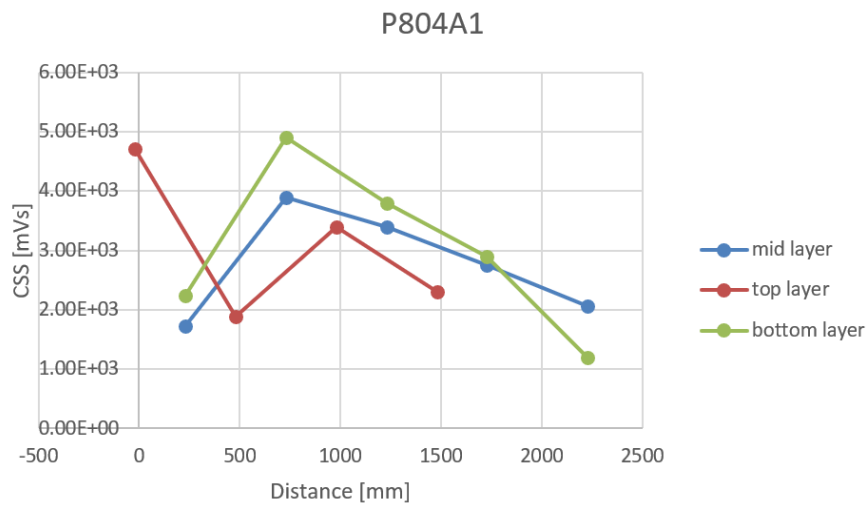
Fig.A2. 12 CCS-Distance P804A1

Other specimens

Attenuation curves of other specimens (including 300mm beams, 800mm beams, and low strength concrete beams) are given in Table.A2. 5.

Table.A2. 5 Attenuation curves of other specimens
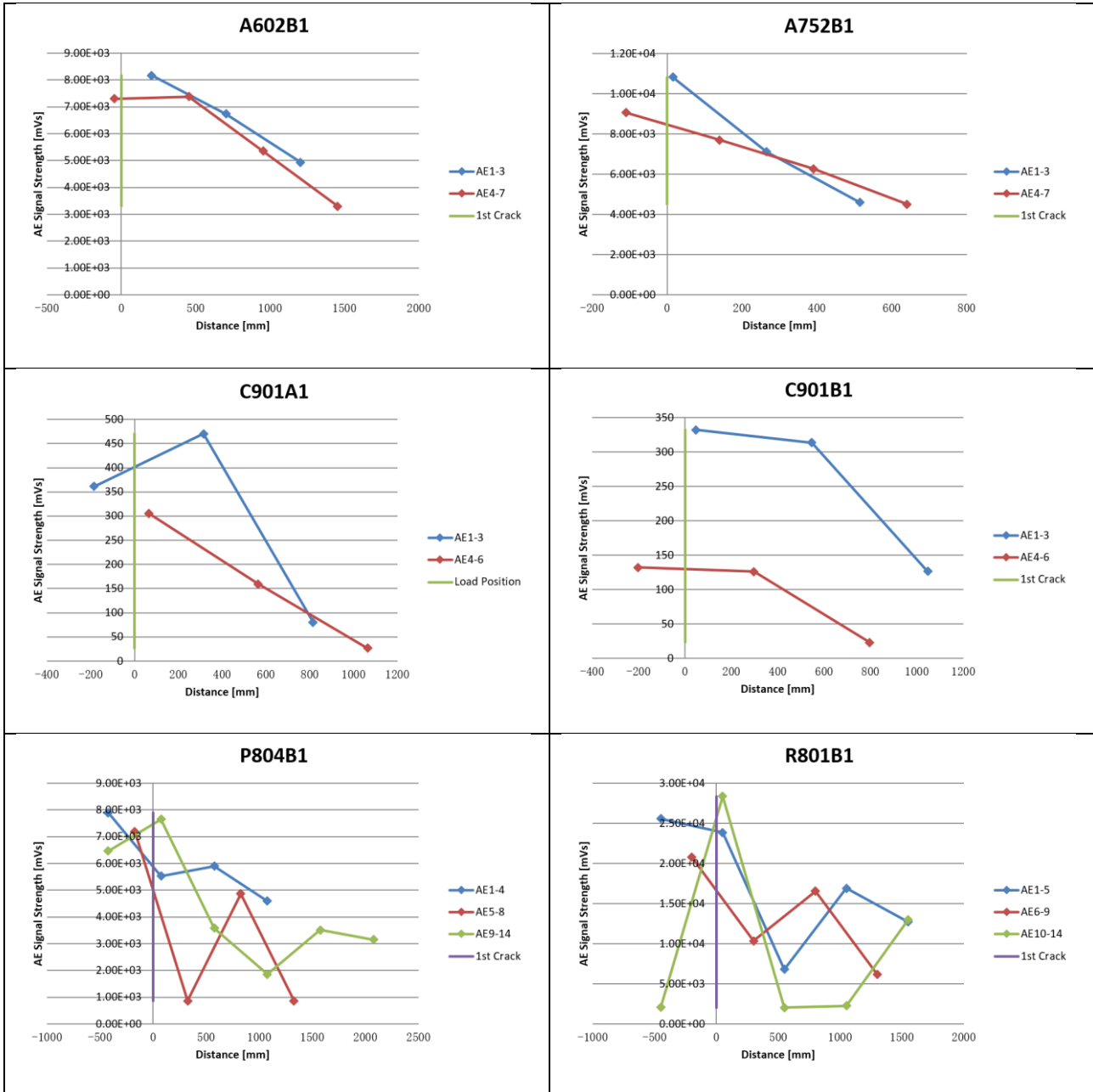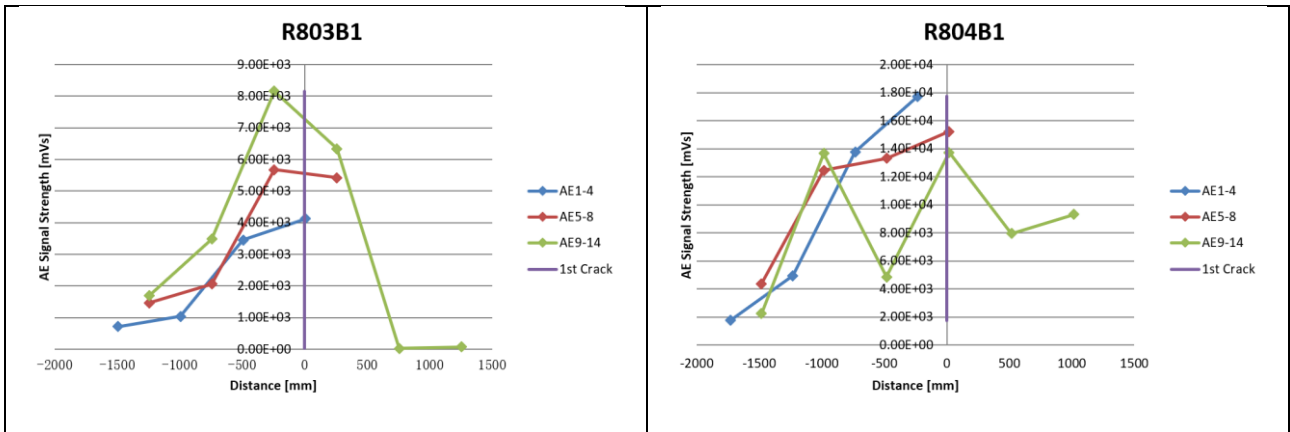
Appendix 3

Attenuation with cracks

A crack detected by the LVDT farthest from loading point is selected to investigate attenuation with cracks, to make sure there are enough AE sensors working in cracked zone.

R501B1

In R501B1, as shown in Table.A3. 1, the crack farthest from loading point is detected by LVDT2 at 191.4kN level. According to the corresponding Load-Time curve, the crack occurs at load step 6, and the corresponding energy release is in the time period 16170-16250s (Fig.A3. 1).

Table.A3. 1 LVDT plot and corresponding AE plot (R501B1)
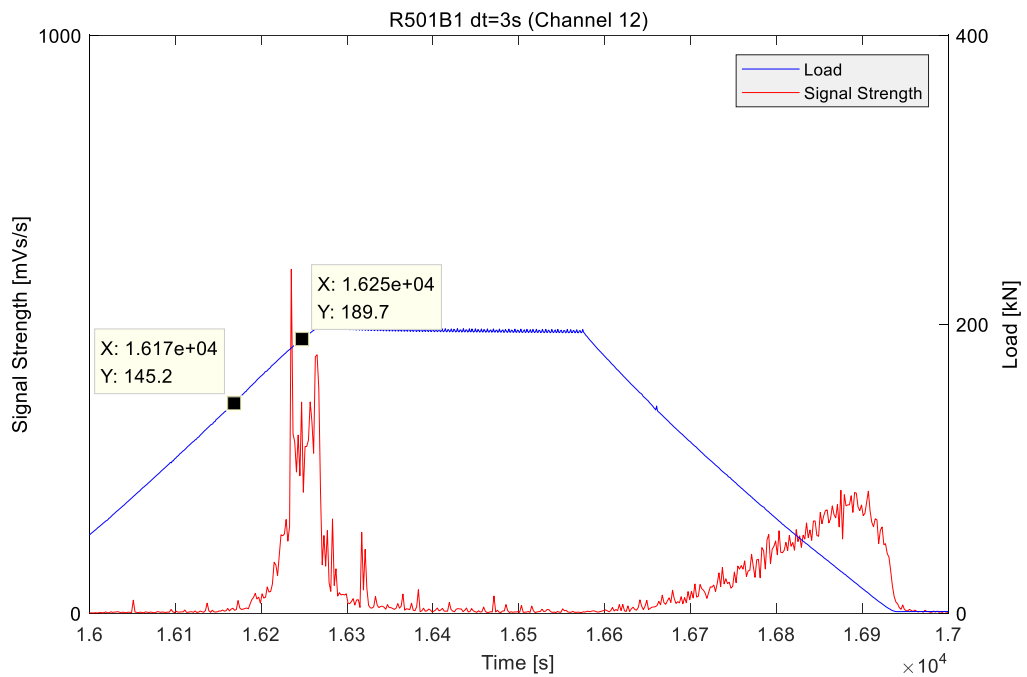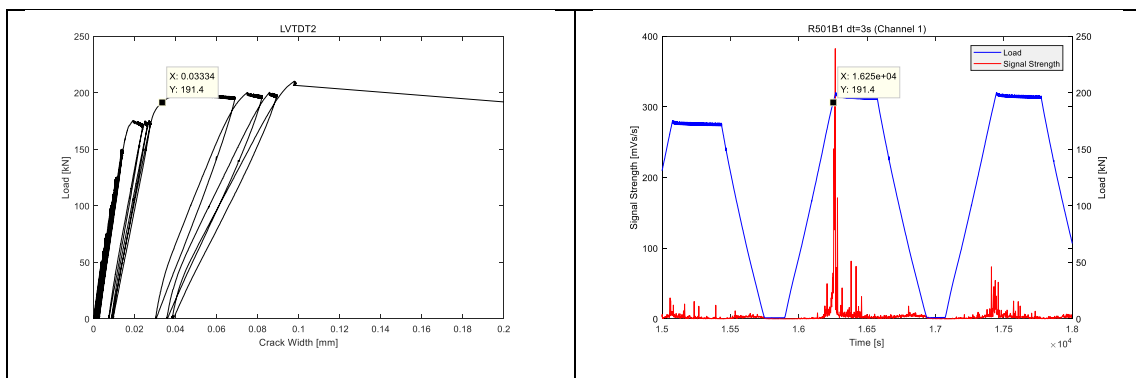
Fig.A3. 1 SS-time curve of R501B1

Crack pattern of load step 6 is shown in Fig.A3. 2. CCS of each sensor against horizontal distance is plotted in Fig.A3. 3.
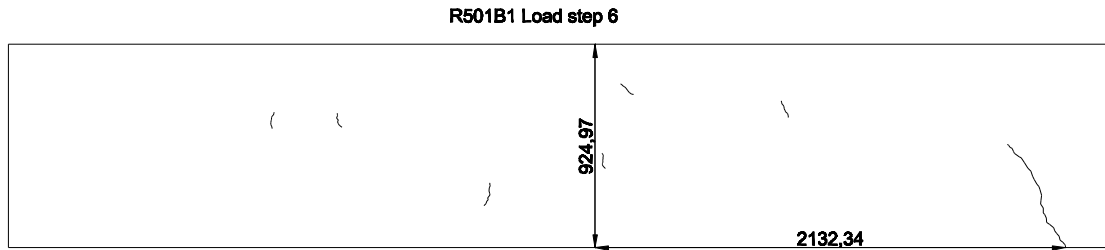
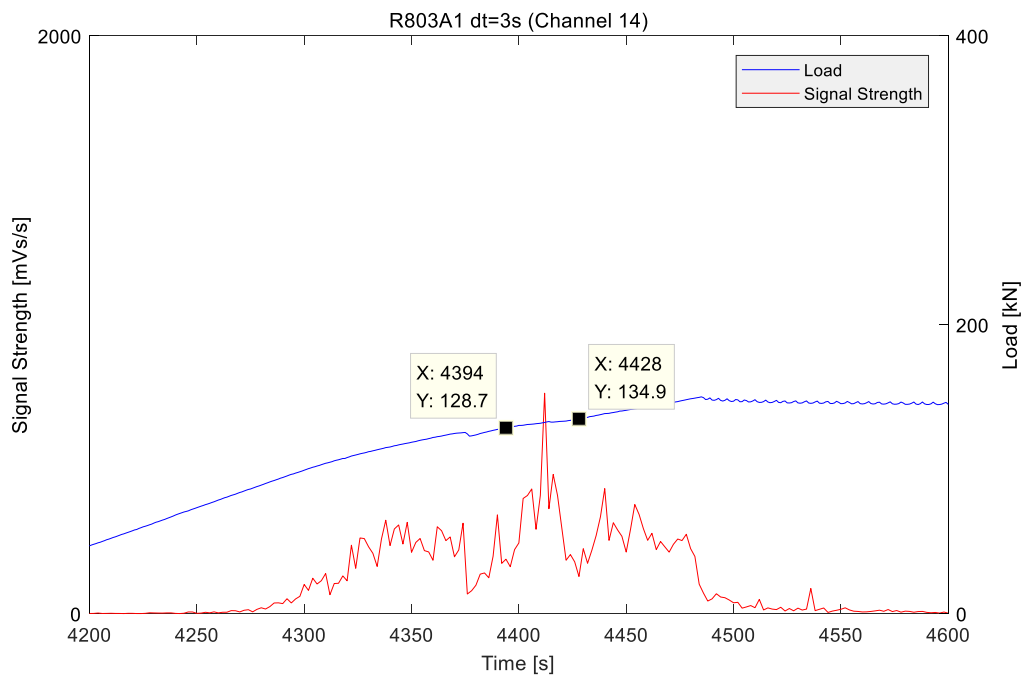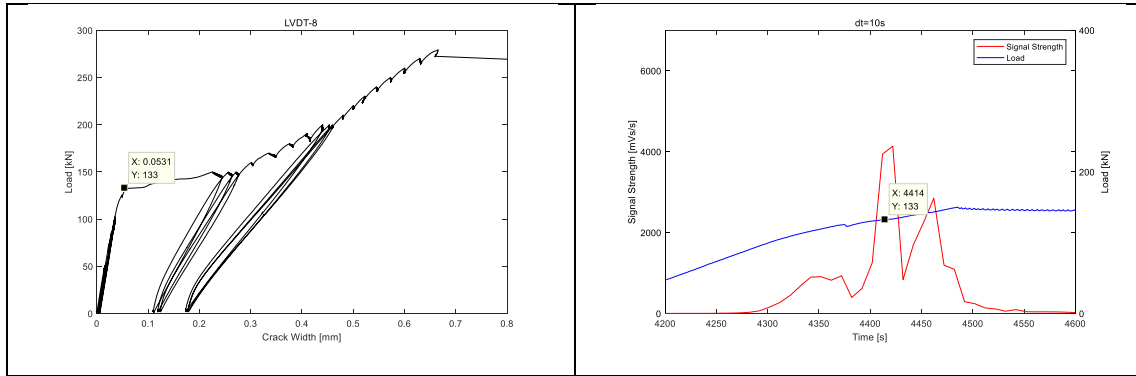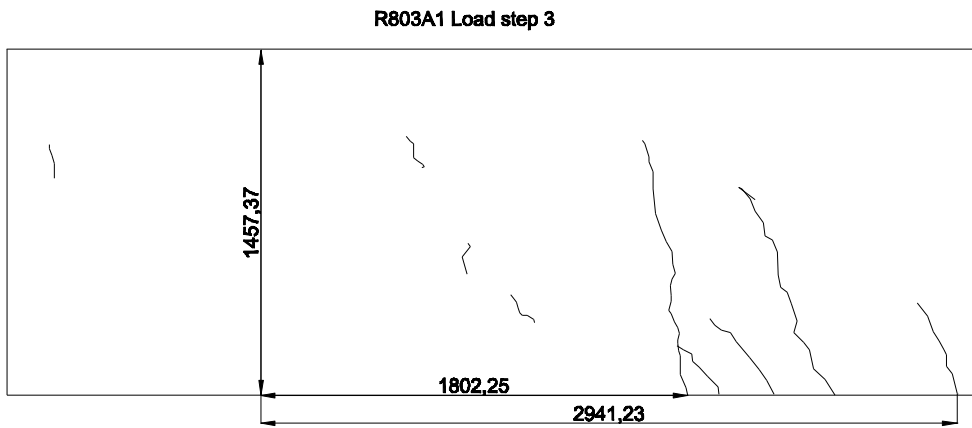**Fig.A3. 2 Crack pattern of load step 6**
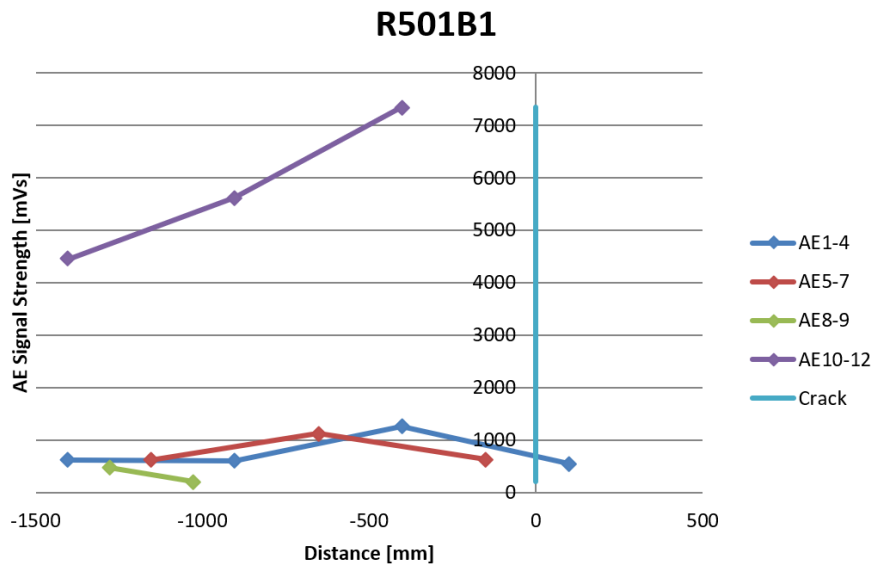
Fig.A3. 3 CCS-Distance R501B1

R803A1

In R803A1, as shown in Table.A3. 1, the crack farthest from loading point is detected by LVDT8 at 133kN level. According to the corresponding Load-Time curve, the crack occurs at load step 3, and the corresponding energy release is in the time period 4394-4428s (Fig.A3. 4).

Table.A3. 2 LVDT plot and corresponding AE plot (R803A1)

Fig.A3. 4 SS-time curve of R803A1

Crack pattern of load step 3 is shown in Fig.A3. 5. CCS of each sensor against horizontal distance is plotted in Fig.A3. 6

R803A1 Load step 3
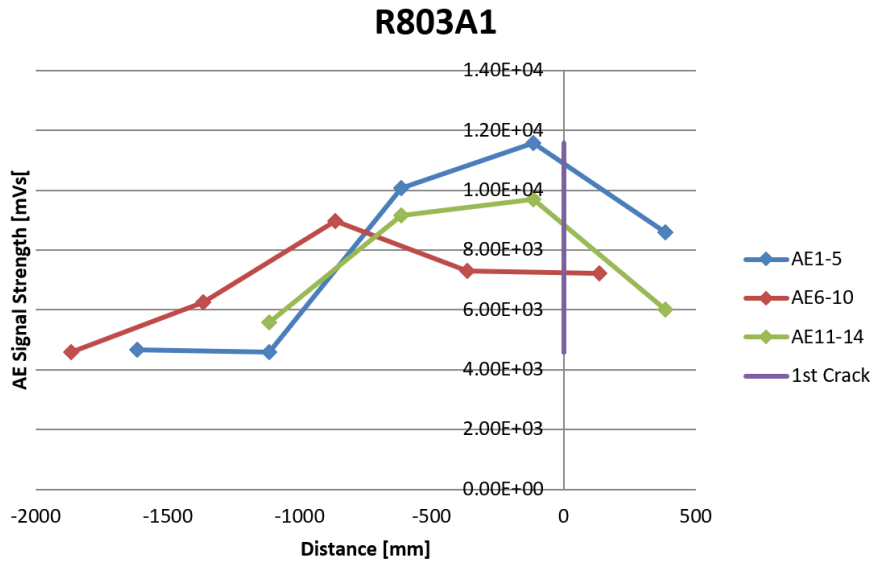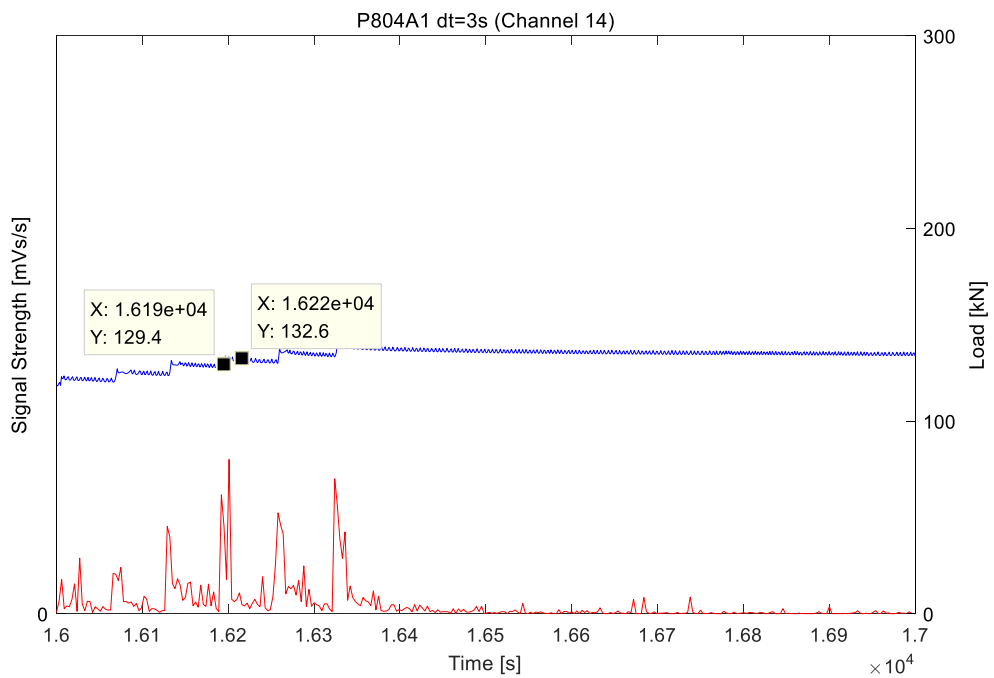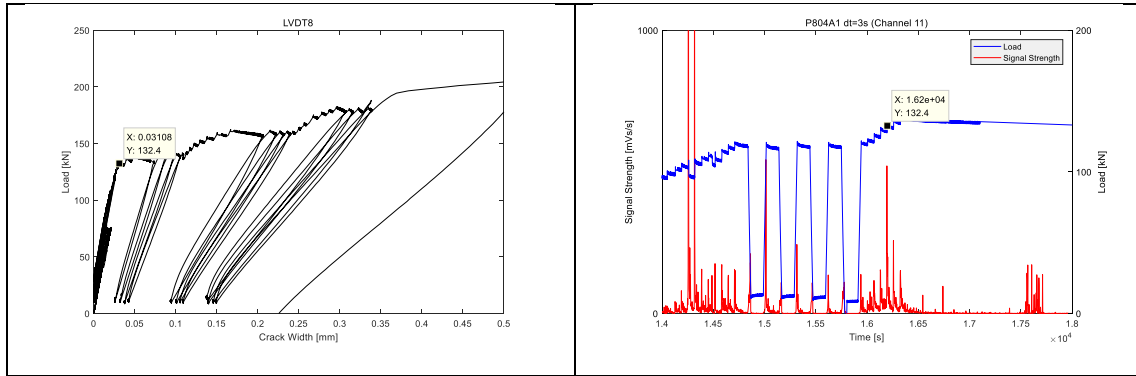

Fig.A3. 5 Crack pattern of load step 3

Fig.A3. 6 CCS-Distance R803A1

P804A1

In P804A1, as shown in Table.A3. 3, the crack farthest from loading point is detected by LVDT8 at 132.4kN level. According to the corresponding Load-Time curve, the crack occurs at load step 6, and the corresponding energy release is in the time period 16190-16220s (Fig.A3. 7).

Table.A3. 3 LVDT plot and corresponding AE plot (P804A1)

Fig.A3. 7 SS-time curve of P804A1

Crack pattern of load step 6 is shown in Fig.A3. 8. CCS of each sensor against horizontal distance is plotted in Fig.A3. 9.
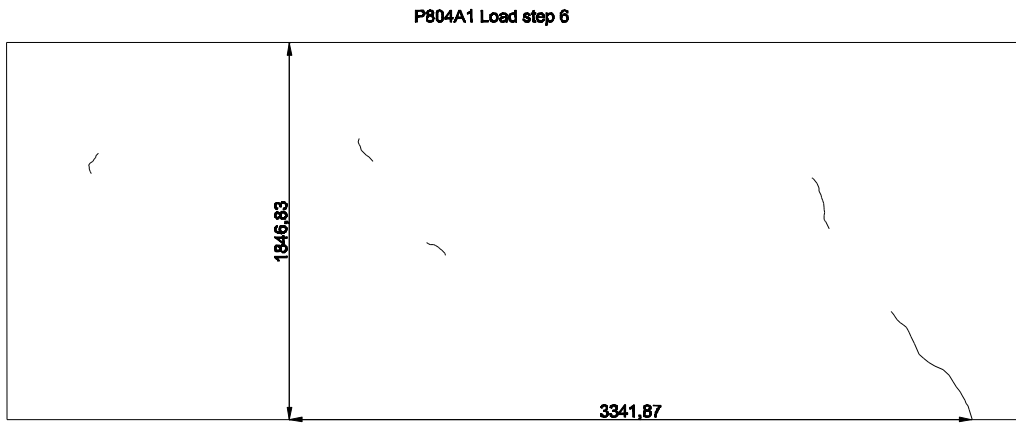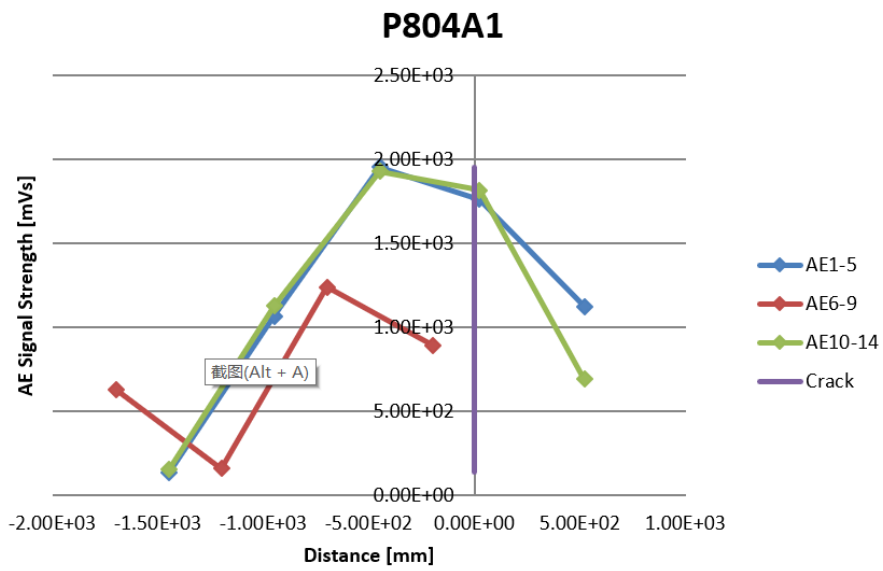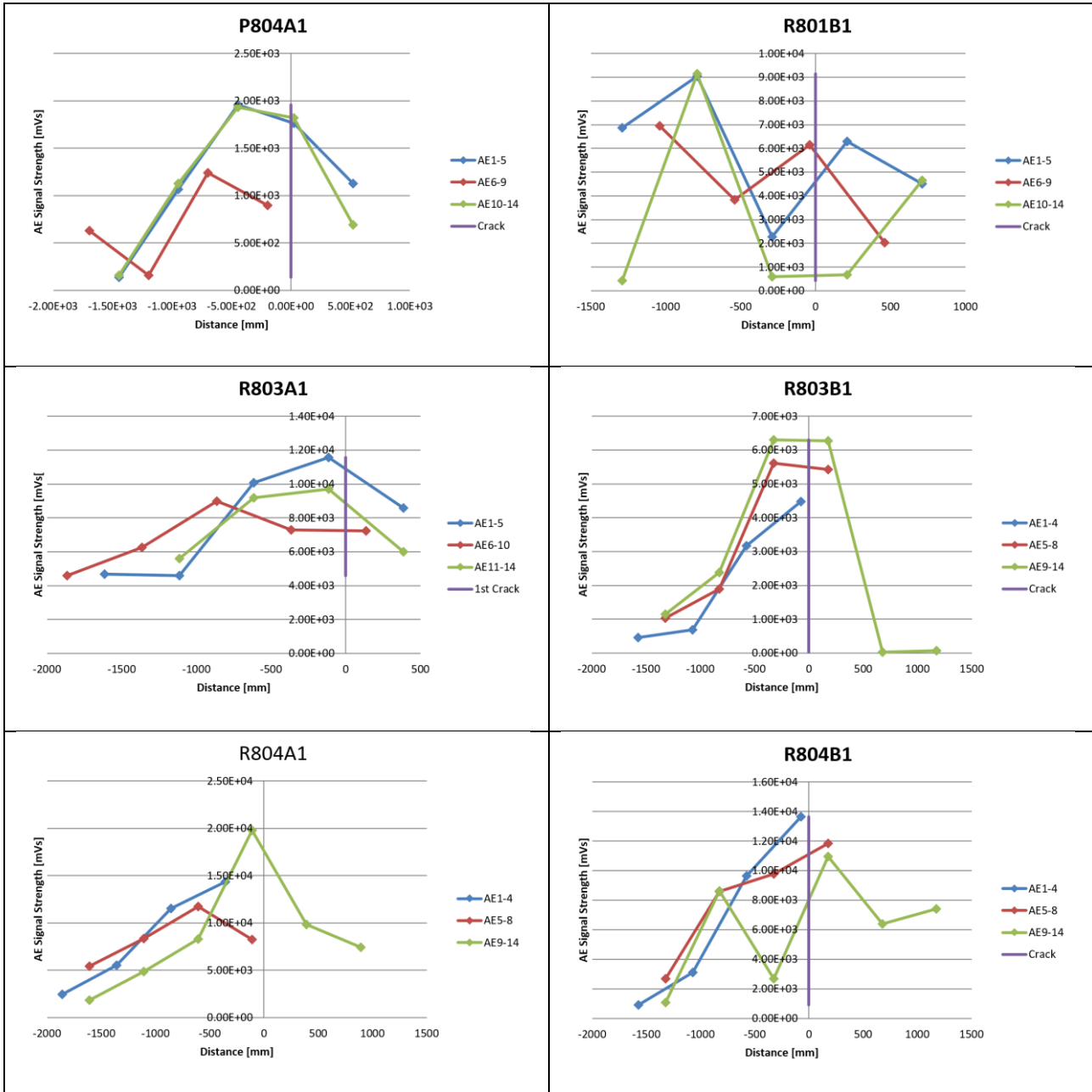
Fig.A3. 8 Crack pattern of load step 6

Fig.A3. 9 CCS-Distance P804A1

Other specimens

Attenuation curves of other specimens (800mm beams) are given in Table.A3. 4.

Table.A3. 4 Attenuation curves of other specimens

Reference

1. Hellier, C., *Handbook of nondestructive evaluation.* 2001.
2. Blitz, J. and G. Simpson, *Ultrasonic methods of non-destructive testing.* Vol. 2. 1995: Springer Science & Business Media.
3. Grosse, C.U. and M. Ohtsu, *Acoustic emission testing.* 2008: Springer Science & Business Media.
4. Koekkoek, R.T. and Y.Yang, *Measurement Report on the Transition between Flexural and Shear Failure of RC Beams without Shear Reinforcement*, in 2016.
5. Ziehl, P. and A. Pollock, *Acoustic emission for civil structures*, in *Acoustic Emission*. 2012, InTech.
6. Vahaviolos, S.J. *Acoustic emission: standards and technology update*. 1999. ASTM.
7. Y.Yang, L. Pahlavan, and D.A. Hordijk, *Analysis of Acoustic Emission from a shear test on a large scale reinforced concrete beam.* EWGAE, 2017.
8. Yang, Y., D. Hordijk, and A. de Boer, *Acoustic emission measurement in the proof loading of an existing bridge affected by ASR.* IALCCE 2016, 2016.
9. Tariq, H., et al., *The linear variable differential transformer (LVDT) position sensor for gravitational wave interferometer low-frequency controls.* Nuclear Instruments and Methods in Physics Research Section A: Accelerators, Spectrometers, Detectors and Associated Equipment, 2002. **489**(1-3): p. 570-576.
10. Karihaloo, B.L., *Fracture Mechanics & Structural Concrete(Concrete Design & Construction Series).* 1995.
11. Brühwiler, E. and F. Wittmann, *The wedge splitting test, a new method of performing stable fracture mechanics tests.* Engineering fracture mechanics, 1990. **35**(1-3): p. 117-125.
12. Fernández-Canteli, A., et al., *Determining fracture energy parameters of concrete from the modified compact tension test.* Frattura ed Integrità Strutturale, 2014(30): p. 383.
13. Morse, P.M. and K.U. Ingard, *Theoretical acoustics.* 1968: Princeton university press.
14. Berryman, J.G. and H.F. Wang, *Elastic wave propagation and attenuation in a double-porosity dual-permeability medium.* International Journal of Rock Mechanics and Mining Sciences, 2000. **37**(1-2): p. 63-78.